Syracuse University

SURFACE

Dissertations - ALL

January 2015

Beyond Standard Model Physics under the ground and in the sky

Bithika Jain
Syracuse University

Follow this and additional works at: https://surface.syr.edu/etd

Part of the Physical Sciences and Mathematics Commons

Abstract

Cosmology and particle physics are in an exciting data-rich era, with several collider and astronomical searches underway. In this dissertation, we have explored some problems which are not addressed by the standard models of particle physics and cosmology. The implications of the Higgs discovery and lack of new physics results are far reaching. To better understand the nature of Higgs and its connections to electroweak symmetry breaking, we have performed a model independent study of spin-1 contributions in gauge extensions of Standard model. The null results of all low energy supersymmetric searches has lead to the development of Split SUSY models which are based only on gauge unification and dark matter as guiding principles. We study in detail the cosmic probes of Split SUSY using indirect dark matter detection constraints and hints of small tensor to scalar ratio. We also investigate the phenomenological viability of models with light dilatons that ameliorate the cosmological constant problem by studying conformal phase transitions using holography. Finally, we have also checked the robustness of soft-wall geometry by including higher curvature terms in the five dimensional bulk action.

Beyond Standard Model Physics under the ground and in the sky

by

Bithika Jain

B.Sc. (Physics) St. Xavier's College, Mumbai, 2007

M.Sc. (Physics) Indian Institute of Technology, Kanpur, 2010

DISSERTATION

Submitted in partial fulfillment of the requirements for the degree of

Doctor of Philosophy in Physics

Syracuse University

August 2015

To my parents

and

Prayush

In loving memory of Nani

and

Chelsea.

Acknowledgements

Over the past five years, I have worked, interacted and made friends with many physicists. Unfortunately, space makes it impossible to thank them all individually and I hope anyone I do not mention here will forgive me. I would first and foremost like to thank my advisor, Jay Hubisz. His vast knowledge of and passion for theoretical physics never ceased to inspire me. I am specially indebted to him for his encouragement and for his endless patience. I would also like to thank the other members of my defense committee Simon Catterall, Jack Laiho, Carl Rosenzweig, Mark Bowick, and Leonid Kovalev for taking time out of their busy schedules to read and critique my work. I am grateful to Syracuse University theoretical physics faculty at Syracuse and Cornell, Maxim Perelstein, JiJi Fan, Simon Catterall and Jack Laiho, for their many excellent questions regarding my work, and valuable insights. I would specially like to thank my academic adviser Joseph Schecter, for his patience and candid advice. To Don Bunk, Jack Collins and Nicolas Rey-Le Lorier, I want to extend my gratitude for helping me with much of what I learned during my research at Syracuse and Cornell. I would also like to thank Ogan Ozsoy, Jayanth Neelakanta, Prashant Mishra, for all of the conversations and questions every weekend. And also for all the beer we shared. I would specially like to thank Maxim Perelstein, JiJi Fan for listening to and critiquing my work.

I would like to thank Priyotosh Bandopadhyay and Sandipan Kundu, for productive conversations at different points of time over the past five years. This would also be the right place to express my gratitute towards my previous mentors, Ajay Patwardhan and Pankaj Jain. Their mentorship and advice helped shape my research interests. It has been a pleasure to share an office with Aarti raghuraman and Jessica Esquivel , and I want to thank them for their innumerable help and for bearing with me. None of this would have been possible without the love and support of my parents and family, and I am deeply indebted to them. Thank you Prayush for all

the love and support you have given me in these past five years, you are truly the best collaborator. This would also be the right place to thank my friends for all the good times and incisive conversations, specially Aahana, Jahnavi, Neha, Aanindeeta, Soham, Shaon, Tatha, Pavan, Ishaan, Ankita, Preyas, Prerit, Gizem, Swetha, Shiladitya, Mandakini, Raghav, Anirudha, Sourav, Samit, Hardik, Arun in no particular order. Finally my sincerest gratitude goes towards all the physicists and mathematicians before my time, on whose shoulders we are standing. Without their curiosity and perseverence, we would still be at the center of our solar system.

List of Papers

Chapters 2, 3, 4 and 5 of the dissertation comprise of work carried out for the following papers, respectively:

1. *Higgs Decays in Gauge Extensions of the Standard Model*, Phys.Rev. D89 (2014) 035014 , Don Bunk, Bithika Jain , and Jay Hubisz

2. *Spin-One Top Partner: Phenomenology*, JHEP 1408, 022 (2014), Jack H. Collins, Bithika Jain , Maxim Perelstein and Nicolas Rey-Le Lorier

3. *Heavy Gravitino and Split SUSY in the Light of BICEP2*, JHEP 1407, 073 (2014), JiJi Fan, Bithika Jain and Ogan Ozsoy

4. *Soft-Wall Light Dilatons*, Work in progress, Don Bunk, Bithika Jain , and Jay Hubisz

List of conventions and symbols

Throughout this dissertation, we have adopted the following conventions:

- Greek indices $\mu, \nu, \lambda, ...$ label the components of four-vectors and take values $0, 1, 2, 3$.

- Repeated indices are summed over.

- The metric has a $(+, -, -, -)$ signature unless stated otherwise

- We work in units such that $\hbar = c = 1$. This results in units where

  $$[\text{Mass}] = [\text{Energy}] = [\text{Momentum}] = [\text{Length}^{-1}] = [\text{Time}^{-1}].$$

- The σ^i are the Pauli matrices:

  $$\sigma^1 = \begin{pmatrix} 0 & 1 \\ 1 & 0 \end{pmatrix} \qquad \sigma^2 = \begin{pmatrix} 0 & -i \\ i & 0 \end{pmatrix} \qquad \sigma^3 = \begin{pmatrix} 1 & 0 \\ 0 & -1 \end{pmatrix}$$

- We further define $\sigma^\mu \equiv (\mathbb{1}, \sigma)$ and $\bar{\sigma}^\mu \equiv (\mathbb{1}, -\sigma)$.

- The Dirac matrices are

  $$\gamma^\mu = \begin{pmatrix} 0 & \sigma^\mu \\ \bar{\sigma}^\mu & 0 \end{pmatrix}$$

- We employ the Feynman slash notation $\not{p} \equiv \gamma^\mu p_\mu$.

- We can use the Dirac matrices as a basis for 4×4 matrices Γ_A which consist of:

$$
\begin{array}{ll}
1 & \text{one of these} \\
\gamma^\mu & \text{four of these} \\
\gamma^{\mu\nu} = \gamma^{[\mu}\gamma^{\nu]} \equiv -i\sigma^{\mu\nu} & \text{six of these} \\
\gamma^{\mu\nu\rho} = \gamma^{[\mu}\gamma^\nu\gamma^{\rho]} & \text{four of these} \\
\gamma^{\mu\nu\rho\sigma} = \gamma^{[\mu}\gamma^\nu\gamma^\rho\gamma^{\sigma]} & \text{one of these}
\end{array}
$$

- Latin indices $a, b, c, ...$ label the components of tensors with respect to an arbitrary orthonormal basis and take values $0, 1, 2, 3$.

- The Riemann tensor is defined as $R^\lambda_{\mu\sigma\nu} \equiv \partial_\sigma \Gamma^\lambda_{\mu\nu} - \partial_\nu \Gamma^\lambda_{\mu\sigma} + \Gamma^\lambda_{\sigma\rho} \Gamma^\rho_{\mu\nu} - \Gamma^\lambda_{\nu\rho} \Gamma^\rho_{\mu\sigma}$.

- The Ricci tensor is defined as $R_{\mu\nu} \equiv R^\lambda_{\mu\lambda\nu}$.

- The energy momentum tensor $T_{\mu\nu}$ is related to the matter action S_m by $T_{\mu\nu} = -\frac{2}{\sqrt{-g}} \frac{\delta S_m}{\delta g^{\mu\nu}}$.

Throughout this dissertation, we have used the following abbreviations:

- AdS: Anti-de Sitter

- AdS-S: Anti-de Sitter-Schwarzschild

- BSM: Beyond the Standard Model

- CC: Cosmological Constant

- CPT: Charge-Parity-Time

- CKM: Cabibbo-Kobayashi-Maskawa

- CMB: Cosmic Microwave Background

- CFT: Conformal field theory

- DOF: Degrees of Freedom

- DM: Dark matter

- EFT: Effective Field Theory

- EM: Electromagnetic

- EWSB: Electroweak symmetry breaking

- ETC: Extened Technicolor

- FRW: Friedmann-Robertson-Walker

- GR: General Relativity

- KK: Kaluza-Klein

- NDA: Naive Dimensional Analysis

- PMNS: Pontecorvo-Maki-Nakagawa-Sakata

- PNGB: Pseudo-Nambu-Goldstone Boson

- QED: Quantum Electrodynamics

- QCD: Quantum Chromodynamics

- QFT: Quatum field theory

- RG: Renormalization Group

- RS: Randall Sundrum

- SBSI: Spontaneous breaking of scale invariance

- SM: Standard Model

- SMPP: Standard Model of Particle Physics

- SUSY: Supersymmetry

- TC: Technicolor

- vev: vacuum expectation value

Contents

List of Figures

List of Tables

Chapter 1

Introduction

1.1 The Two Standard Models

Over the last 50 years, through the heroic efforts of experimental and theoretical physicists, two large branches of physics have each made a historic transition. A very successful attempt has been made to (1) understand the laws governing the whole physics reality down to the smallest imaginable scales and (2) to find a quantitative description of the properties of the entire Universe on the largest scales. As the Universe is known to be expanding and cooling, these two quests became linked in the earliest epochs, and hence particle physics and cosmology are necessarily connected. The connection between these two fields is nicely illustrated by the cosmic uroboros 1.1.

Today, benefiting from the huge technological developments during the last century, gigantic underground accelerators and spacecrafts probe everyday these two extreme realizations of physics. So what is more precisely the situation of particle physics and cosmology? At the end of the last century both fields were mature enough to give birth to Standard Models. Both only need a few free parameters to explain the huge wealth of data even if most of these parameters could not be explained yet in terms of a "fundamental theory". But what is new is that these models enable to

deduce consequence of particle physics in cosmology and vice verse, one of the most outstanding result of modern science. The past five years have a been very exciting period for particle physics. The LHC has been working very well. We now have plenty of physics results and the major discovery of the much awaited Higgs boson. LHC has already entered the second phase of its explorations as it has now ramped up the energy of the proton collisions to 13 TeV. Some of the open questions beyond the Standard Model of particle physics are: [1]:

- What is the nature of the Higgs boson and electroweak symmetry breaking?

- Why are there three generations of quarks and leptons? Are quarks and leptons really fundamental, or are they in turn made up of even more fundamental particles?

- What is the nature of neutrinos? [2]

- How to fit in gravity?

- What is the nature of the astrophysical dark matter?

- What is the origin of the difference between matter and antimatter, and is it related to the origin of the matter in the Universe?

As confirmed by the latest Planck results, cosmology provides three fundamental questions about todays universe [6]:

- What is dark energy?

- What is dark matter?

---

[1]This is, by no means a complete list of unanswered questions.

[2]First sign of the existence of BSM physics. We have many unknowns here -Are neutrinos Majorana or Dirac fermions? What is the absolute mass scale of neutrinos and what is their hierarchy (normal or inverted)? What are the precise values of PMNS matrix elements, and especially the CP violation phase? And finally are there sterile neutrinos, i.e. neutrino interacting only with the Higgs and other lepton doublets but not W or Z?

- Why is there matter and not antimatter?

- How do we explain cosmic inflation?

May be part (or all) of these questions can be resolved by particle physics.

In the rest of this chapter we first present the relevant details of the standard models for particle physics and cosmology. We then focus on the problems associated with both the standard models. Later we discuss beyond standard model (BSM) scenarios with special focus on Higgs Physics, Hierarchy Problem, Dark matter and models based on conformal dynamics. Finally, we summarize and present a more detailed outline of the rest of the dissertation.

1.1.1 Standard Model of Particle Physics

The standard model (SM) of elementary particle physics is a non-abelian gauge field theory [7, 8] of microscopic interactions [9, 10] based on the symmetry group $SU(3)_C \otimes SU(2)_L \otimes U(1)_Y$. It was officially announced by J. Ilioupolus at the ICHEP conference in London in July 1974. Since then, the SM has been beautifully confirmed by all experiments. All new particles discovered fit perfectly in it's framework. The language of the SM of particle physics is that of a relativistic quantum field theory (QFT), which is a consistent framework that incorporates both special relativity and quantum mechanics.

The Lagrangian of the SM is made up of four differents parts named after illustrious scientists:

$$\mathcal{L}_{SM} = \mathcal{L}_{YM} + \mathcal{L}_{WD} + \mathcal{L}_{Yu} + \mathcal{L}_{H} \tag{1.1}$$

The first is the Yang-Mills part [8], $\mathcal{L}_{YM}$, which describes the low energy gauge groups of the SM, $SU(3)$ for color (C) [11–13], $SU(2)$ for weak isospin (T_3), and $U(1)$ for hypercharge Y [3]. The second part of the Lagrangian, is the Weyl-Dirac part

---

[3]$SU(2)_L \otimes U(1)_Y$ describes the electroweak (EW) interactions where the weak hypercharge Y is the U(1) generator and is linked to the electric charge(Q) and weak isospin (T_3) by $Y = (Q - T_3)$.
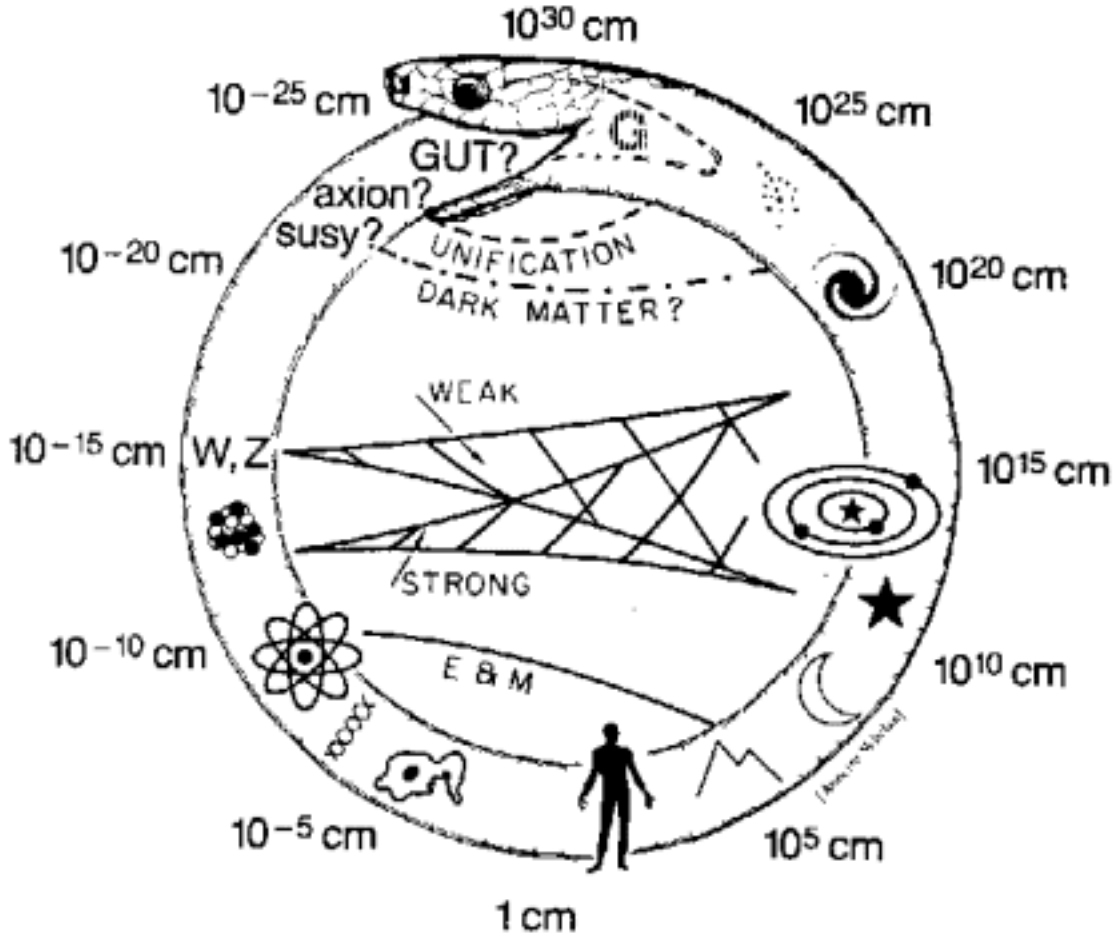
Figure 1.1: The Cosmic Uroboros represents the universe as a continuity of vastly different size scales, of which the largest and smallest may be linked by gravity. Sixty orders of magnitude separate the very smallest from the very largest. Traveling around the serpent from head to tail, we move from the scale of the cosmic horizon to that of a galaxy supercluster, a single galaxy, the solar system, the sun, the moon, a mountain, a human, a single-celled creature, a strand of DNA, an atom, a nucleus, the scale of the weak interactions, and approaching the tail the extremely small size scales on which physicists hope to find evidence for Supersymmetry (SUSY), dark matter particles such as the axion, and a Grand Unified Theory. There are other connections between large and small: electromagnetic forces are most important from the scale of atoms to that of mountains; strong and weak forces govern both atomic nuclei and stars; cosmic inflation may have created the large-scale of the universe out of quantum-scale fluctuations [1].

describing the fermion fields and their gauge interactions. The fermions can be split in two categories, (i) quarks which are triplets under the color gauge groups, and (ii) leptons which have no color. Within each category some transform as weak doublets, some as weak singlets. The partial Lagrangian $\mathcal{L}_{YM} + \mathcal{L}_{WD}$ exhibits large global symmetries. Each types of fermions, have a global $U(3)$ transformation symmetry. However, most of it is explicitly broken by the third part, Yukawa interactions [14], by which fermion pairs interact with spinless particles. The global symmetries of $\mathcal{L}_{YM} + \mathcal{L}_{WD}$ simplify the Yukawa couplings. The 3×3 matrices of Yukawa couplings are neither real nor diagonal, they are called the Cabibbo-Kobayashi-Maskawa (CKM) [15, 16] and Pontecorvo-Maki-Nakagawa-Sakata (PMNS) [17–20] for quarks and leptons respectively. Note that to generate masses for charged fermions we have already introduced a spinless boson Higgs field, H [4], which transforms as a weak doublet, color singlet and has a hypercharge as well, $(\mathbf{1}, \mathbf{2}, \frac{1}{2})$. The fourth and the final part of the SM is the Lagrangian which describes the Higgs Doublet, itsinteractions with the gauge fields and with itself [21–26]

$$\mathcal{L}_H = (D_\mu \Phi)^\dagger (D^\mu \Phi) - V(\Phi), \tag{1.2}$$

where the potential can be written as:

$$V(\Phi) = -\mu^2 \Phi^\dagger \Phi + \lambda \left(\Phi^\dagger \Phi\right)^2 \tag{1.3}$$

Assuming the dimensionful parameter to be positive ($\mu^2 > 0$), the scalar field acquires a non-trivial vacuum expectation value (vev) $\langle \Phi \rangle = v > 0$, which in turn breaks the electroweak symmetry via the symmetry breaking pattern,

$$SU(2)_L \times U(1)_Y \to U(1)_{em}$$

---

[4]Mass terms for fermions and gauge bosons are forbidden by the gauge principle

4 EW sector:	α_{em}		m_Z	v	m_H
2 Strong sector:	α_s		Θ_{QCD}		
12 Fermionic :	λ_i where $i = u, d, b, t, c, s, e, \mu, \tau$				
4 CKM:	$\theta_{12}, \theta_{23}, \theta_{13}$		δ_{13}		
6 PMNS:	$\theta_{12}, \theta_{23}, \theta_{13}$		δ_{13}	$\alpha_{1,2}$	
28 total parameters					

Table 1.1: The 28 parameters of SM of particle physics.

. This electroweak symmetry breaking (EWSB) gives masses to the matter and gauge fields. To see this, we expand the Higgs doublet around this minimum via

$$\Phi(x) = \frac{1}{\sqrt{2}} \begin{pmatrix} -i\sqrt{2}\varphi^+(x) \\ v + h(x) + i\varphi^3(x) \end{pmatrix} \tag{1.4}$$

[5] where the scalars $\varphi^\pm$ and φ^3 represent the three Goldstone bosons associated with the symmetry breaking in question. They can be identified with the longitudinal degrees of freedom of the massive $W^\pm$ and Z bosons. The scalar, h denotes the physical Higgs boson, which is necessary to unitarize WW scattering[6]. The kinetic term of the Higgs gives rise to masses for the gauge bosons. The physical Higgs boson,h also acquires a mass after EWSB. The radiative corrections to this mass are the origin of the gauge hierarchy problem, which will be discussed extensively in the next subsection. The fermion masses are generated by means of the Yukawa interactions.

We can now enumerate the free parameters of SM, which have been tabulated in Table. 1.1. In the gauge sector, the electroweak part needs 4 parameters i.e the electromagnetic (EM) fine structure constant α, the mass of the Z boson, m_Z, the Higgs vacuum expectation value, v, and the Higgs mass m_H, then the strong sector

---

[5]$\Phi(x) = \frac{1}{\sqrt{2}} \begin{pmatrix} 0 \\ v \end{pmatrix}$ is the vacuum state in this parameterization.

[6]In fact, the physical Higgs particle,h is not required for the generation of the gauge boson masses, which could also be implemented by means of a general non-linear sigma model, as explained in e.g [27]

has 2 parameters , α_s - the strong coupling constant and a strong CP phase, Θ_{QCD} [7]. In the fermion sector [28, 29], Yukawa couplings give 12 real free parameters corresponding to the fermion masses. CKM (quark-mixing matrix) and PMNS (lepton mixing matrix) matrices can be parametrized by 3 angles and 1 CP violating phase each. If we assume that the neutrino is of Majorana type, 2 other parameters, $\alpha_{1,2}$ are necessary for the PMNS matrix giving a total of 10 parameters for fermion mixing matrices. Thus, we have 28 parameters, which are unrelated at least within the context of the theory. It should be noted that the number of parameters within the SM varies slightly among phenomenologists depending on precisely how minimal the model under consideration is and in particular how the neutrinos are treated [8].

The SM has several *exact* and *approximate* symmetries. We have already mentioned the local gauge symmetry, $SU(3)_C \otimes SU(2)_L \otimes U(1)_Y$. In the absence of fermion masses, the Weyl-Dirac (matter) Lagrangian has an accidental [9] global symmetry,

$$Q_L^i \to U_{Q_L}^{ij} Q_L^j$$
$$u_R^i \to U_{u_R}^{ij} u_R^j$$
$$d_R^i \to U_{d_R}^{ij} d_R^j$$
$$L_L^i \to U_{L_L}^{ij} L_L^j$$
$$e_R^i \to U_{e_R}^{ij} e_R^j \tag{1.5}$$

Owing to five independent $U(3)$ symmetries, the global flavor symmetry of the matter Lagrangian is $[U(3)]^5$. As we have already mentioned, these global flavor symmetries are violated by the Yukawa couplings of the fermions to the Higgs field. Only a very small subgroup of $[U(3)]^5$ is not violated, corresponding to the baryon and lepton number. Thus baryon number and lepton number are *accidental global symmetries* of the SM. When the Higgs field acquires a vev, it is seen that, baryon number and

---

[7]This parameter arises from the quantum effects which describe the QCD vacuum

[8]Originally, the neutrinos were assumed to be massless and the PMNS matrix diagonal.

[9]A symmetry shared only by a part of the Lagrangian is called an accidental symmetry.

lepton number are anomalous, but $B - L$ is not [30]. This disallows a Majorana mass term for neutrino. Neutrino mass is definitely physics beyond the standard model [31].

The Higgs potential in invariant under $SO(4)$, which acts on the real components of the complex doublet of the Higgs field. As $SO(4) \sim SU(2L) \times SU(2R)$, the four vector, made up of four real components of the Higgs, transform as a **(2,2)**. The first $SU(2L)$ is the weak gauged isospin. The diagonal sum of these two SU(2)s, is known as the *custodial symmetry* [32–34]. It is broken both by the Yukawa couplings, and by the couplings to hypercharge.

SM also exhibits some *discrete symmetries* [35]. Locality and reality of the Lagrangian implies that the SM is invariant under the combined operation of CPT. The chiral character of weak isospin breaks parity. SM explicitly breaks CP as the three family CKM matrix can accommodate only one complex phase.

Though this is a very brief overview of the SM, it is certainly evident that the theory has far too much arbitrariness to be the final story. For instance, the finite number of parameters seem to be unrelated. The hope is to have a more complete theory which will explain the relationships between these parameters. The complications of the SM can also be described in terms of a number of problems. However, before we discuss them, it would be useful to look at the standard model of cosmology.

1.1.2 Standard Model of Cosmology

The Standard model of Cosmology (SMC) is based on ideas as old as the SM of particle physics. Determining the precise date when the SMC was in place is a little murky (to say the least). The Modern cosmology is well described by the standard "ΛCDM" Big bang model. This model is an application of general relativity (GR) to the entire universe.

The model is based on the Friedmann-Lemaître-Robertson-Walker Cosmology [36–42] It assumes that the universe is spatially isotropic and homogeneous which leads

us to the Robertson-Walker metric (kinematics). This is given by,

$$ds^2 = -dt^2 + a^2(t) \left[\frac{dr^2}{1 - kr^2} + r^2(d\theta^2 + sin^2\theta d\phi^2) \right], \quad (1.6)$$

where $a(t)$ is the scale factor and geometrically, k describes the curvature of the spatial sections. Here, t is the cosmic time, which is the proper time as measured by a comoving observer (one at constant spatial coordinates). To simplify calculations often, τ, the conformal time is used. Then the metric reduces to, $ds^2 = a(\tau)^2 \left[-d\tau^2 + \frac{dr^2}{1-kr^2} + r^2(d\theta^2 + sin^2\theta d\phi^2) \right].$ [10].

The dynamics is contained in differential equations governing the evolution of the scale factor. These come when we assume a simplified description for the cosmological matter, that it behaves like a perfect fluid. Einstein equations when applied to cosmology, yield the Friedmann equations

$$H^2 \equiv \left(\frac{\dot{a}}{a}\right)^2 = \frac{8\pi G}{3} \sum_i \rho_i - \frac{k}{a^2}$$

$$\frac{\ddot{a}}{a} + \frac{1}{2} \left(\frac{\dot{a}}{a}\right)^2 = -4\pi G \sum_i p_i - \frac{k}{2a^2} \quad (1.7)$$

where an overdot denotes a derivative with respect to cosmic time t and i indexes all different possible types of energy in the universe. H is the *Hubble parameter* (sometimes called the Hubble constant [43]), given by $H = \dot{a}/a$. These equations relates the rate of increase of the scale factor, as encoded by the Hubble parameter, to the total energy density of all matter in the universe.

Energy conservation equation tells us that the expansion of the universe (as specified by H) can lead to local changes in the energy density. Lastly, within the fluid approximation and with the assumption that the pressure is a single valued function of the energy density, we can define an equation of state parameter, w by $p \equiv \rho$.

---

[10]$k = +1$ corresponds to positively curved spatial sections, ; $k = 0$ corresponds to local flatness, and $k = 1$ corresponds to negatively curved spatial sections

It should be noted that, $w = 0$ corresponds to pressureless matter, or dust—any collection of massive non-relativistic particles would qualify. Similarly, $w = 1/3$ corresponds to a gas of radiation, whether it be actual photons or other highly relativistic species. For cosmological constant, $w = -1$, which implies that the energy density is constant. Thus, this energy is constant throughout spacetime; we expect that the cosmological constant is related to the *vacuum energy*. From observations, we know that the dominant component of energy density in the present universe is neither dust nor radiation, but rather is "dark energy" which may be a vacuum energy (cosmological constant), a dynamical field, or something even more dramatic. This component is characterized by an equation of state parameter $w \sim -1$. Note that the matter- and radiation-dominated flat universes begin with $a = 0$; this is a singularity, known as the Big Bang.

Measurements of matter density and specifically of the ordinary baryonic matter indicates that most of the matter density must therefore be in the form of non-baryonic dark matter, which we will abbreviate to simply "dark matter" (DM) [44–49] Every known particle in the SM of particle physics has been ruled out as a candidate for this DM. We know that DM has been non-relativistic for a long time (cold) and weakly interacts with ordinary matter. Moreover, the supernova studies have provided direct evidence for a nonzero value for Einstein's cosmological constant. This indicates that the universe has an accelerating expansion. Moreover, the universe implied by combining the supernova results with direct determinations of the matter density is spectacularly confirmed by measurements of the cosmic microwave background (CMB). CMB is an almost isotropic blackbody spectrum, with temperature approximately, $T_0 = 2.7K$ and thus contributed to radiation. Therefore, the early universe was dominated by radiation. At early times the CMB photons were energetic enough to ionize hydrogen atoms and therefore the universe was filled with a charged plasma (and hence was opaque). This phase lasted until the photons redshifted enough to allow protons and electrons to combine, during the era of re-

combination. Shortly after this time, the photons decoupled from the now-neutral plasma and free-streamed through the universe.

Our premier precision observational tools indicate that the CMB [50, 51] is not a perfectly isotropic radiation bath. CMB anisotropies [11] are widely recognized as one of the most powerful probes of cosmology and early-Universe physics. Given a set of initial conditions and assumptions concerning the background cosmology, the angular power spectrum of the CMB anisotropies can be computed numerically to high precision using linear perturbation theory [52]. The combination of precise experimental measurements and accurate theoretical predictions can be used to set tight constraints on cosmological parameters.

However, at the time of their decoupling, different photons were released from regions of space with slightly different gravitational potentials. Since photons redshift as they climb out of gravitational potentials, photons from some regions redshift slightly more than those from other regions, giving rise to a small temperature anisotropy in the CMB observed today. On smaller scales, the evolution of the plasma has led to intrinsic differences in the temperature from point to point. In this sense the CMB carries with it a fingerprint of the initial conditions that ultimately gave rise to structure in the universe. Careful analysis of all of the features of the CMB power spectrum (the positions and heights of each peak and trough) provide constraints on essentially all of the cosmological parameters.

At temperatures below 1 MeV, the weak interactions are frozen out and neutrons and protons cease to interconvert. The neutrons have a lifetime which is slightly larger that the age of the universe in this epoch and they begin to gradually decay into protons and leptons. Soon thereafter, however, we reach a temperature somewhat below 100 keV, and Big-Bang nucleosynthesis (BBN) begins [53]. At that point the neutron/proton ratio is approximately 1/7. Of all the light nuclei, it is energetically favorable for the nucleons to reside in ^4He, for every two neutrons and fourteen

---

[11]Anisotropies in the CMB are treated as small fluctuations about a FRW metric whose evolution is described by GR.

1 temperature:	T_0			
1 timescale:	H_0			
4 densites:	Ω_Λ	Ω_{CDM}	Ω_B	Ω_ν
1 pressure:	$w \equiv p/\rho$			
1 mean free path:	τ_{reion}			
4 fluctuation descriptions:	A	n	$n' \equiv dn/dlnk$	$r \equiv T/S$
12 total parameters				

Table 1.2: The 12 Parameters of ΛCDM.

protons, we end up with one helium nucleus and twelve protons. Thus, about 25% of the baryons by mass are converted to helium. Nucleosynthesis also gives information about the baryon asymmetry in the universe.

This completes the standard cosmological model, also known as the ΛCDM model [54–56] The number of parameters required to describe this model varies to some extent depending on the tastes of individual cosmologists. However, a typical count gives the number of required parameters as 12, which are listed in Table 1.2 The ΛCDM model can be extended by adding cosmological inflation, quintessence and other elements that are current areas of speculation and research in cosmology.

1.2 Problems of the Standard Models

The two Standard Models are certainly distinct, since none of the parameters of the ΛCDM can be derived using the SM of particle physics (SMPP) for example, one needs to know at least the value of H_0 (and then the full SMPP would give Ω_ν) or the addition of T_0 and information about baryogenesis (to get Ω_B). It is also the case that very few of the SM parameters have much bearing on the ΛCDM, since only the physics of photons, protons, neutrons and electrons is of primary importance for physical cosmology, with the neutrino sector being less important, and the rest being largely irrelevant (except indirectly, through the relationship with higher energy physics beyond the SM). Because the sets of parameters are essentially disjoint, then

any fundamental answer to the question of 'Life, the Universe and Everything' will have to explain the parameters of both SMs.

Even though SMPP has achieved many impressive experimental successes it fails to provide an explanation to some experimental and theoretical issues. On the experimental side, neither the observed dark matter density can be explained (the SM lacking an appropriate natural candidate for it [57]) nor the baryon asymmetry of the Universe can be accounted for, mainly because the SM does not provide sizeable CP violation sources and a strong enough first-order electroweak phase transition [58]. Also, it gives no reason why the three gauge couplings of the Standard Model gauge group almost meet at a large unification scale, but not quite [59].

On the theoretical side there is no plausible explanation for the huge hierarchy between the electroweak scale, responsible for the mass of the weak gauge bosons, and the Planck scale, apparent in the weakness of gravitational interactions. As the only fundamental scalar particle in the Standard Model, the newly discovered Higgs boson causes peculiar problems in its perturbative field theory description. In the presence of a physical cut-off scale, its mass turns out to be extremely sensitive to quantum corrections. This means that we would expect such a scalar to acquire a mass close to the cut-off scale. On the other hand, electroweak symmetry breaking and the unitarity of WW scattering require the Higgs mass to stay sufficiently below the TeV scale. This tension is called the "gauge hierarchy problem" or "hierarchy problem". Moreover, in SM, the Yukawa couplings are inputs. They are experimentally found to be hierarchal, with values as low as $\sim 3 \times 10^{-6}$, and intrafamily mass ratios as large as 40. The anarchic flavor structure of the Standard Model needs an explanation (also known as the flavor hierarchy problem [60]). Clearly, the discussion of hierarchy problem indicates that SM should be treated as an effective field theory (EFT). Thus for an accurate description of nature at arbitrarily high energies we would need higher dimensional operators. With one important exception [12], none of the high energy

---

[12]It appears that neutrino data favors augmenting the SM by a unique dimension 5 operator, but this operator is suppressed by a superheavy mass scale.

experiments have observed clear evidence for any such higher dimension operators.

Another fine-tuning problem is the strong CP problem which is associated with the parameter θ_{QCD}. Once it was realized that $U(1)_A$ is not a symmetry of QCD and a non-abelian gauge symmetry explains the complicated nature of QCD's vacuum. This arises from the θ_{QCD} $g_s^2 G\widetilde{G}$ term in the QCD Lagrangian, which breaks P,T and CP symmetry. Gravity is also not fundamentally unified with the other interactions in the SM, and it is also not quantized. There is another difficulty, namely the cosmological constant (CC) problem. As, mentioned in the previous section, CC can be thought of as the energy of vacuum. There seems to be a link between the Higgs boson and the cosmological constant. Latest Planck results ($\Omega_{vac} \sim 0.7$) confirmed that acceleration is taking place at present. It is therefore tempting to identify the constant energy density of the vacuum ρ_{vac} to the EW vacuum. But, this gives $\rho_{vac} \sim -10^8 GeV^4$, highly incompatible with the cosmology measurements $\rho_{vac} = \Omega_{vac}\rho_{cri} \sim 10^{48} GeV^4$. This is the cosmological constant problem.

It is clear that SM of particle physics requires a number of new ingredients. Infact, the problems of elementary particle physics and cosmology have increasingly merged. The framework of ΛCDM is a towering achievement, describing to great accuracy the physical processes leading to the present day universe. However, there remain outstanding issues in cosmology. Many of these come under the heading of initial condition problems:the universe as we know it can only arise for very special and finely-tuned initial conditions. We need a more complete description of the sources of energy density in the universe. The most severe of these problems eventually led to a radical new picture of the physics of the early universe - *cosmological inflation*. The theory of inflation provides a solution to the horizon, flatness and "unwanted relics" problem. If the only matter in the universe is radiation and dust, then in order to have density parameter, Ω_{total} to be in the observed range today requires:

$$0 \leq 1 - \Omega \leq 10^{-60} \tag{1.8}$$

This remarkable degree of tuning is the flatness problem. The next problem stems from the existence of particle horizons. Horizons exist because there is only a finite amount of time since the Big Bang singularity, and thus only a finite distance that photons can travel within the age of the universe. The horizon problem is simply the fact that the CMB is isotropic to a high degree of precision, even though widely separated points on the last scattering surface are completely outside each others horizons. Certainly, the causal structure of ΛCDM needs to be modified. The symmetry between particles and antiparticles, firmly established in collider physics, naturally leads to the question of why the observed universe is composed almost entirely of matter with little or no primordial antimatter. There is strong cosmological evidence for dark energy and dark matter, but we have no explaination for their observed values.

Particle physics and cosmology are facing a particularly intriguing moment. Theoretically both are described by Standard Models with few parameters (triumph for Occams Razor) and extremely robust against precise experimental data. In particle physics, its been 40 years without BSM discovery, despite the huge number of models predicting new physics close to the EW scale now extensively probed by LHC. In cosmology, ΛCDM is still a good fit despite the reduction of allowed parameter space volume by 10^5 during the last 15 years. Experimental findings are even more tantalizing: the cosmological constant is very small but not 0 (1998), the SM Higgs exists at a mass of 125 GeV [61, 62] and is apparently fine-tuned (2013). Both are pointing away from naturalness, even if the latter is still fresh and needs the full LHC program to be really conclusive. Despite this quite unique situation for physics, the future should be paved by the understanding of current puzzles.

1.3 Beyond Standard Model

For past few decades, several extensions of Standard Model [13] have been proposed, which could solve some or all of the problems mentioned above in order to generalize the SM. In order to go beyond the SM we can follow several avenues.

1.3.1 Experiments

This is the traditional way of making progress in science. We need experiments to explore energies above the currently attainable scales and discover new particles and underlying principles that generalize the Standard Model. This avenue is presently important due to the current explorations of the Large Hadron Collider (LHC) at CERN, Geneva.

LHC

This experiment is exploring physics above the weak scale with a center of mass energy of up to 14 TeV. At the LHC, proton-proton collisions were recorded between spring 2010 and autumn 2012. The quantity of data recorded by general purpose experiments ATLAS and CMS are proportional to the integrated luminosity L, expressed in fb^{-1}, as the number N of events expected for a given process of crosssection σ is $N = L\sigma$. Cross-sections are expressed in pb ($10^{-36}cm^2$) or fb ($10^{-39}cm^2$) . LHC accumulated about $5fb^{-1}$ and $20fb^{-1}$ of data per experiment at a center of mass energy $\sqrt{s} = 7$ TeV and 8 TeV, respectively. These two data sets are referred to as 'LHC Run I'. Run 1 of the LHC has taken probes of the SM to a new level, not only by the discovery of the Higgs boson H (125) [63] and the absence of other new particles, but also via precision measurements in Electroweak (EW) and QCD sector. Run 2 of LHC began in May, 2015 when particles collided at $\sqrt{s} = 13$ TeV. It is to be expected that Run 2 of the LHC will provide important improvements in the sensitivity of LHC probes

---

[13]From henceforth, by Standard Model we mean the Standard Model of particle physics.

of possible dimension-6 operators. These improvements will come not only from the greater statistics, but also from the greater kinematic range that will strengthen the power of the associated Higgs production kinematics and the triple-gauge couplings constraints, in particular. At the moment we know that the SM is very effective: LHC Run 2 data will give us a better idea just how effective it is, and perhaps provide some pointers to the nature of the new physics that surely lies beyond it at higher energies.

Dark Matter Searches

There are several DM candidates: weakly interacting massive particles (WIMPs) [64–67], asymmetric DM [68–71], axions [72–75], right-handed or sterile neutrinos [76–78]. Alternatively, DM may be in a so-called hidden sector, which has its own set of matter particles and forces, through which the DM interacts with other currently unknown particles. It is assumed that all these candidates would have non-gravitational interactions through which they may be detected. DM may interact with one or more of the four catergories of particles:nuclear matter, leptons, photons and other bosons, and other dark particles. These interactions may then be probed by four complementary approaches: direct detection (XENON100, CREST II), indirect detection (HESS), particle colliders (LHC), and astrophysical probes (Planck). Astrophysical/cosmological datasets are rich, rapidly evolving, and hold several candidate dark matter signals. However, the discovery of a compelling dark matter signal is only the beginning. Complementary experiments are required to verify the initial discovery, to determine whether the particle makes up all of dark matter or only a portion, and to identify its essential properties, such as its interactions, spin, and mass, and to determine its role in forming the large scale structures of the Universe that we see today. A balanced dark matter program is required to carry out this research program to discover and study dark matter and to transform our understanding of the Universe on both the smallest and largest length scales.

Neutrinos

There are several experiments aimed at understanding the neutrino physics specifically neutrino masses, mixing (NovA, T2K, Kamiokande, DUNE, PINGU,JUNO, INO)

1.3.2 Add new particles and/or interactions.

This ad hoc technique is not well guided but it is possible to follow if by doing this we are addressing some of the questions mentioned before

1.3.3 More general symmetries.

Symmetries play a vital role in SM, it is then natural to use this as a guide and try to generalize it by adding more symmetries. These can be of the two types:

Internal Symmetries: GUTs

More general internal symmetries leads to consider *grand unified theories (GUTs)* in which the symmetries of the SM are themselves the result of the breaking of yet a larger symmetry group [79–82],

$$G \rightarrow SU(3)_C \otimes SU(2)_L \otimes U(1)_Y$$

The fundamental idea of GUTs is that at energies higher than a certain energy threshold, M_{GUT} the group symmetry is G and that, at lower energies, the symmetry is broken down to the SM gauge symmetry. This would occur by a chain of symmetry breakings. This reduces the number of parameters in the theory to just one gauge coupling. This would "run" at low energies and give rise to the three different couplings of the SM. These theories allow for baryon number violation. The baryon number violating interactions can also explain the baryon asymmetry in the universe.

Non-minimal (greater that SU_5) GUTs can easily predict nonzero neutrino masss $\sim 10^{-5} - 10^2$ eV, which can allow for observable neutrino oscillations. This proposal indeed is very elegant however the biggest problem is that these models require a great deal of fine tuning of the parameters. Lastly, GUTs do not include gravity[14].

Spacetime symmetries 1: SUSY

Supersymmetry (SUSY) is one of the most popular ways to reduce the large corrections to Higgs mass [15], it extends the symmetry structure of SM by a symmetry linking fermions and bosons [85]. A SUSY transformation turns a bosonic state into a fermionic state, and vice versa. The operator Q that generates such transformations is an anticommuting spinor, with

$$Q|\text{Boson}\rangle = |\text{Fermion}\rangle \qquad \text{and} \qquad Q|\text{Fermion}\rangle = |\text{Boson}\rangle$$

In an interacting QFT, the forms for such symmetries are restricted by the the Haag-Lopuszanski-Sohnius extension [85] of the Coleman-Mandula theorem [86].

1. **MSSM**

   In the lowest SUSY, we have only a minimal number of fermions and bosons in a multiplet - called supermultiplet (alternatively we can say that it has only one supersymmetric generator). While models with more than one supersymmetry generator are useful tools to study the structure of gauge theories, we will focus on the phenomenologically most interesting case of $\mathcal{N} = 1$ SUSY [87, 88], with $\mathcal{N}$ referring to the number of supersymmetries (the number of distinct copies of $Q, Q^\dagger$) [16]. The generalisation of SM to $\mathcal{N} = 1$ SUSY is remarkably

---

[14]A more thorough discussion of GUTs can be found in [83].

[15]For more details see [84]

[16]Models with more than one SUSY generator are called "Extended" SUSY. Extended SUSY in 4 dimensional(4D) field theories cannot allow for chiral fermions or parity violation as observed in the SM. So we will not discuss such possibilities further, although extended SUSY in higher-dimensional field theories might describe the real world if the extra dimensions are compactified in an appropriate way.

Names		spin 0	spin 1/2	$SU(3)_C$, $SU(2)_L$, $U(1)_Y$
squarks, quarks	Q	$(\widetilde{u}_L \ \widetilde{d}_L)$	$(u_L \ d_L)$	$(\,\mathbf{3}\,,\,\mathbf{2}\,,\,\frac{1}{6})$
($\times 3$ families)	$\overline{u}$	$\widetilde{u}_R^*$	$u_R^\dagger$	$(\,\overline{\mathbf{3}}\,,\,\mathbf{1}\,,\,-\frac{2}{3})$
	$\overline{d}$	$\widetilde{d}_R^*$	$d_R^\dagger$	$(\,\overline{\mathbf{3}}\,,\,\mathbf{1}\,,\,\frac{1}{3})$
sleptons, leptons	L	$(\widetilde{\nu} \ \widetilde{e}_L)$	$(\nu \ e_L)$	$(\,\mathbf{1}\,,\,\mathbf{2}\,,\,-\frac{1}{2})$
($\times 3$ families)	$\overline{e}$	$\widetilde{e}_R^*$	$e_R^\dagger$	$(\,\mathbf{1}\,,\,\mathbf{1}\,,\,1)$
Higgs, higgsinos	H_u	$(H_u^+ \ H_u^0)$	$(\widetilde{H}_u^+ \ \widetilde{H}_u^0)$	$(\,\mathbf{1}\,,\,\mathbf{2}\,,\,+\frac{1}{2})$
	H_d	$(H_d^0 \ H_d^-)$	$(\widetilde{H}_d^0 \ \widetilde{H}_d^-)$	$(\,\mathbf{1}\,,\,\mathbf{2}\,,\,-\frac{1}{2})$

Table 1.3: Chiral supermultiplets in the Minimal Supersymmetric Standard Model. The spin-0 fields are complex scalars, and the spin-1/2 fields are left-handed two-component Weyl fermions.

Names	spin 1/2	spin 1	$SU(3)_C$, $SU(2)_L$, $U(1)_Y$
gluino, gluon	$\widetilde{g}$	g	$(\,\mathbf{8}\,,\,\mathbf{1}\,,\,0)$
winos, W bosons	$\widetilde{W}^\pm \ \widetilde{W}^0$	$W^\pm \ W^0$	$(\,\mathbf{1}\,,\,\mathbf{3}\,,\,0)$
bino, B boson	$\widetilde{B}^0$	B^0	$(\,\mathbf{1}\,,\,\mathbf{1}\,,\,0)$

Table 1.4: Gauge supermultiplets in the Minimal Supersymmetric Standard Model.

easy, each of the known fundamental particles is therefore either in chiral or gauge supermultiplet, and must have a superpartner with spin differing by 1/2 unit. Quarks and leptons are taken to be the fermionic components of chiral multiplets, thereby adding to SM their spin-0 superpartners, the squarks and sleptons. The gauge bosons are spin-1 components of vector supermultiplets, introducing new spinors superpartners, the gluinos, the winos and the bino. The SM Higgs need to be replaced by 2 scalar Higgs bosons of opposite hyper-charge, both forming chiral supermultiplets, creating a vector-like pair of spinor doublets. The particle content of MSSM is summarized in Tables [1.3,1.4].

If SUSY was unbroken all sparticles would have same mass as their SM counterparts and we would have definitely observed them. Untill now, none of the

superpartners of SM have been discovered. A clear indication that SUSY is broken in the vacuum state chosen by nature. The gauge hierarchy problem of SM can be resolved by weak-scale SUSY. The bare mass of SM higgs receives large quantum corrections. For instance, a fermion f with yukawa coupling, λ_f, contributes to the Higgs mass as

$$m_h^2 \approx m_{h0}^2 - \frac{\lambda_f^2}{8\pi^2} N_c^f \int^\Lambda \frac{dp}{p^2} \approx m_{h0}^2 + \frac{\lambda_f^2}{8\pi^2} N_c^f \Lambda^2 \qquad (1.9)$$

where m_h is the physical Higgs boson mass, m_{h_0} is the bare Higgs mass and the remaining term is the $m_{h1-loop}^2$, the loop correction. N_c^f are the number of colors of fermion f, Λ is the largest energy scale for which SM is valid. If we assume that SM is valid upto $\Lambda \sim M_{Pl}$ and still the top quark has Yukawa coupling, $\lambda_t \simeq 1$, then the 1-loop contribution to the Higgs mass, $m_{h1-loop}^2 \sim 10^{30} m_h^2$, or we can say that there exists a fine-tuning of 1 part in 10^{30}.

SUSY moderates this fine-tuning. If SUSY was exact, the Higgs mass would receive no perturbative corrections. With SUSY breaking, Higgs mass is

$$m_h^2 \approx m_{h0}^2 + \frac{\lambda_f^2}{8\pi^2} N_c^f \left(m_{\widetilde{f}}^2 - m_f^2 \right) ln \left(\Lambda^2 / m_{\widetilde{f}}^2 \right) \qquad (1.10)$$

where $\widetilde{f}$ is spartner of fermion. The quadratic dependence on Λ is reduced to a logarithmic one, and even when $\Lambda \sim M_{Pl}$ and $m_{\widetilde{f}}$ is not too far above m_h, there would be at most 1% fine-tuning. The large value of top Yukawa in SM implies that stops (top-partners) would play a special role in canceling loops of SM tops. This basic idea has been explored in Chapter 3 in context of $spin-1$ top partners in SUSY.

MSSM improves the unification of the three gauge couplings and moves the gauge unification scale to values around $M_{GUT} \simeq 10^{16}$ GeV, large enough to avoid predicting unobserved proton decays [89–92]. It can provide a weakly interacting dark-matter candidate, and it might help explaining the matter-

antimatter asymmetry. The feature that makes it most relevant to LHC physics is that it predicts new fundamental particles at the TeV scale.

In the MSSM, supersymmetry breaking is simply introduced explicitly. This is because we parameterize our ignorance of the correct model for SUSY breaking by introducing extra terms. The SUSY breaking couplings should be soft (of positive mass dimension) in order to be able to naturally maintain a hierarchy between the electroweak scale and the Planck (or any other very large) mass scale. This means in particular that dimensionless supersymmetry-breaking couplings should be absent. The number of free parameters exceeds 100, which makes the MSSM scenario somewhat unpredictive. This parameter set includes complex gaugino masses and trilinear mixing parameters, which are strongly constrained by electric dipole moments, or a general flavour sector with 6×6 matrices for the squark masses, clearly not reflecting the observed flavour symmetries. For direct LHC searches with their given energy range and their limited precision, we can reduce this set to the LHC-relevant parameters, usually referred to as the phenomenological MSSM (pMSSM). Its specific assumptions are: no R-parity violation, no new sources of CP violation, mass degenerate first and second generation scalars, and no flavour-changing neutral currents. These assumed symmetry properties automatically avoid a large number of indirect constraints on the supersymmetric Lagrangian and allow for a dark-matter candidate. They leave us with 19 supersymmetric model parameters at the TeV scale.

SUSY introduces many new fields, in particular sfermions and thus many new sources of FCNC and CP violation. A generic extension has 44 CP violating terms [93]. This poses a severe problem and ways to control these sources have to be devised. There is a connection between the SUSY breaking terms and resolution of (s)fermion mass problem. There are many ideas but as yet no compelling models.

The effective cosmological constant, Λ_{eff} which arises if we set the bare cosmological constant to be zero but assume that there is non zero vaccuum energy: $\langle T_{\mu\nu} \rangle = \rho_{vac} g_{\mu\nu}$. So we have,

$$\Lambda_{eff} = 8\pi G_N \rho_{vac} \equiv \frac{\Lambda^4}{M_{Pl}^2} \tag{1.11}$$

Now, we would expect that ρ_{vac} receives non zero contribution from symmetry breaking: if SUSY breaking occurs around 1 TeV then $\Lambda \leq 10^{-30} M_{Pl} \sim 10^{-3} eV$. This is very unnatural fine tuning of parameters. Hence, the Cosmological Constant problem is not resolved in SUSY. Cosmology of a non-SUSY method which gives a more promising perspective on CC problem is explored in Chapter 5.

Finally, the first run of LHC has not detected any light SUSY partners yet, although the light Higgs mass would require that. Typical SUSY searches look for jets (and leptons) plus missing energy, where the missing energy stems from the LSP, which stands at the end of a chain of subsequent decays of supersymmetric particles. Assuming the SUSY partners to be approximately degenerate, the current measurements push the lower bound on squark and slepton masses to the several hundred GeV (depending on the specific scenario) [94] , i.e. right below the TeV scale, where NP should appear in order not to reintroduce a hierarchy problem. Therefore, todays point of view about SUSY is such that Higgsinos, stops, and the gluino should not be too far above the weak scale, while the rest of the SUSY spectrum, including the squarks of the first two generations, can be heavier and beyond the current LHC reach, see e.g. [95]. It will be interesting to observe whether (natural) SUSY will survive the second run of LHC.

2. **Split-SUSY** A major motivation for BSM physics has been to invent models which resolve the naturalness problem of the Higgs mass. As we have just seen above low-scale SUSY has a 30 decimal fine tuning. Developments in the

string theory in past decade suggest that there exists a "landscape" of long lived metastable vacua [96]. This can help in resolving the CC problem, if the SUSY breaking at higher scales is favored [97]. If we allow the approximate chiral symmetries protect the fermions of the supersymmetric SM down to the TeV scale, then sparticle spectrum would split in two (i) the scalars (squarks and sleptons) that get a mass at the high-scale of supersymmetry breaking $\widetilde{m}$, which can be as large as the GUT scale, and (ii) the fermions (gauginos and higgsinos) which remain near the electroweak scale and can account for both gauge-coupling unification and DM. The only light scalar in this theory is a finely-tuned Higgs. Such theories are called Split -SUSY [98–100]. They predict that gauginos and higgsinos would exist at TeV scale. The virtues of this approach include simplicity, automatic amelioration of SUSY flavor and CP problems, preservation of gauge coupling unification and the lightest neutralino being a dark matter (DM) candidate.

High-scale SUSY with a split spectrum has become increasingly interesting given the current experimental results. A supersymmetric scale above the weak scale could be naturally associated with a heavy unstable gravitino, whose decays populate the DM particles. In an anomaly mediation based mini-split scenario [101], the gravitino exists around the PeV scale and the lightest TeV scale neutralino (in particular, wino) is a component of DM. The constraints on these DM candidates are discussed in Chapter 4.

More general spacetime symmetries 2: Extra dimensions and other strongly coupled theories

1. **Strongly coupled theories**

   The discovery of a Higgs boson, which is so far very consistent with the SM, has greatly changed the landscape of allowed models of electroweak symmetry breaking (EWSB). The first to be excluded are Technicolor/Higgsless mod-

els [102–105]. [17]. Technicolor(TC) was created in the era in which the W and Z bosons were heavy and all known fermions comparatively light. In the first approximation, therefore, the fermions are massless and TC is essentially a pure QCD-like theory which naturally generates the weak scale, in analogy to the way the strong scale is generated by QCD through its running coupling constant. By itself, TC requires a new gauge group and additional fermions, i.e., techniquarks. TC is, however, an incomplete theory. Extended Technicolor (ETC) was introduced [107, 108] to accomodate light fermion masses, but even the charm quark begins to push the limits on ETC from rare decay processes. Hence, one is led to various schemes to accomodate heavier fermion masses, such as Walking Technicolor [109–112] and Multi-Scale Technicolor [113, 114]. After the discovery of the top quark in 90s [115, 116], dynamical models of EWSB evolved into Topcolor Assisted Technicolor, where a new Technidynamics can coexist and the top quark acquires a dynamical mass through Topcolor. However, a severe problem with TC theories is that they are higgsless theories, i.e. their spectrum does not contain a sharp scalar resonance such as the one discovered at the LHC. In walking TC theories, there is a candidate that could be narrow and even lighter than those from TC, but they are still heavier than the boson found at the LHC [117]. It is therefore reasonable to look for other versions of composite models which include a light scalar particle in the spectrum

We will now focus on models which allow for a natural electroweak symmetry breaking from strong dynamics at a scale f and the strong dynamics produces a light composite Higgs doublet. The possibility of composite Higgs was first considered by Georgi and Kaplan in the 80's, when they realised that the Higgs boson can be naturally lighter than other composite resonances if it emerges as a Pseudo Nambu-Goldstone(PNGB) [118, 119] boson of an enlarged global

---

[17]A very good review of the various models based on strong dynamics can be found in [106]

symmetry of the strong sector. In this context, the electroweak scale v is dynamically generated and can be smaller than the scale f, which distinguishes them from TC theories, where no such separation of scales exists, and which sets the scale of the heavy resonances of the strong sector. An important imprint of PNGB models and the generated Higgs potential is that the Higgs couplings are modified compared to the SM [18]. These deviations can be considerably large, thus these models are heavily constrained from electroweak precision tests [120–122]. There are stronger constraints from CP-violating and FCNC processes if the EWSB is communicated to fermions via the same mechanism as in ETC.

Although the gap between v and f can be explained, the former still suffers from radiative corrections. This is the motivation for the so-called collective symmetry breaking, which is realized in a class of models called little Higgs [123–126]. In these models, the global symmetry is larger than necessary to accommodate the four Goldstone bosons that can be identified with the scalar degrees of freedom of the Higgs. Since the electroweak gauge group is enlarged as well, there are additional gauge bosons which become heavy by eating the additional Goldstone bosons. If now either the SM gauge bosons or the additional bosons couple to the Higgs there is a leftover global symmetry, which ensures that the Higgs remains massless. If both couple to the Higgs, the latter acquires a mass, which is only logarithmically divergent, see [127] for further details.

To get a light Higgs naturally, a further variant of Composite Higgs scenario exists. In the scenario where Higgs is a PNGB, the Higgs field emerges as the PNGB of a global symmetry that is broken by strong dynamics [118, 128, 129]. Making the global symmetry approximate results in a potential for the Higgs field. In this way, a light SM like Higgs in the low energy theory can be arranged.

---

[18]Note that for $f \to \infty$ we recover the SM Higgs couplings, since the effects of the heavy resonances decouple.

This potential of the Higgs below the symmetry breaking scale is such that the Higgs acquires a VEV, like in the SM. Fluctuations about this VEV lead to a light Higgs particle in the spectrum. This consideration attains more plausibility in light of the recent discovery of a Higgs like particle at mass c lose to 125 GeV. This class of theories includes previously mentioned, little Higgs models [125, 130, 131] and twin Higgs models [132, 133]. If the dynamics above the scale at which the global symmetry is broken involves strong conformal dynamics, the flavor scale can again be separated from the electroweak scale, allowing new contributions to flavor violating processes to be small enough to satisfy the existing constraints.

BSM models with strong conformal dynamics in the UV can also provide a way to explain the fermion mass hierarchy of the SM. In the scenario referred to as the Partial Compositeness (PC) [134], the SM fermions do not constitute part of the conformal sector. However, they acquire a mass by mixing to the composites of the conformal sector. Depending on the dimension of the composite operator with which they mix, the resulting mass can be made to vary by several orders of magnitude [134]. This allows a simple explanation of the observed hierarchy in the fermion masses, making these class of models even more appealing.

We therefore see that conformal dynamics can play an important role in BSM models that try to address the hierarchy problem while remaining consistent with flavor constraints. If the conformal symmetry is broken spontaneously, the spectrum below the breaking scale contains the NGB, the dilaton. The form of the dilaton couplings is fixed by the requirement that conformal symmetry be realized nonlinearly. In the context of realistic BSM models, the theory at high energies has only an approximate conformal symmetry, which is spontaneously broken at low energies. This results in a mass for the dilaton in the low energy theory, and affects its couplings to other light states. It becomes important to understand the conditions under which the dilaton can be light,

27

and its couplings to the SM fields in these scenarios. This is because if the dilaton is light, it may be accessible at the present colliders, and would signal involvement of conformal dynamics in the real world. However, in these BSM models, conformal symmetry is expected to be explicitly broken by operators that grow in the infrared to become strong at the breaking scale. Therefore, at least naively, there is no reason to expect a light dilaton in the low energy effective theory. This explicit breaking could also significantly affect the predictions for the couplings of the dilaton in a spontaneously broken CFT. This has motivated several studies of the mass and couplings of the dilaton in realistic scenarios.

2. **Warped Extra-dimensions**

In the late 90's, the idea of composite Higgs re-emerged in the guise of warped extradimensional models [135–138]. Later it was realized that the pseudo-Goldstone idea with collective breaking can be easily realized in extra dimensional models, where the Higgs is identified with a component of the gauge field, giving rise to the holographic composite Higgs models [139, 140], building on earlier important work [141–148]. The generic features of these constructions have been condensed into a simple 4D effective description [149, 150]. These are all viable models of natural EWSB, where strong dynamics produces a light composite Higgs [19].

We will now discuss in detail the BSM models which involve Warped Extra dimensions. Around the time when AdS/CFT correspondence was conjectured, Randall and Sundrum proposed a mechanism to address the hierarchy problem using extra dimensions [135] . The class of BSM theories that incorporate this mechanism are studied under the name of Randall Sundrum (RS) models. Via the AdS/CFT correspondence, RS models are closely related to BSM theories

---

[19]A very good overview of composite Higgs models in light of the discovery of the Higgs boson can be found in [151] and references therein.
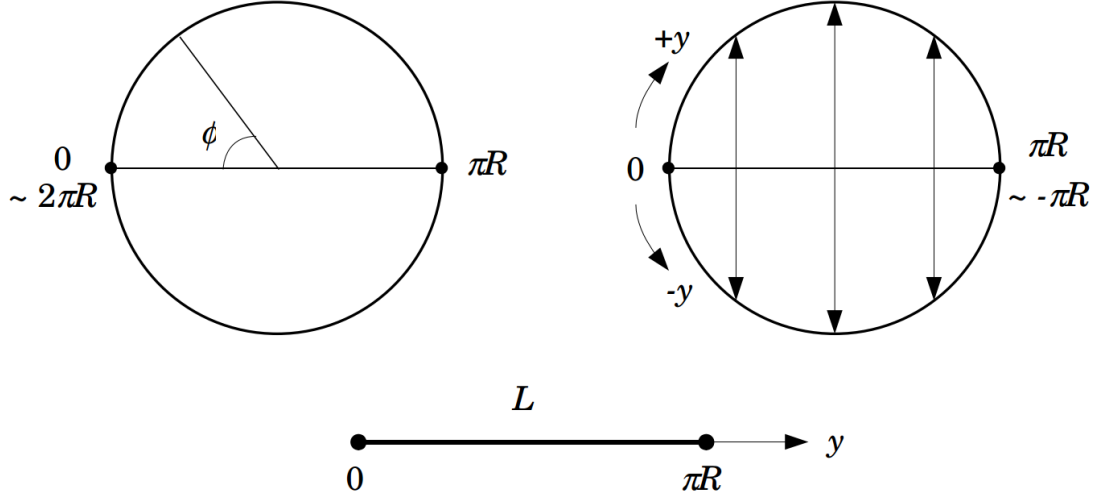
Figure 1.2: $S^1/\mathbb{Z}_2$ orbifold

based on conformal dynamics . In this section, we develop the basic setup of the RS models and elaborate some of its important features. In particular, we outline how they address the hierarchy problem in the SM. We then use the duality to relate to the corresponding features of BSM scenarios involving conformal dynamics that are dual to the RS models. In RS models, a slice of AdS space in 4+1 dimensions is considered. The metric in this space can be written as

$$ds^2 = e^{-2ky}\eta_{\mu\nu}dx^\mu dx^\nu - dy^2 \qquad (1.12)$$

where the extradimensional coordinate, y goes from y_0 to y_1. This finite extradimension is compatified on a circle whose upper and lower halves are identified (see Fig. 1.2). In the setup, the location, y_0 is identified with the hidden/ultraviolet (UV) and y_1 with the visible/infrared (IR) brane. The exponential factor e^{-ky} in 1.12 is called the warp factor of this geometry. Such a geometry can be obtained as a static solution of Einstein equations in the following way. Consider the 5D gravity action with a cosmological constant in the bulk and brane tensions on the two branes, expressed by the following bulk

action

$$S = \int d^5 x \sqrt{g} \left(-\frac{1}{2\kappa^2} \mathcal{R} - \Lambda \right) - \int d^4 x \sqrt{g_{ind0}} V_0(\phi) - \int d^4 x \sqrt{g_{ind1}} V_1(\phi). \quad (1.13)$$

Here $\kappa^{-2} \equiv 2M_*^3$, with M_* being the 5D planck scale, Λ is the bulk cosmological constant and V_0, V_1 are the brane tensions on the hidden and the visible branes respectively. $\sqrt{g_{ind(0,1)}}$ are the induced metrices, obtained from the full background metric $\sqrt{g}$. In order to solve the Einstein equations of motion for this set up, we find that

$$k = \sqrt{\frac{-\Lambda \kappa^2}{6}}, \quad V_{UV} = -V_{IR} = 6k/\kappa^2 \quad (1.14)$$

Note that there is no reason for this coincidence except for the stabilization for the set-up and the requirement for a flat brane metric. The situation is similar to the cosmological constant problem in the SM. The compactification radius is not set by this relation but once it takes on its value, the set-up remains stable. The radius itself is related to the 55-component of the metric tensor (with some gauge dependence) and can be fixed via a Goldberger-Wise mechanism [152], in which interaction with a bulk scalar induce a potential for this field, see [153] for details.

Given this static background geometry, the natural step is to consider the gravitational fluctuations about this background. To be able to use this geometrical construction for a real world scenario, we must be able to recover 4D gravity in the low energy limit. Consider small fluctuations about the full RS metric in 1.12. Without going into explicit details of the calculation, we outline the steps involved in getting the spectrum in the low energy. By expanding the 5D graviton as a linear combination of 4D fields, we can obtain all the fields present in the 4D theory. This expansion is generically called as Kaluza-Klein (KK) decomposition of a 5D field into 4D fields. Under this expansion, all the

4D fields get a profile in the extra dimension. The profile is a function of the extra dimension, and is the coefficient multiplying the corresponding 4D field in the KK decomposition.

Once the SM fields are included in a QFT based on this background geometry, this construction can serve as a BSM scenario that addresses the hierarchy problem. Such models are called as the RS models. In its earliest version, all the SM fields including the Higgs were considered localized on the IR brane. The later variants kept the Higgs localized on or towards the IR brane, but allowed the fermion and the gauge fields to propagate in the extra-dimension.

RS models allow us to reformulate the Cosmological Constant Problem. In these models there is an exact cancellation between the bulk and brane cosmological constants (double-fine tuning). A relevant question to ask is why should this occur? The Goldberger-Wise mechanism of radius stabilization offers a partial resolution of this problem. However, the requirement that the backreaction of the scalar field on the geometry remain small meant that only slight mistunes in the brane tensions could be accommodated. In the recent past some progress has been made aimed at resolving this issue [154–157].

RS models are closely related to BSM scenarios based on conformal dynamics, through the AdS/CFT duality. In this way, several important features of RS models can be understood from a dual point of view. Consider concretely the case of two brane RS models. In the AdS/CFT dictionary, the coordinate corresponding to the fifth dimension of AdS space is associated with the renormalization scale in the dual theory. Making a change of coordinates in AdS space from y to z, where z is defined as $z = e^{ky}/k$ the renormalization scale μ in the dual CFT is related to z as $\mu \sim 1/z$ [158]. RS models with two branes are therefore dual to a strongly coupled theory that is well approximated by a CFT in the energy regime between the two branes. The hidden brane corresponds to the UV cut-off of the theory. The visible brane corresponds to the scale where

the CFT is spontaneously broken [158]. The boundary conditions on the bulk fields at the UV brane determine the coefficients of the deformation (in the UV) of the CFT in the dual picture. The RS geometry contains a massless graviscalar mode in the low energy, the radion. This mode corresponds to the freedom to move the distance between the two branes, and is identified with the NGB of spontaneously broken conformal invariance, the dilaton, on the 4D side of the correspondence. The AdS geometry is stabilized by adding a Goldberger-Wise (GW) scalar ϕ to the theory. In the dual picture, this corresponds to deforming the CFT by a primary scalar operator $\mathcal{O}$. The boundary condition for ϕ on the UV brane is related to the strength of this deformation. Presence of ϕ that stabilizes the RS geometry generates a mass for the radion. Correspondingly, the deformation of CFT by $\mathcal{O}$ generates a mass for the dilaton.

In the RS scenario, the SM fields could be localized to the IR brane, or could propagate in the bulk. In the dual 4D theory, the brane localized fields correspond to composites of the conformal dynamics. The bulk fermionic fields in RS models correspond to elementary fields that mix with CFT operators of a given scaling dimension. The scaling dimension is related to the 5D mass parameter of the fermion in the AdS space. The gauge fields that propagate in the bulk correspond to global symmetries of the conformal dynamics that are weakly gauged. We see that AdS/CFT duality allows us to match BSM scenarios in RS models to those involving conformal dynamics.

1.4   Summary and Plan of the Dissertation

We are now faced with the "Lonely Higgs problem". The Higgs has been discovered but there is no direct or indirect sign of new physics. This has changed the landscape of allowed models of electroweak symmetry breaking a.k.a solutions to the hierarchy problem. To test their validity, precision Higgs phenomenology is of great interest;

especially for the upcoming 14 TeV LHC run. Complete characterization of Higgs production and decay and thus of the Higgs couplings is needed. Most extensions of the Standard model contain new spin-1 fields, like the Kaluza-Klein modes in extra-dimensional theories, same spin partners in Little Higgs models, spin-1 top partners in supersymmetric variants, or any extension of SM with exotic spin-1 fields coupling to the electroweak sector. Such gauge extensions of the Standard model are important as the dominant contribution to the diboson Higgs decays, $H \to \gamma\gamma$ and $H \to Z\gamma$, comes from the charged spin-1 states in the SM. The W boson can contribute differently to these channels in extensions of the Standard Model. Moreover, new spin 1 states appear which could modify Higgs decay rates and in certain cases also yield a non-zero tree level S parameter. In chapter 2 we will focus on a model independent study of the spin-1 contributions in gauge extensions of the Standard Model [159].

Top partners are a well motivated target for collider searches, as they can be crucial in cancellation of Standard Model loop contributions and need to be at or below the TeV scale to satisfy the naturalness criteria. The current lore has models with top partners of spin-0, when solutions to hierarchy problem are given by supersymmetry, or spin-1/2, when shift symmetry or higher dimensional gauge symmetry is used. Both these possibilities have been extensively covered by experimental searches. An alternate possibility, which has received far less attention is a spin-1 top partner (a.k.a. a "swan"). This was proposed by Cai, Cheng and Terning [160], in a supersymmetric model where the left handed top quark is identified with a gaugino of an extended gauge group and its superpartner is a spin-1 top partner . In Chapter 3, we will discuss the phenomenology of these spin 1 top partners.

The existence of non-luminous, cold Dark Matter (DM) is one of the most glaring pieces of evidence for Beyond the Standard Model physics. Competitive bounds from collider searches, direct detection and indirect detection have made the DM puzzle enticing. High-scale SUSY with a split spectrum has become increasingly interesting given the current experimental results. A supersymmetric scale above the weak scale

could be naturally associated with a heavy unstable gravitino, whose decays populate the DM particles. In an anomaly mediation based mini-split scenario, the gravitino exists around the PeV scale and the lightest TeV scale neutralino (in particular, the wino) is a component of DM. In Chapter 4 we will see how by using cosmic probes like indirect detection, and ensuring that DM relic abundance from gravitino decays does not overclose the universe, we can set upper bounds on the temperature at the outset of radiation domination (reheating temperature, T_R) [161].

The cosmological constant problem can be reformulated in the brane world models. In Chapter 5 we will discuss a soft-wall realization of the Randall Sundrum geometry where the infrared brane plays a lesser role as a cutoff for large curvature effects and low energy observables such as spectrum of states are largely insensitive to its position. We will explore the finite temperature behavior of such models by studying geometries which include a horizon or a black brane along the extra dimension in the presence of non-trivial scalar field vacuum expectation value. A first order geometric phase transition proceeds via bubble nucleation between the two different gravity solutions. In Chapter 6, we explore the effects of higher curvature terms on these Soft-Wall geometries.

Chapter 2

Higgs Decays in Gauge Extensions of the Standard Model

2.1 Introduction

The discovery of a higgs-like resonance at about 125 GeV [162, 163] that is so far consistent with expectations from the Standard Model (SM) [164–168], has altered the landscape of allowed models of electroweak symmetry breaking (EWSB). The absence of signals in other searches (i.e. for supersymmetry, and or new resonances) suggests the existence of a gap between the mass of this scalar and other new physics which may be responsible for maintaining the light mass of this scalar field. A current priority in experimental particle physics is an exhaustive study of this new resonance in terms of a more complete characterization of its production and decays.

Strong dynamics and/or extra dimensions may still play an important role in protecting the scale of electroweak mass generation from unacceptably large quantum corrections. The lightness of the higgs could be attributable to it being a pseudo-goldstone boson resulting from the spontaneous breakdown of a global symmetry [118, 119], or perhaps conformal invariance of an underlying strongly coupled theory [154, 155, 169–171]. It could also be due to geometric warping [135, 172]. In these cases,

the interactions of the light scalar field may be "higgs-like," although discrepancies relative to the SM predictions generically arise in such theories [149, 150, 173–177]. In such cases vector resonances often play an important role in the unitarization of scattering amplitudes of massive SM degrees of freedom [104, 105, 178–188], and have important phenomenological consequences [189, 190] Extra dimensional solutions to the hierarchy problem predict the existence of a tower of new states beyond those of the SM called Kaluza-Klein (KK) modes. In such constructions, the gauge bosons of the SM are expected in most models to have corresponding KK-mode partners that appear at energy scales above the inverse size of the extra dimension, along with towers of other spin-1 exotics that are often a key component of such models [139, 140].

An additional ingredient that may play a vital role in making such theories compatible with other low-energy observables is that of collective symmetry breaking, the mechanism underlying the success of little higgs theories in solving the hierarchy problem [123–126]. In these models additional global symmetries, and the particles that complete the SM spectrum into full multiplets of these groups, protect the higgs mass from one- or higher-loop order corrections. Additional spin-1 states - same spin partners of SM gauge bosons - play a vital role in the cancellation of quadratic divergences in the low-energy effective theory.

In general models of strongly interacting EWSB, including partial UV completions of many little higgs theories, there are also accompanying composite degrees of freedom, beyond those whose masses are protected by spontaneously broken symmetries. The spectrum of these resonances can be described as a consequence of the pattern of symmetry breaking that occurs below the scale of confinement in a strong sector. At a minimum, the strong sector must incorporate a custodial $SU(2)$ symmetry in order to protect against unacceptably large contributions to the T-parameter [33, 191]. In analogy with QCD, in which the lowest lying vector resonances fit into a representation of the surviving $SU(3)_V$ in the $SU(3)_L \times SU(3)_R \rightarrow SU(3)_V$ chiral symmetry breaking coset, strongly interacting EWSB is expected to at least con-

tain a multiplet of vector resonances fitting into $SU(2)_C$ multiplets resulting from a $SU(2)_L \times SU(2)_R \to SU(2)_C$ symmetry breaking pattern. The techniques of effective lagrangians and hidden local symmetry [192–200] are particularly convenient methods of parameterizing low energy effective theories that include such vector and/or axial vector resonances.

It is well-known that higgs production and decay rates can be a bellwether for new physics, especially in the light-higgs window, where numerous channels are available for study. The majority of higgs events arise from gluon fusion, a one-loop process strongly sensitive to exotic particles with QCD charge which obtain some significant portion of their mass from the higgs mechanism. In a similar fashion, higgs decays to the di-photon final state are highly sensitive to new particles with non-trivial electro-weak quantum numbers. In this vein, the hitherto unobserved higgs decay channel $H \to Z\gamma$ which also occurs only at one-loop order in the SM is another crucially important probe of physics beyond the standard model. Due to the fact that the rate for the clean final state $l^+l^-\gamma$ is rather small, the LHC limits are still weak [201], and the channel has been a focus of only limited theoretical study [202–206]. However, the LHC will soon be exploring the electroweak scale more thoroughly at a center of mass energy scale at or near 13 TeV. Of order 100 fb^{-1} of data are necessary to begin probing the rate expected in the SM, with this luminosity goal achievable in the next couple years of LHC data-taking.

Spin-1 states play a vital role in contributing to the $h \to Z\gamma(\gamma\gamma)$ channels [207, 208]. The dominant contribution to both amplitudes in the SM is from virtual W bosons running in loops, with virtual top quarks giving the next largest piece of the amplitudes. In extensions of the SM, the higgs-WW coupling is often modified, generating corrections to these amplitudes. Exotic spin-1 states also appear in numerous constructions (such as those described above) and should give contributions at one-loop as well. In this work, we study generic virtual spin-1 contributions to higgs decays, using the most general set of vector self-interaction terms consistent

with $U(1)_{\text{EM}}$ gauge invariance. We have calculated skeleton amplitudes that we have made available as Mathematica readable files for use by those wishing to calculate such amplitudes in their model of choice [209]. We exhibit the utility of these amplitudes in the context of an explicit moose construction with resonances that model vectors and axial vectors in strongly coupled extensions of the SM that preserve a custodial $SU(2)$ symmetry. The model, which is a modification of the construction detailed in [210] with the addition of a higgs-like resonance, exhibits the full range of possibilities for the couplings associated with vector self-interactions. Additionally, the model incorporates a dimension-6 operator with a coefficient whose value affects the S-parameter (which is typically large in models where strong dynamics plays a role in electroweak symmetry breaking [120–122, 211–213]).

The organization of this paper is as follows. In Section 2.2, we describe a framework for constructing gauge invariant low-energy effective theories that allow for modified higgs couplings to both SM and exotic spin-1 states, and also allow for a complete range of vector cubic and quartic self-interactions consistent with $U(1)_{\text{EM}}$. In Section 2.3, we describe the relevant Feynman rules in a generic framework, and outline our parameterization for the one-loop amplitudes. In Section 2.4, we construct an explicit model in which we derive the Feynman rules relevant for a calculation of the $h \to \gamma\gamma(Z\gamma)$ amplitudes. In Section 2.5, we explore the decay rates over the parameter space of the model, paying particular attention to correlations between the tree-level contribution to the S-parameter, the $h \to \gamma\gamma$ rate, and the $h \to Z\gamma$ rate as these are of especial interest in these types of effective theories [214, 215]. We conclude in Section 2.6. Mathematica files containing skeleton amplitudes (and couplings for our explicit calculation) that can be used in generic gauge extensions of the SM can be downloaded online [209].

2.2 General Vector Interactions

Diagonalization of the quadratic part of actions that arise in gauge extensions of the standard model often result in mixing of the SM vector fields with exotic ones. This mixing results in shifted gauge boson self interactions such that the W, Z, and higgs boson couplings differ from those of the SM. In addition, the light fields will also generically have direct couplings to heavy exotica. The higgs boson couplings to the gauge fields will also depend on how the observed scalar higgs is embedded into the complete mechanism of gauge symmetry breaking, including both electroweak breaking and the breaking of the extended gauge sector. In this section, we describe the classes of actions we consider, and we then characterize the most general self-interactions of the vector fields with each other and with the higgs, under the constraint that all interactions be gauge invariant.

2.2.1 The Quadratic Action

We consider a generic gauge group G with a kinetic term constructed from the usual gauge-invariant field strengths:

$$\mathcal{L}_{\text{kin}} = -\frac{1}{4}\text{Tr } V_{\mu\nu}V^{\mu\nu}. \tag{2.1}$$

The trace in this equation is over all generators of the UV gauge group, and at a minimum, this complete gauge group must contain the electroweak group $SU(2)_L \times U(1)_Y$, either trivially as a product structure, or embedded into a higher rank group.

To describe the breaking of this gauge group down to $U(1)_{\text{EM}}$, we construct a low energy effective theory in which complete gauge invariance is realized non-linearly in an effective field theory. The gauge symmetry breaking of the extended gauge sector can be parameterized by a set of Σ-fields whose vacuum expectation values determine the spectrum. The mass terms for the spin-1 fields arise from a sum over the kinetic

terms for these Σ-fields:

$$\mathcal{L}_{\mathrm{mass}} = \sum_l \frac{f_l^2}{4} \mathrm{Tr} \ |D_l^\mu \Sigma_l|^2. \tag{2.2}$$

Mass mixing between the gauge eigenstates arises from these kinetic terms when the sigma fields are expressed in terms of their vacuum expectation values $\Sigma_l \to \Sigma_l^0$. These vev's are taken such that the desired breaking pattern $G \to U(1)_{\mathrm{EM}}$ is obtained.

In the spirit of low energy effective theory, we should consider terms involving additional insertions of the Σ fields that may contribute to the low energy effective action. Such operators are non-renormalizable, and should be thought of as the product of having integrated out some UV dynamics, which may be either strongly or weakly coupled. The most phenomenologically interesting class of operators from the standpoint of electroweak precision or contributions to higgs decay phenomenology is the addition of wave function mixing operators:

$$\mathcal{L}_{\mathrm{WF}} = \epsilon_{ij} \mathrm{Tr} \ V_{\mu\nu}^i \Sigma_{ij} V^{j\mu\nu} \Sigma_{ij}^\dagger. \tag{2.3}$$

Such operators are closely analogous with the operator that corresponds to integrating out UV dynamics which contributes to the oblique S-parameter:

$$\mathcal{O}_S = \frac{1}{\Lambda^2} H \tau^a H^T W_{\mu\nu}^a B^{\mu\nu}. \tag{2.4}$$

In fact such operators, with properly chosen coefficients, can contribute to a reduction in the severity of electroweak precision constraints in models of vector and axial-vector resonances such as those that appear in extra dimensional models of electroweak symmetry breaking, in strongly coupled UV completions of little higgs models, and generically in various $L - R$ symmetric variants of gauge extensions of the SM. We further discuss the correlations between electroweak precision observables and the higgs decay rates in Section 2.5.

2.2.2 Vector boson self-interactions

The most general set of 3-point interactions involving two charged vectors with a neutral one (here displaying only the γ or the Z), that are consistent with conservation of electric charge, are given by:

$$\mathcal{L}_3 = -i \sum_{X,Y} g_\gamma^{X,Y} X_\mu^+ Y_\nu^- A^{\mu\nu} + g_Z^{X,Y} X_\mu^+ Y_\mu^- Z^{\mu\nu} + G_Z^{X,Y} \left(X_{\mu\nu}^+ Y^{-\mu} - X_{\mu\nu}^- Y^{+\mu} \right) Z^\nu$$
$$+ e \left(X^{+\mu\nu} X_\nu^- - X^{-\mu\nu} X_\nu^+ \right) A_\mu \tag{2.5}$$

where X and Y are vector fields. These may be either SM $W^\pm$ bosons, or exotic vector resonances. The first three of these terms clearly transform trivially under electromagnetic gauge transformations, while the 4th manifests gauge invariance only after considering transformations of the quartic interactions. $\mathcal{L}_3$ thus contains interactions of the SM gauge fields with each other with possibly modified coupling values and interactions of exotic charged states with the photon and Z. While the last coupling is fixed by gauge invariance, the others are free parameters up to inter-relations arising from the need to preserve full gauge invariance of the complete UV gauge structure giving rise to these interactions.

Similarly, the 4 point interactions take the form[1]

$$\mathcal{L}_4 = -\sum_{X,Y} A_\mu Z_\nu X_\rho^+ Y_\sigma^- \left(2a_{\gamma Z}^{XY} g^{\mu\nu} g^{\rho\sigma} - b_{\gamma Z}^{XY} g^{\mu\rho} g^{\nu\sigma} - c_{\gamma Z}^{XY} g^{\mu\sigma} g^{\rho\nu} \right)$$
$$-\sum_X e^2 A_\mu A_\nu X_\rho^+ X_\sigma^- \left(2g^{\mu\nu} g^{\rho\sigma} - g^{\mu\rho} g^{\nu\sigma} - g^{\mu\sigma} g^{\rho\nu} \right). \tag{2.6}$$

For the mixed γZ coupling, the coefficients are determined by the requirement of overall gauge invariance of the full theory. Electromagnetic gauge invariance forces the $\gamma\gamma$ quartic couplings to be equal to the square of the electromagnetic coupling constant.

---

[1] Up to interactions with more than two derivatives such as $\frac{1}{\Lambda^4} F^4$ non-renormalizable operators, where F is the field strength corresponding to the spin-1 fields in the effective theory.

2.2.3 Higgs interactions

For the purposes of this paper, we maintain a semi-model independent attitude regarding the origin of the observed higgs-like scalar field. We take an effective field theory approach, assuming the higgs is a CP even singlet under electromagnetism, and we allow its couplings to the various vector fields to be free parameters. Inspired by the higgs low-energy effective theorems, in which the SM higgs interactions are derived (in the approximation that $p_H \to 0$) by substituting occurrances of the weak scale vacuum expectation value with $v \to v(1 + h/v)$, we scale all non-linear sigma model vev's by $f_i \to f_i(1 + a_i h/f_i)$, where the a's are free parameters of the low energy effective theory. Applying this formalism to the Σ_l kinetic terms in Eq. (2.2), we have

$$\mathcal{L}_{\text{h-V}} = \sum_l \left(2a_l \frac{h}{f_l} \right) \frac{f_l^2}{4} \text{Tr} \, |D_l^\mu \Sigma_l|^2. \tag{2.7}$$

Specific models will generate different values for these coefficients, although there are constraints from requiring perturbative unitarity of the effective theory [190]. Particularly, they need not be $\mathcal{O}(1)$, and indeed can be much smaller in some models.

2.3 Diagrams

We have computed the most general possible diagrammatic structure for loop processes involving the contributions of virtual spin-1 fields to effective operators coupling the scalar higgs to field strengths for vector bosons. The loops of consequence in amplitudes for $h \to \gamma\gamma(Z\gamma)$ involve charged vector bosons running in loops through both "triangle" and "fishing" diagrams, shown in Figure 2.1.

As discussed in Section 2.2, the vertex structure for the interactions is non-standard in generic models, and we characterize the Feynman rules relevant for the computation in Figure 2.2.

With the assistance of the FeynCalc package for Mathematica [216], we have cal-
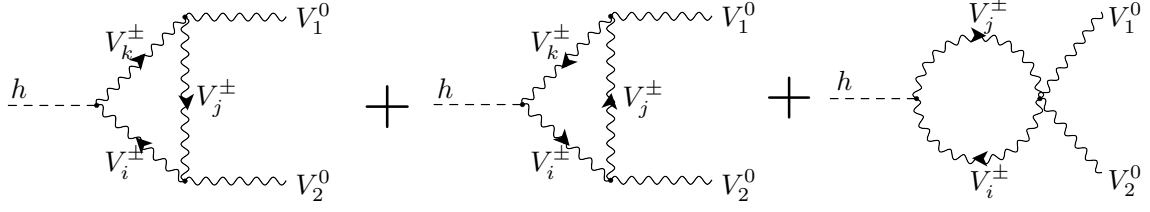
Figure 2.1: One-loop diagrams contributing to the scalar decay rate to neutral vector bosons (i.e. the photon or Z) in gauge extensions of the SM. There is an implied summation over all charged spin-1 fields in the model. The arrows on the charged vector field propagators indicate direction of charge flow. We refer to the sub-amplitudes corresponding to these diagram types as $\mathcal{A}$, $\mathcal{A}^\times$, and $\mathcal{A}^\propto$, respectively.

culated the diagrams corresponding to the range of possible vertex structures shown in Figure 2.2 by turning on one form of coupling at a time. For the triangle diagrams, this corresponds to computing 3×3 matrices of amplitudes, $[\mathcal{A}(M_i^2, M_j^2, M_k^2)]_{\alpha\beta}$ and $[\mathcal{A}^\times(M_i^2, M_j^2, M_k^2)]_{\alpha\beta}$, for each of the possible charge flow directions, taking each vertex to have one of g^0, g^+, or g^- set to one, with all others turned off. For the fishing diagrams, we compute a vector of diagrams, $[\mathcal{A}^\propto(M_i^2, M_j^2)]_\alpha$, with each of the $\lambda^{(1,2,3)}$ couplings set to one, the others to zero. These individual amplitudes are divergent, and we report the finite and divergent parts of these diagrams (computed in unitary gauge) in an online repository of Mathematica files [209]. The full amplitude in a specific model is then obtained by contracting these arrays of sub-diagrams with arrays of couplings that are specific to a given model. The summation over virtual spin-1 fields and their associated couplings to the higgs and external neutral gauge fields is given by:

$$\mathcal{M}^{\mu\nu}_{V_0^1 V_0^2} = \sum_{ijk\alpha\beta} [\kappa_h]_{ki} [\mathcal{A}^{\mu\nu}(M_i^2, M_j^2, M_k^2)]^{\alpha\beta} [g_{V_0^1}]^\alpha_{ji} [g_{V_0^2}]^\beta_{kj}$$

$$\mathcal{M}^{\times\mu\nu}_{V_0^1 V_0^2} = \sum_{ijk\alpha\beta} [\kappa_h]_{ik} [\mathcal{A}^{\times\mu\nu}(M_i^2, M_j^2, M_k^2)]^{\alpha\beta} [g_{V_0^1}]^\alpha_{ij} [g_{V_0^2}]^\beta_{jk}$$

$$\mathcal{M}^{\propto\mu\nu}_{V_0^1 V_0^2} = \sum_{ij\alpha} [\kappa_h]_{ji} [\mathcal{A}^{\propto\mu\nu}(M_i^2, M_j^2)]^\alpha [\lambda_{V_0^1 V_0^2}]^\alpha_{ij}, \tag{2.8}$$

where V_0^1 and V_0^2 are the external neutral gauge fields, either γ or Z. These contri-

43

$$= i\kappa_{ij}\eta_{\mu\nu}$$

$$= -i\left[g_{ij}^{0}\left(k_{\rho}\eta_{\mu\nu} - k_{\nu}\eta_{\mu\rho}\right) + \right.$$
$$g_{ij}^{+}\left(q_{\mu}\eta_{\nu\rho} - q_{\rho}\eta_{\mu\rho}\right) +$$
$$\left. g_{ij}^{-}\left(p_{\nu}\eta_{\mu\rho} - p_{\mu}\eta_{\nu\sigma}\right)\right]$$

$$= -i\left[2\lambda_{ij}^{(1)}\eta_{\mu\nu}\eta_{\rho\sigma} - \lambda_{ij}^{(2)}\eta_{\mu\rho}\eta_{\nu\sigma} - \lambda_{ij}^{(3)}\eta_{\mu\sigma}\eta_{\nu\rho}\right]$$

Figure 2.2: Feynman rules for vertices with general interaction structure. Rules for vertices with 2 charged particles are shown, as these are what are relevant for the calculation. All momenta are assumed to be entering the vertices, and arrows indicate charge flow.

butions must then be summed together to obtain the full amplitude due to spin-1 contributions.

In the next sections we explore contributions to the higgs partial widths in a specific extension of the SM that exhibits the full generality of the couplings and diagrams that have been discussed thus far.

2.4   A Specific Model:

Vector and Axial-Vector Resonances

If the 126 GeV resonance is produced as a composite of TeV scale strong dynamics, it is likely that there are a host of other composite states with masses not far above the electroweak scale. These states should occupy representations of the symmetries of the UV theory. The approximate $SU(2)_L \times SU(2)_R$ global symmetry of the low energy theory, which enforces the absence of tree-level corrections to the oblique T-parameter, dictates that the symmetries of the UV should reflect at least this

global symmetry, with a spontaneous breaking pattern $SU(2)_L \times SU(2)_R \to SU(2)_V$, mimicking the custodial symmetry breaking pattern of the SM. In analogy with QCD, there may be vector and axial vector states, transforming non-linearly as the broken and unbroken generators for these symmetries. The $SU(2)$ structure implies that these states should fall into triplets with a charged and neutral vector in each: $\rho_V^{\pm,0}$ and $\rho_A^{\pm,0}$. If these states are light in comparison with the scale associated with non-perturbativity of the effective theory, then they can enter in loop processes and give calculable contributions to the effective interactions of the scalar resonance.

Axial vector resonances are especially interesting from the perspective of electroweak precision due to the fact that their contribution to the S-parameter can partially cancel contributions from the vector resonances [213]. In this section, we study the couplings of charged vector and axial vectors relevant for the higgs decay rates to $\gamma\gamma$ and γZ in the context of a model which thoroughly explores the range of possibilities for exotic gauge boson self-interactions.

2.4.1 Effective Lagrangian for Vectors and Axial Vectors

A completely generic implementation of axial vector resonances is difficult from the perspective of the low energy effective theory in which only transformations under the unbroken global $SU(2)_C$ are invariants of the phenomenological Lagrangian [192, 193]. Axial vectors can be implemented in different ways while remaining consistent with the unbroken $SU(2)_C$ [217, 218]. To have a concrete model to study, which should have some features of actual strongly coupled theories while also allowing concrete results from computation, we study the theory described by the moose diagram shown in Fig. 2.3. We note that this is precisely the moose studied in [210], although we are considering the effects of adding a singlet h to these models which is coupled in a delocalized way to gauge fields.

The model incorporates a $SU(2)_1 \times SU(2)_2$ gauge extension of the SM, with degrees of freedom referred to as vector and axial vector triplets of resonances. We
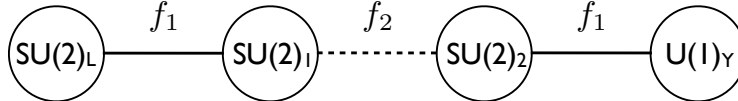
Figure 2.3: The moose diagram that we study that incorporates vector and axial vector resonances

impose a $L - R$ symmetry to preserve custodial $SU(2)$. This $L - R$ symmetry forces the link vevs between $SU(2)_L - SU(2)_1$ and $SU(2)_2 - U(1)_Y$ to be equal - both are given by f_1. Additionally imposing the parity symmetry requires that the couplings associated with $SU(2)_1$ and $SU(2)_2$ be equal - in our case $g_1 = g_2 \equiv g_\rho$. This P_{LR} is broken explicitly by the SM hypercharge interactions, as $U(1)_Y$ corresponds to gauging only the t_3 generator of $SU(2)_R$. This is the usual case in the SM, where it is the hypercharge interactions (as well as the fermion Yukawa couplings) that violate custodial symmetry. In writing the action for this theory, we take the usual canonically normalized gauge kinetic terms for the 4 gauge groups:

$$\mathcal{L}_{\text{gauge-kin}} = -\frac{1}{4} \left[W_{\mu\nu}^{a\ 2} + X_{(1)\mu\nu}^{a\ 2} + X_{(2)\mu\nu}^{a\ 2} + B_{\mu\nu}^2 \right]. \tag{2.9}$$

Strongly coupled models of electroweak symmetry breaking are commonly afflicted by severe electroweak precision constraints, even with a custodial symmetry imposed. Finding models in which the oblique S-parameter is small is the biggest challenge [120–122]. Generically, tree level contributions to the S-parameter arise from mixing of the vector and axial vector states with the SM gauge fields. In [210], it was shown that it is possible to reduce the S parameter with a higher dimensional operator that kinetically mixes $SU(2)_1$ and $SU(2)_2$, analogous with a similar technique in holographic technicolor models [219]. As discussed above, this kinetic mixing gives rise to non-trivial structure for the interaction vertices for the gauge fields once the quadratic Hamiltonian is diagonalized. The gauge invariant kinetic mixing term

we consider is given by

$$\mathcal{L}_{\mathrm{WF}} = -\frac{1}{2}\epsilon \, \mathrm{Tr}\left[X_{(1)\mu\nu}\Sigma_{12}X_{(2)}^{\mu\nu}\Sigma_{12}^{\dagger}\right], \qquad (2.10)$$

where Σ_{12} is the nonlinear sigma model link field corresponding to the central line connecting the $SU(2)_1$ and $SU(2)_2$ gauge groups in the moose. The spin-1 cubic and quartic interactions arise from both the standard and wave-function mixing kinetic terms. Note that the parameter ϵ must be constrained $-1 < \epsilon < 1$ to avoid ghosts in the field theory, and that there are limits which strongly imply that S must remain positive [220].

The gauge kinetic terms for the Σ-fields determine the structure of the mass matrix for the gauge fields. We consider the following Lagrangian for these gauge kinetic terms:

$$\mathcal{L}_{\Sigma-\mathrm{kin}} = \frac{f_1^2}{8}\mathrm{Tr}\left[|D_\mu\Sigma_{L1}|^2\right] + \frac{f_2^2}{8}\mathrm{Tr}\left[|D_\mu\Sigma_{12}|^2\right] + \frac{f_1^2}{8}\mathrm{Tr}\left[|D_\mu\Sigma_{2Y}|^2\right], \qquad (2.11)$$

where the gauge covariant derivatives correspond to bi-fundamentals under the gauge groups neighboring the link; for the link field Σ_{ij}, we have $D_\mu = \partial_\mu - ig_i\hat{A}_\mu^i + ig_j\hat{A}_\mu^j$.

For the scalar higgs interactions, we again impose the $L - R$ symmetry:

$$\mathcal{L}_{\mathrm{higgs}} = h\left\{a_h\frac{f_1}{4}\mathrm{Tr}\left[|D_\mu\Sigma_{L1}|^2\right] + b_h\frac{f_2}{4}\mathrm{Tr}\left[|D_\mu\Sigma_{12}|^2\right] + a_h\frac{f_1}{4}\mathrm{Tr}\left[|D_\mu\Sigma_{2Y}|^2\right]\right\}, \quad (2.12)$$

forcing the higgs couplings to the $L - 1$ and $2 - Y$ kinetic terms to be identical.

2.4.2 Couplings in the four site model

The couplings of the hamiltonian eigenstates, which follow after diagonalization of the quadratic part of the action, can be straightforwardly derived. Due to the wave-function mixing, however, the normalization condition for the states is modified. The normalization condition for the eigenvectors in the presence of the wave-function

mixing term is instead (as emphasized in [210]) $v_n^T Z v_n = 1$, where we have

$$Z_0 = \begin{pmatrix} 1 & 0 & 0 & 0 \\ 0 & 1 & \epsilon & 0 \\ 0 & \epsilon & 1 & 0 \\ 0 & 0 & 0 & 1 \end{pmatrix} \tag{2.13}$$

for the neutral gauge bosons and

$$Z_\pm = \begin{pmatrix} 1 & 0 & 0 \\ 0 & 1 & \epsilon \\ 0 & \epsilon & 1 \end{pmatrix} \tag{2.14}$$

for the charged ones. The eigenvectors thus satisfy the following relation:

$$M^2 \vec{v}_n = m_n^2 Z \vec{v}_n \tag{2.15}$$

where M^2 is the mass matrix of the quadratic lagrangian that follows from the Σ-field kinetic terms in Eq. (2.11). To avoid ghost instabilities, we must constrain ϵ to the interval $-1 < \epsilon < 1$. The components of the eigenvectors, $\vec{v}_n$, are ordered based on the moose structure in Figure 2.3, from left to right. The couplings of the physical states are then obtained by expressing the original Lagrangian in terms of the eigenvector solutions to Eq. (2.15).

2.4.3   Higgs interactions

As an example of the interactions of the mass and kinetic eigenstates, we give the Feynman rules for interactions of the scalar higgs with the charged gauge fields in Table 2.1. We have performed an expansion in g/g_ρ and g'/g_ρ, presuming that the two exotic gauge groups have large (but still perturbative) coupling constants. We have used the definitions $c_f \equiv f_1/\sqrt{f_1^2 + 2f_2^2}, s_f \equiv \sqrt{2}f_2/\sqrt{f_1^2 + 2f_2^2}$, and $v \equiv$

hW^+W^-	$i\frac{2M_W^2}{v}\left(a_h\frac{s_f^3}{\sqrt{2}}+b_hc_f^3\right)$
$h\rho_V^+\rho_V^-$	$i\frac{\sqrt{2}M_\rho^2}{v}a_hs_f$
$h\rho_A^+\rho_A^-$	$i\frac{\sqrt{2}M_A^2}{v}s_fc_f\left(a_hc_f+\sqrt{2}b_hs_f\right)$
$hW^+\rho_A^-$	$i\frac{2M_WM_A}{v}s_fc_f\left(a_h\frac{s_f}{\sqrt{2}}-b_hc_f\right)$

Table 2.1: Feynman rules corresponding to interactions of the singlet field h with charged gauge bosons in the 4-site model shown in Figure 2.3. We have only kept the lowest order terms in the $\frac{g}{g_\rho}$ expansion; in fact all interactions are non-vanishing at order g^2/g_ρ^2. The charge reversed Feynman rules are identical.

$f_1f_2/\sqrt{f_1^2+2f_2^2}$. When $a_h/f_1 \neq b_h/f_2$, the higgs has interactions which change the "flavor" of gauge field at the vertex. For models in which gauge boson self-interactions also allow a change in the flavor of charged gauge boson, a larger class of diagrams than in the SM is allowed.

It is possible that other higher dimensional operators of the form $hV_{\mu\nu}^2$ exist due to strong coupling effects, giving both a direct contribution to higgs decay amplitudes, and also contributing to new loop structures. We discuss this first possibility later, in Section 2.4.6. The latter possibility leads to contributions which are suppressed both by loop factors and the cutoff scale. We neglect such contributions in this work.

2.4.4 γ and Z-boson Interactions with charged spin-1 fields

The quartic interactions of the photon are constrained by gauge invariance to be simply the electric charge squared, with no "flavor" changing of the gauge fields at the vertex. In the 4-site model under consideration, the quartic Feynman rules are all of the form

$$\lambda_{ij}^{(1)}=\lambda_{ij}^{(2)}=\lambda_{ij}^{(3)}=\begin{cases} e^2 & i=j \\ 0 & i\neq j \end{cases} \tag{2.16}$$

where the electric charge is given in terms of the fundamental model parameters as

$$e^2=e_0^2\left(1-\frac{2e_0^2(1+\epsilon)}{g_\rho^2}+\mathcal{O}(e_0^4/g_\rho^4)\right), \tag{2.17}$$

with $e_0^2 \equiv g^2 g'^2/(g^2 + g'^2)$.

For the cubic interactions, the presence of the wave function mixing term induces off-diagonal couplings of the photon to charged spin-1 fields. The interactions, to order $1/g_\rho^2$, are given in Table 2.2.

$\gamma W^+ W^-$	g_0	$e\left(1 + \epsilon c_f^4 \left(\frac{g}{g_\rho}\right)^2\right)$
	g_+	e
	g_-	e
$\gamma W^+ \rho_A^-$	g_0	$e\epsilon c_f^2 \sqrt{\frac{2}{1-\epsilon}} \left(\frac{g}{g_\rho}\right)$
$\gamma \rho_V^+ \rho_V^-$	g_0	e
	g_+	e
	g_-	e
$\gamma \rho_V^+ \rho_A^-$	g_0	$e\epsilon c_f^2 (1+\epsilon) \sqrt{\frac{1+\epsilon}{1-\epsilon}} \frac{1}{2\left(\epsilon c_f^2 + \frac{1}{2}(1+\epsilon)s_f^2\right)} \left(\frac{g}{g_\rho}\right)^2$
$\gamma \rho_A^+ \rho_A^-$	g_0	$e\left(\frac{1+\epsilon}{1-\epsilon} - \epsilon c_f^4 \left(\frac{g}{g_\rho}\right)^2\right)$
	g_+	e
	g_-	e

Table 2.2: These are the non-vanishing (at order g/g_ρ^2) cubic interactions of the photon with the charged gauge bosons associated with the moose diagram in Figure 2.3. The expression for e in terms of the fundamental parameters (to order g^2/g_ρ^2) is given in Eq. 2.17.

The corresponding interactions of the Z-boson with charged spin-1 fields are algebraically much more complicated. We have made the full set of couplings, valid to order g^2/g_ρ^2, available as Mathematica code [209].

2.4.5   Loop level contributions to $h \to Z\gamma$ and $h \to \gamma\gamma$

The following results are analytic expressions that are valid to lowest order in the g/g_ρ expansion, and correspond to the low energy theorem limit where $m_h, m_Z \ll 2m_{V^\pm}$.

The amplitudes are proportional to the usual transverse tensor structure

$$e^2 \left(g^{\alpha_1 \alpha_2} p_{\gamma^1} \cdot p_{\gamma^2} - p_{\gamma^1}^{\alpha_1} p_{\gamma^2}^{\alpha_2} \right) \mathcal{M}_{\gamma\gamma}$$

$$eg \cos \theta_w \left(g^{\alpha_1 \alpha_2} p_Z \cdot p_\gamma - p_Z^{\alpha_1} p_\gamma^{\alpha_2} \right) \mathcal{M}_{Z\gamma} \tag{2.18}$$

For the 4-site model, performing the summations of Eq. 2.8, we find:

$$\mathcal{M}_{\gamma\gamma} = \frac{\epsilon^2 f_1 \log \frac{\Lambda^2}{M_A^2}}{4\pi^2 f_2^3 (1-\epsilon)^2} (a_h f_2 - b_h f_1) + \frac{7}{8\pi^2 f_1 f_2} (2 a_h f_2 + b_h f_1)$$

$$+ \frac{\epsilon}{8\pi^2 f_2 (1-\epsilon)^2} \left[a_h \sqrt{2} \frac{c_f}{s_f} \left(c_f^2 \epsilon + 3 s_f^2 (2-\epsilon) \right) + b_h \left(12 s_f^2 (1-\epsilon) - 10 c_f^2 \epsilon - 6 \frac{c_f^4}{s_f^2} \epsilon \right) \right] \tag{2.19}$$

$$\mathcal{M}_{Z\gamma} = \frac{\epsilon \log \frac{\Lambda^2}{M_A^2}}{2\sqrt{2}\pi^2 (1-\epsilon)^2} \frac{c_f}{s_f^3} \frac{(a_h f_2 - b_h f_1)}{f_1^2 + 2 f_2^2} \left[\epsilon \left(1 - \tan^2 \theta_w \right) - \frac{1}{2} s_f^2 (1-\epsilon) \left(1 + \tan^2 \theta_w \right) \right]$$

$$+ \frac{7}{16\pi^2 f_1 f_2} \left[(2 a_h f_2 + b_h f_1) \left(1 - \tan^2 \theta_w \right) + \left(a_h f_2 s_f^2 + b_h f_1 c_f^2 \right) \left(1 + \tan^2 \theta_w \right) \right]$$

$$+ \frac{\epsilon}{16\pi^2 (1-\epsilon)^2} \frac{f_1}{f_2^2} \left\{ a_h \left[\left(3 s_f^2 (2-\epsilon) + \epsilon c_f^2 \right) \left(1 - \tan^2 \theta_w \right) - \frac{3}{2} s_f^2 (1-\epsilon) \left(1 + \tan^2 \theta_w \right) \right] \right.$$

$$\left. + b_h \left[\left(6\sqrt{2} \frac{s_f^3}{c_f} (1-\epsilon) - 2\sqrt{2} c_f s_f \epsilon - 3\sqrt{2} \frac{c_f}{s_f} \epsilon \right) \left(1 - \tan^2 \theta_w \right) + \frac{3}{\sqrt{2}} s_f c_f (1-\epsilon) \left(1 + \tan^2 \theta_w \right) \right] \right\} . \tag{2.20}$$

In the $\epsilon \to 0$ limit, when the non-renormalizable operator incorporating wavefunction mixing is turned off, the results are finite and given by

$$\mathcal{M}_{\gamma\gamma} = \frac{7}{8\pi^2 f_1 f_2} (2 a_h f_2 + b_h f_1) \tag{2.21}$$

$$\mathcal{M}_{Z\gamma} = \frac{7}{16\pi^2 f_1 f_2} \left[(2 a_h f_2 + b_h f_1) \left(1 - \tan^2 \theta_w \right) + \left(a_h f_2 s_f^2 + b_h f_1 c_f^2 \right) \left(1 + \tan^2 \theta_w \right) \right] . \tag{2.22}$$

51

For our numerical analysis, we use these formulae to compare against the standard model expectations for these amplitudes.

2.4.6 $h \to Z\gamma$ and $h \to \gamma\gamma$ from higher dimensional operators

There are tree-level contributions to the $hZ\gamma$ and $h\gamma\gamma$ couplings inherited from strong-coupling effects [206] that couple the scalar h directly to the field strengths of the two middle $SU(2)$ groups in the moose. These terms serve as counter-terms for divergences that appear in loop amplitudes such as those given in the previous subsection. We have not considered tree level couplings to the "fundamental" W and Z bosons in the effective field theory (the gauge groups on either end of the moose) but since there is mixing after symmetry breaking takes place, there is an effective tree level $hZ\gamma$ coupling. The tree level L-R symmetric lagrangian before spontaneous breaking is assumed to take the form

$$\frac{c}{4\Lambda} h \left[(\rho_1^{\mu\nu \ a})^2 + (\rho_2^{\mu\nu \ a})^2 \right] + \frac{c_\epsilon}{2\Lambda} h \text{Tr} \left[\rho_{1 \ \mu\nu} \Sigma_{12} \rho_2^{\mu\nu} \Sigma_{12}^\dagger \right] \tag{2.23}$$

where c is an unknown coefficient parametrizing the effects of UV strongly-coupled dynamics. Like the WF mixing term, c_ϵ is an addtional coefficient parametrizing the "mixing" between the two heavy vectors. After the theory is expressed in the mass basis, the resulting lagrangian term is

$$\frac{(c + c_\epsilon)}{2\Lambda} \frac{eg \cos\theta_w}{g_\rho^2} \left(1 - \tan^2\theta_w \right) h Z_{\mu\nu} A^{\mu\nu} + \frac{(c + c_\epsilon)}{2\Lambda} \frac{e^2}{g_\rho^2} h A_{\mu\nu} A^{\mu\nu}. \tag{2.24}$$

Note that the additional contributions to the amplitudes both scale in the same way, and with the same sign as functions of the coefficients c and c_ϵ. Generically, strong coupling effects are expected to produce values of the c parameters that are of order g_ρ^2, such that these terms serve as counter-terms to absorb the divergences in the amplitudes for the higgs decay rates.

2.5 Results

Current LHC constraints on the higgs couplings favor a SM-like coupling of the higgs to Z bosons. The hW^+W^- coupling is given in Table 2.1, and the hZZ coupling is of a similar form. To leading order in the g/g_ρ expansion, for massive vectors V, we have

$$\frac{g_{hVV}}{g_{hVV}^{\text{SM}}} = a_h \frac{s_f^3}{\sqrt{2}} + b_h c_f^3 + \mathcal{O}(g^2/g_\rho^2). \tag{2.25}$$

In plotting our results, we constrain $g_{hVV}/g_{hVV}^{\text{SM}} = 1$, enforcing a relationship between a_h and b_h. We choose to eliminate b_h with this relation, and vary a_h. We have also restricted the W-boson mass to the SM value, fixing one combination of f_1 and f_2. To leading order in g/g_ρ, we set

$$v^2 = \frac{f_1^2 f_2^2}{f_1^2 + 2f_2^2}, \tag{2.26}$$

with $v \equiv 246$ GeV.

One of the motivations for considering an effective field theory which contains an axial vector is to study the interplay between electroweak precision and the higgs decay rates. In strongly coupled models of electroweak symmetry breaking or in their holographic counterparts, ameliorating the tree-level contributions to S is a particular challenge [220–222]. In adjusting the parameter ϵ, the relationship between the axial-vector and vector resonances change:

$$\frac{M_\rho^2}{M_A^2} = c_f^2 \frac{1-\epsilon}{1+\epsilon} + \mathcal{O}(g^2/g_\rho^2), \tag{2.27}$$

and the tree-level contributions to the S parameter vary accordingly [210]:

$$\Delta S \approx \frac{2\sin^2\theta_w}{\alpha} \frac{g^2}{g_\rho^2}(1+\epsilon)\left(1 - c_f^4\frac{1-\epsilon}{1+\epsilon}\right) \approx \frac{4\sin^2\theta_w}{\alpha s_f^2}\frac{M_W^2}{M_\rho^2}\left(1 - c_f^2\frac{M_\rho^2}{M_A^2}\right). \tag{2.28}$$

In Figure 2.4, we show the value of ϵ that is required for the tree level value of S
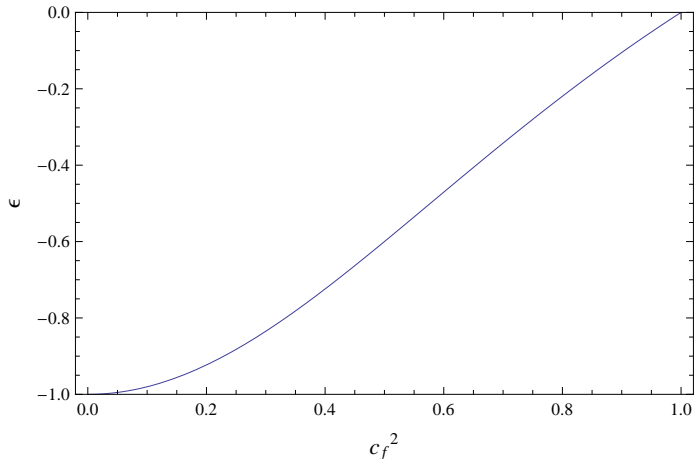
Figure 2.4: Values of ϵ for which the S parameter vanishes as a function of the angle $c_f^2 \equiv f_1^2/(f_1^2 + 2f_2^2)$. The high and low ranges of c_f correspond to large hierarchies between the vev's f_1 and f_2. The large c_f limit, in which $f_1 \to \infty$, is the decoupling limit for the vector and axial vector.

to be zero. We note that negative $\mathcal{O}(1)$ values must be taken to completely set S to zero for a large range of c_f. It is only in the $c_f \to 1$ limit that only small values of epsilon are necessary. However, that limit corresponds precisely to the decoupling limit $f_1 \to \infty$, in which both the vector and axial vector masses become large.

For $\mathcal{O}(1)$ negative values of ϵ, the normal hierarchy between the vector and axial vector resonances is inverted, and the S-parameter can be reduced to zero. Note, however, that such large values of ϵ exceed expectations from application of naive dimensional analysis [223], and there are arguments against such an inverted spectrum following from studies of holographic technicolor models [220]. For the purposes of this work, however, we are motivated more by phenomenological exploration. For example, one question of merit is whether there exists a correlation between values of S and loop corrections to the $h \to \gamma\gamma(Z\gamma)$ rates that may persist generically in more realistic models of electroweak symmetry breaking. In this spirit, we display results for ranges of ϵ following only the requirements that the theory remain perturbative and that the spectrum be tachyon-/ghost-free.

In Figure 2.5, we display the vector and axial vector masses (for the choice $g_\rho = 4$)

as a function of ϵ for various choices of c_f. The black vertical lines display the value of ϵ for which the tree-level S-parameter vanishes. Note that the inverted spectrum is required for the tree-level contribution to S to vanish. The leading order (in the g/g_ρ expansion) expressions for the vector and axial vector masses are given by

$$
\begin{aligned}
M_\rho^2 &= \frac{g_\rho^2 f_1^2}{4(1+\epsilon)} \\
M_A^2 &= \frac{g_\rho^2(f_1^2 + 2f_2^2)}{4(1-\epsilon)}.
\end{aligned}
\tag{2.29}
$$
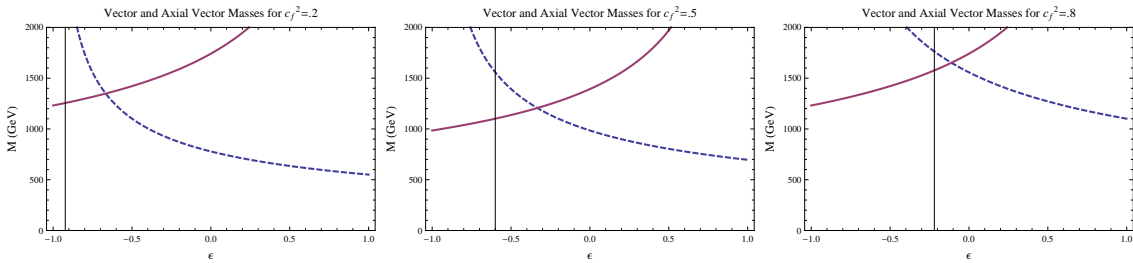
Figure 2.5: The values of M_ρ (dashed) and M_A (solid) as a function of ϵ for $c_f^2 = .2, .5$, and $.8$, respectively. The value of g_ρ has been fixed at $g_\rho = 4$ in this figure, however the masses scale linearly with g_ρ, so long as it is large compared with electroweak gauge couplings. The black vertical lines correspond to the values of ϵ for which the tree-level contribution to S vanishes.

We have added the amplitudes calculated in Section 2.4.5 to the SM top quark contributions for both $h \to \gamma\gamma$ and $h \to Z\gamma$, and calculated the partial decay widths to these final states in the 4-site model. Comparing with the SM rates[2], we display the ratio $\Gamma(h \to XX)/\Gamma_{\mathrm{SM}}(h \to XX)$ as functions of ϵ and a_h for 3 representative values of the angle c_f. While significant enhancements or suppressions are possible in the theory, we find that when the $h \to \gamma\gamma$ rate is SM-like (as suggested by current LHC data), the contributions to $h \to Z\gamma$ are either close to SM-like as well, or experience a large suppression (where the branching ratio is approximately 1/10'th that of the SM). In Figure 2.6, we display the decay rates in the branching fractions for these

---

[2]We utilize the higgs low energy theorem limits for both the SM W contribution and the new physics contribution to make this comparison.
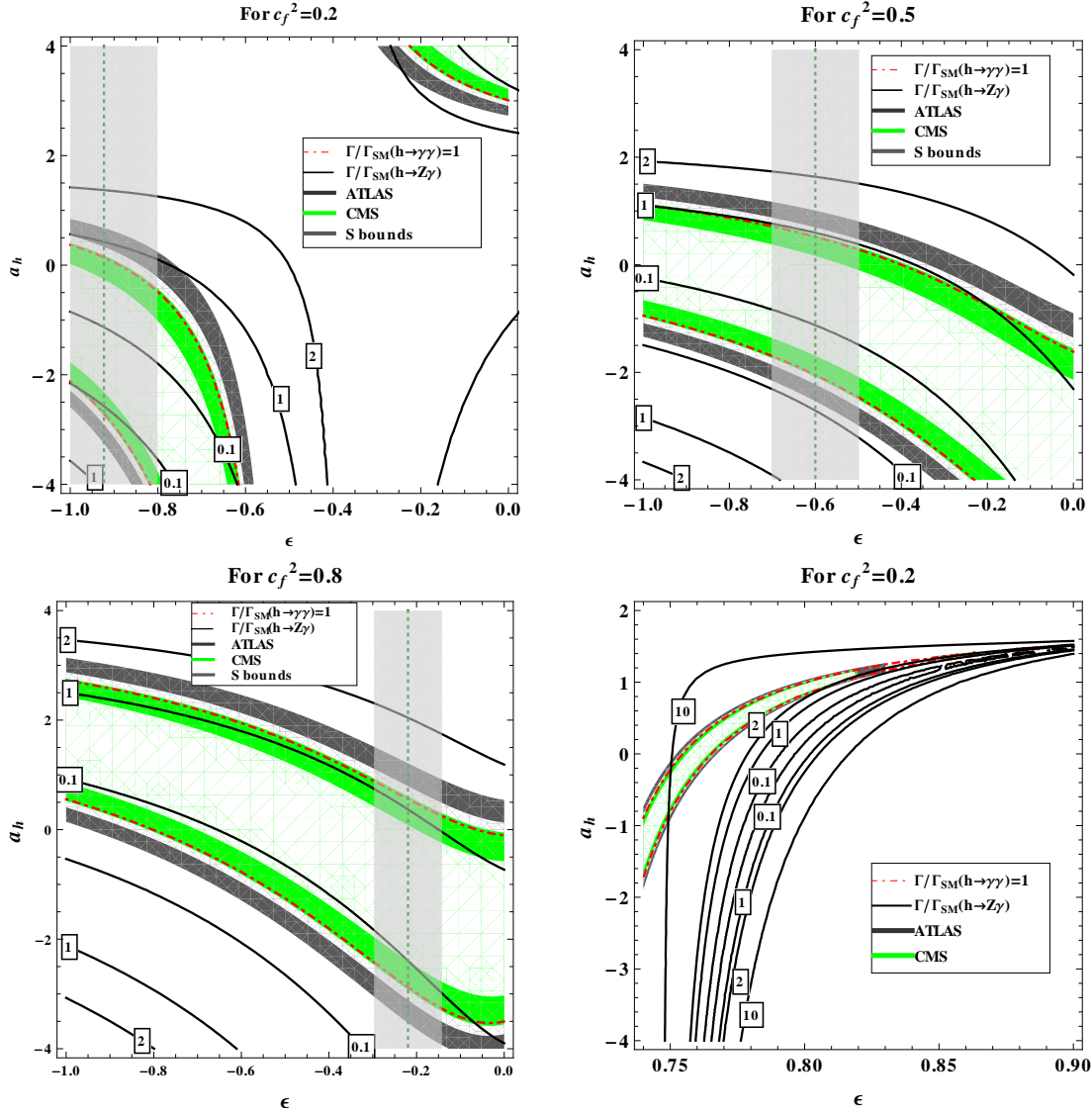
Figure 2.6: This figure displays the ratio of the higgs partial widths to the $Z\gamma$ and $\gamma\gamma$ final states in relation to the expectation in the SM. The figures represent the scenario where direct contributions from higher dimensional operators are neglected. Loop diagrams from the vector and axial vector states are taken into account. The three plots are for $c_f^2 = 0.2, 0.5,$ and 0.8. The light grey shaded region corresponds to the value of ϵ for which the S-parameter obeys current experimental constraints [2]. The dark grey and green bands correspond respectively to the 1σ bands for the ATLAS [3] and CMS [4] experimental results for $h \to \gamma\gamma$.

final states relative to SM expectations. In this plot we have taken the contributions from the higher dimensional operators discussed in Section 2.4.6 to be vanishing (i.e.

$c = c_\epsilon = 0$). Adding these operators with non-trivial coefficients changes the contour bands, as Shown in Figure 5.2. In both Figure 2.6 and Figure 5.2, we have kept the ratio of the cutoff scale and the axial vector masses fixed at $\Lambda/M_A = 2$. Since M_A varies with ϵ and c_f, the cutoff changes in these plots as well. While the shape of the contours does not change significantly with the addition of these operators, it is important to note that the relative size of the $h \to \gamma\gamma$ rates vs the $h \to Z\gamma$ rates differ significantly. For example, with the higher dimensional operator coefficients set to zero, there is mostly only a suppression of the $h \to Z\ gamma$ rates when the $\gamma\gamma$ rate is SM-like. In contrast, when the higher dimensional operators are added with coefficients consistent with naive dimensional analysis, the $Z\gamma$ rate can either be signficantly suppressed relative to SM predictions (see left panel in Figure 5.2), or potentially enhanced (see right panel in Figure 5.2) depending on the sign of their coefficients.
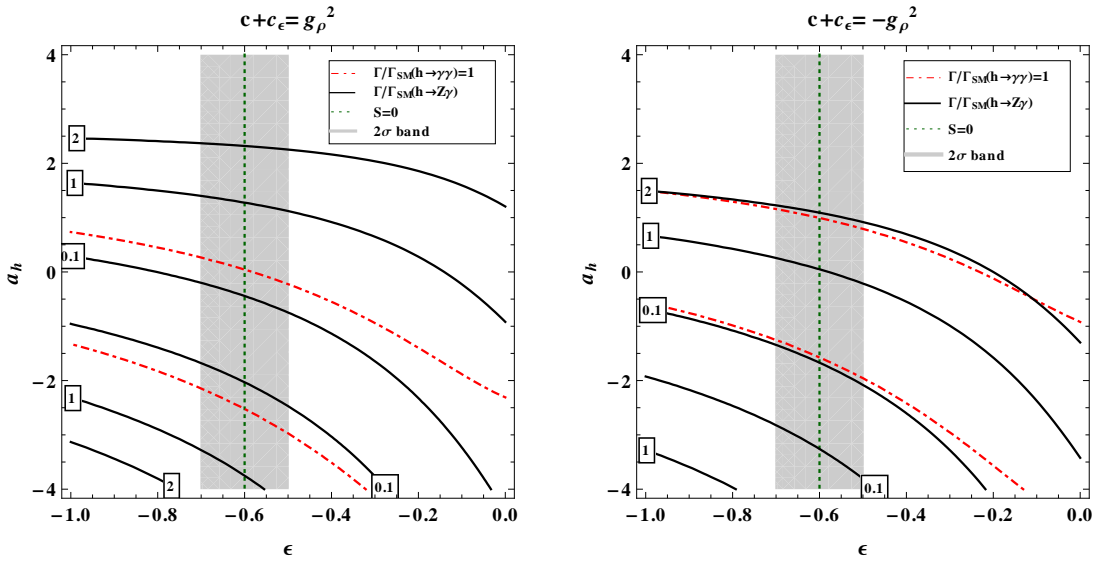
Figure 2.7: This figure displays the ratio of the higgs partial widths to the $Z\gamma$ and $\gamma\gamma$ final states in relation to the expectation in the standard model when dimension 5 operators coupling the higgs field directly to exotic field strengths are added, interfering with the loop level contributions of states in the low energy effective theory. In the two plots, we have taken $c + c_\epsilon = g_\rho^2$ (left) and $c + c_\epsilon = -g_\rho^2$ (right). For these plots, we have taken $c_f^2 = 0.5$. We have fixed the cutoff scale Λ at twice the mass of the axial-vector resonance, which varies as a function of ϵ and c_f as shown in Figure 2.5.

2.6 Conclusions

We have considered the effects of electroweak/TeV scale spin-1 resonances on the phenomenology of a higgs-like scalar resonance. In particular, we have calculated the effects of such fields on the di-boson decays: $h \to \gamma\gamma$ and $h \to Z\gamma$. A very general framework for calculations of spin-1 contributions has been constructed, with application to arbitrary gauge extensions of the SM made possible via Mathematica files that have been made available online [209]. In these files, the quantum effects of vector-resonances and SM gauge fields have been presented as functions of generic couplings that may arise in extra dimensional models, little higgs models, strongly coupled theories, or various other SM extensions with exotic spin-1 resonances that couple to the electroweak sector.

The results of this calculation have been applied to a benchmark phenomenological model for dynamical electroweak symmetry breaking that contains a composite scalar resonance in the spectrum. In particular, the effects of a class of models with vector and axial-vector triplets on scalar phenomenology have been computed and found to generate potentially large contributions to the $\gamma\gamma$ and γZ branching fractions of the 125 GeV resonance. Contributions to the higgs decay rates are especially interesting in these scenarios, as the divergence structure of the decay amplitudes is dependent on the value of the parameter that determines the size of tree-level contributions to the S-parameter.

Future runs of the LHC, including both energy and luminosity upgrades, are likely to strongly constrain the viability of many gauge extensions of the SM via probes of the higgs, particularly once we measure its decay rate to the $Z\gamma$ final state. The correlations of this channel with electroweak precision constraints and the $h \to \gamma\gamma$ rate are particularly interesting in light of the current state of the allowed landscape of well-motivated gauge extensions of the SM. We have provided here a set of tools which we hope will be a valuable resource as we test such theories against LHC data.

Chapter 3

Spin-One Top Partner: Phenomenology

3.1 Introduction

Discovery of the Higgs boson brought into sharp focus the long-standing theoretical problem of the Standard Model (SM), the hierarchy problem. If the SM is the complete description of physics up to scale Λ, radiative corrections generate a contribution to the Higgs mass parameter of order $\Lambda/(4\pi)$. The Higgs mass parameter is now precisely known, $\mu = (126 \text{ GeV})/\sqrt{2} \approx 90 \text{ GeV}$. Unless unrelated contributions to μ cancel, we expect the scale of SM break-down Λ to be of order 1 TeV. This argument strongly motivates experimental searches for non-SM physics at the LHC energies, and an extensive program of such searches is ongoing.

The hierarchy argument does not uniquely fix the nature of new physics at scale Λ, but it does provide some important clues. Precision electroweak measurements constrain the scale at which generic strong-coupling extensions of the SM may become relevant to ~ 10 TeV or above. This indicates that the solution to the hierarchy problem must rely on weakly-coupled physics, unless significant fine-tuning is involved. All known weakly-coupled solutions to the hierarchy problem involve new particles

at the scale $\Lambda \lesssim$ TeV. Loops of these particles introduce additional contributions to the Higgs mass parameter, which cancel the leading contribution of SM loops. Such cancellations can occur naturally due to symmetries; known examples are supersymmetry, shift symmetry, and gauge symmetry extended to models with extra compact dimensions of space. Each of these symmetries can be implemented in a variety of ways, leading to a large zoo of possible explicit models for non-SM physics at the TeV scale. Most of these models have a rich spectrum of new states, and their masses are typically extremely model-dependent, making it difficult to choose optimal targets for experimental searches. However, in all models, the particles canceling the loops of SM tops, the "top partners", play a special role. The large value of the top Yukawa in the SM implies that the top partners must be quite light, below a few hundred GeV, for the model to be natural, independent of model-building details. This makes top partners a particularly well-motivated target for the LHC searches.

The conventional wisdom says that top partners fall into one of two classes: spin-0 partners, or "stops", if the hierarchy problem is solved by supersymmetry; and spin-1/2 partners, if it is solved by shift symmetry or higher-dimensional gauge symmetry. Both these possibilities are extensively covered by experimental searches. There is, however, an alternative possibility, which has so far received far less attention: a spin-1 top partner. An explicit model realizing this scenario was constructed by Cai, Cheng and Terning (CCT) in 2008 [160]. However, to date, no comprehensive study of phenomenology of this model has been performed. The goal of this paper is to rectify this omission.

The paper is organized as follows. We review the CCT model, emphasizing the aspects that will be germane for the discussion of phenomenology, in Section 3.2. We then discuss the two main sources of current constraints on the model, precision electroweak fits (Section 3.3) and direct searches for Z' bosons at the LHC (Section 3.4). In Section 3.5, we discuss how the 125 GeV Higgs boson can be accommodated in this model, and briefly discuss the degree of fine-tuning implied by the constraints. Sec-

	$SU(5)$	$SU(3)$	$SU(2)$	$U(1)_H$	$U(1)_V$	$U(1)_Y$
Q_i	$\mathbf{1}$	$\square$	$\square$	$\frac{1}{6}$	0	$\frac{1}{6}$
$\bar{u}_i$	$\mathbf{1}$	$\overline{\square}$	$\mathbf{1}$	$-\frac{2}{3}$	0	$-\frac{2}{3}$
$\bar{d}_i$	$\mathbf{1}$	$\overline{\square}$	$\mathbf{1}$	$\frac{1}{3}$	0	$\frac{1}{3}$
L_i	$\mathbf{1}$	$\mathbf{1}$	$\square$	$-\frac{1}{2}$	0	$-\frac{1}{2}$
$\bar{e}_i$	$\mathbf{1}$	$\mathbf{1}$	$\mathbf{1}$	1	0	1
H	$\square$	$\mathbf{1}$	$\mathbf{1}$	$\frac{1}{2}$	$\frac{1}{10}$	$\left(\frac{2}{3},\frac{1}{2}\right)$
$\overline{H}$	$\overline{\square}$	$\mathbf{1}$	$\mathbf{1}$	$-\frac{1}{2}$	$-\frac{1}{10}$	$\left(-\frac{2}{3},-\frac{1}{2}\right)$
Φ_3	$\square$	$\overline{\square}$	$\mathbf{1}$	$-\frac{1}{6}$	$\frac{1}{10}$	$\left(0,-\frac{1}{6}\right)$
Φ_2	$\square$	$\mathbf{1}$	$\overline{\square}$	0	$\frac{1}{10}$	$\left(\frac{1}{6},0\right)$
$\overline{\Phi}_3$	$\overline{\square}$	$\square$	$\mathbf{1}$	$\frac{1}{6}$	$-\frac{1}{10}$	$\left(0,\frac{1}{6}\right)$
$\overline{\Phi}_2$	$\overline{\square}$	$\mathbf{1}$	$\square$	0	$-\frac{1}{10}$	$\left(-\frac{1}{6},0\right)$

Table 3.1: Chiral superfields of the model, and their gauge quantum numbers. Here, $i = 1 \ldots 3$ is the flavor index.

tion 3.6 discusses the deviations in the Higgs couplings to gluons and photons induced by the new particles of the CCT model, while Section 3.7 contains a brief sketch of the possible signatures of the model at a 100 TeV hadron collider. We conclude in Section 3.8, and relegate some of the details of the analysis to the Appendix.

3.2 Review of the Model

The model studied in this paper was proposed by Cai, Cheng and Terning (CCT) in [160]. In this section we will review the model.

3.2.1 Structure and Particle Content

The CCT model is a supersymmetric gauge theory, based on a gauge group $G = SU(5) \times SU(3) \times SU(2) \times U(1)_H \times U(1)_V$. The matter superfields of the model, and their gauge quantum numbers, are listed in Table 1.The superpotential has the form

$$
\begin{aligned}
W \;=\; & y_1 Q_3 \Phi_3 \overline{\Phi}_2 + \mu_3 \Phi_3 \overline{\Phi}_3 + \mu_2 \Phi_2 \overline{\Phi}_2 + y_2 \bar{u}_3 H \overline{\Phi}_3 + \mu_H H \overline{H} \\
& + \frac{Y_{Uij}}{M_F} Q_i \bar{u}_j \overline{\Phi}_2 H + \frac{Y_{Dij}}{M_F} Q_i \bar{d}_j \Phi_2 \overline{H} + \frac{Y_{Eij}}{M_F} L_i \bar{e}_j \Phi_2 \overline{H},
\end{aligned}
\tag{3.1}
$$

where $i, j = 1 \ldots 3$ are flavor indices. In addition, one must also add soft SUSY-breaking terms generated at some messenger scale Λ. With the usual motivation of the hierarchy problem, we assume that all soft masses are around the TeV scale; their precise values will not be important for most of our discussion. As will be described in more detail below, SUSY breaking triggers gauge symmetry breaking by causing the four link fields, $\Phi_{2,3}$ and $\overline{\Phi}_{2,3}$, to acquire vacuum expectation values (vevs) of the form

$$
\langle \Phi_3 \rangle = \begin{pmatrix} f_3 & 0 & 0 & 0 & 0 \\ 0 & f_3 & 0 & 0 & 0 \\ 0 & 0 & f_3 & 0 & 0 \end{pmatrix} , \qquad \langle \overline{\Phi}_3 \rangle^T = \begin{pmatrix} \overline{f}_3 & 0 & 0 & 0 & 0 \\ 0 & \overline{f}_3 & 0 & 0 & 0 \\ 0 & 0 & \overline{f}_3 & 0 & 0 \end{pmatrix} ,
$$

$$
\langle \Phi_2 \rangle = \begin{pmatrix} 0 & 0 & 0 & f_2 & 0 \\ 0 & 0 & 0 & 0 & f_2 \end{pmatrix} , \qquad \langle \overline{\Phi}_2 \rangle^T = \begin{pmatrix} 0 & 0 & 0 & \overline{f}_2 & 0 \\ 0 & 0 & 0 & 0 & \overline{f}_2 \end{pmatrix} . \quad (3.2)
$$

Given their connection with SUSY breaking, we assume that all f's are at roughly the same scale, $f \sim$ TeV; we will discuss experimental constraints on f's in detail later in this paper. This pattern of vevs breaks G to $G_{\mathrm{SM}} = SU(3)_c \times SU(2)_L \times U(1)_Y$, with the $SU(3)_c \times SU(2)_L$ identified with the diagonal linear combination of the $SU(3) \times SU(2)$ subgroup of $SU(5)$, and the additional $SU(3) \times SU(2)$ factor in G. The unbroken hypercharge $U(1)_Y$ is given by the linear combination of the diagonal generator T_{24} of $SU(5)$ and the two explicit $U(1)$ factors in G: $Y = \frac{1}{\sqrt{15}} T_{24} + H + V$. The SM gauge couplings at the scale f are related to the G couplings (denoted by hats):

$$
\frac{1}{g_{2,3}^2} = \frac{1}{\hat{g}_{2,3}^2} + \frac{1}{\hat{g}_5^2} , \qquad \frac{1}{g_Y^2} = \frac{1}{\hat{g}_H^2} + \frac{1}{\hat{g}_V^2} + \frac{1}{15\hat{g}_5^2} . \quad (3.3)
$$

Examining the matter field quantum numbers under G_{SM}, it is easily seen that the model contains all of the familiar matter content of the MSSM. In particular, the fields Q_i, $\bar{u}_i$, $\bar{d}_i$, L_i and $\bar{e}_i$ are directly identified with the corresponding MSSM fields,

with the exception of the third-generation quarks which require special treatment. The two Higgs fields of the MSSM, H_d and H_u, are embedded in the H and $\overline{H}$ fields, along with the (non-MSSM) color triplets and anti-triplets $\overline{T}^c$ and $\overline{T}$:

$$
H = \begin{pmatrix} \overline{T}^c \\ H_u \end{pmatrix}, \qquad \overline{H} = \begin{pmatrix} \overline{T} \\ H_d \end{pmatrix}. \tag{3.4}
$$

The last four terms of the superpotential (3.1) then reproduce the full MSSM superpotential. In particular, SM quark and lepton Yukawa couplings are of order f/M_F, and can naturally be small if there is a hierarchy between these scales.

The model also has a rich spectrum of non-MSSM fields. These are listed in Table 2, along with their G_{SM} quantum numbers and R parity. Since SUSY breaking and $G \to G_{\mathrm{SM}}$ breaking occur at roughly the same scale, in this case we list each field and its superpartner separately. Note that the conserved R parity in the CCT model, which plays the same role as the usual R parity in the MSSM, is a convolution of a "global" R parity which commutes with all gauge transformations, and a "twist" transformation, which acts on the $SU(5)$ multiplets as $P_{\mathrm{twist}} = \mathrm{diag}(-1, -1, -1, 1, 1)$. The twist is required because the scalar components of the H and $\bar{H}$ multiplets must be assigned opposite R-parities, $+1$ for the Higgs and -1 for the $\overline{T}$ and $\overline{T}^c$.

Interestingly, some of the fields in Table 2 have the same quantum numbers as MSSM fields, allowing them to mix. In particular, there are three fields with the quantum numbers of the left-handed quark doublet Q, $(\mathbf{3}, \mathbf{2}, 1/6)$: the "off-diagonal" $SU(5)$ gaugino λ, and the link field "inos" Φ_{2t} and $\bar{\Phi}_{3t}$. There are also three fields in the conjugate representation, $(\bar{\mathbf{3}}, \mathbf{2}, -1/6)$: $\bar{\lambda}$, $\bar{\Phi}_{3t}$ and Φ_{2t}. The mass matrix for these fields, before electroweak symmetry breaking (EWSB), is given in Table 3.3. Note that only Q_3 participates in the mixing due to the structure of the superpotential; more generally, we can always relabel the linear combination of the quark doublet fields which couples to $\Phi_3\bar{\Phi}_2$ as Q_3. Because the mass matrix has four columns but only three rows, there will always be a linear combination of Q-like fields which will

be massless at this level, acquiring a mass through ESWB only. We identify this field with the third generation quark doublet of the SM, Q_3^{SM}. The key idea of the CCT model is that for a certain range of parameters, Q_3^{SM} is predominantly the gaugino λ. If that's the case, top-loop contribution to the Higgs mass must be canceled by its superpartner, a spin-1 ("swan") gauge boson $\vec{Q}$. This occurs if [160]

$$
\begin{aligned}
M_5 &\ll \hat{g}_5 f_2, \quad \hat{g}_5 f_3 \ll \mu_3, \quad \hat{g}_5 f_3 \ll \hat{g}_5 \overline{f}_2, \\
\hat{g}_5 \overline{f}_2 &\ll \mu_2, \quad \hat{g}_5^2 \frac{f_2 \overline{f}_2}{M_5 \mu_2} \approx 1, \quad \hat{g}_5 \lesssim y_1.
\end{aligned}
\tag{3.5}
$$

We will assume throughout this paper that these conditions are realized. Another sector in which mixing occurs is the fields with the quantum numbers $(\overline{\mathbf{3}}, \mathbf{1}, -2/3)$: $\overline{u}$ and $\overline{T}$. One of their linear combinations gets a mass of order f, while the other remains massless until EWSB, and is identified with the SM right-handed top. Generating an order-one top Yukawa requires that the massless combination be predominantly $\overline{T}$; the condition for this is

$$
\mu_H \ll y_2 \overline{f}_3.
\tag{3.6}
$$

The dominant coupling of the SM top to the Higgs comes from the $SU(5)$ gaugino-sfermion-fermion interaction of the field $\overline{H}$:

$$
-\sqrt{2} \hat{g}_5 \overline{H}^* \left(-T^{a*} \lambda_5^a\right) \widetilde{\overline{H}} \supset \hat{g}_5 H_d^* \lambda \overline{T}.
\tag{3.7}
$$

Since $\hat{g}_5$ can be $O(1)$ while the other Yukawa couplings in Eq. (3.1) are suppressed by the ratio f/M_F, this explains the mass splitting between the top and the other quarks. The down-type third generation singlet is still $\overline{d}_3$, just like in the MSSM, so the bottom quark still gets its mass from the superpotential Yukawas. From now on we will assume that the gaugino fraction of the third generation doublet is very close to unity, i.e. $\langle Q_3^{SM} | \lambda \rangle \approx 1$. Note that this equality cannot be exact without forcing the bottom quark's mass to vanish since it is proportional to $\left| \langle Q_3^{SM} | Q_3 \rangle \right| \leq \sqrt{1 - \left| \langle Q_3^{SM} | \lambda \rangle \right|^2}$.

Still, assuming that the deviation of $\langle Q_3^{SM} | \lambda \rangle$ from unity is small, the gauge coupling $\hat{g}_5$ must satisfy

$$\hat{g}_5 = \frac{\sqrt{2} m_t}{v \cos \beta} \approx \sqrt{1 + \tan^2 \beta} \, , \tag{3.8}$$

where m_t is the top mass, $v = \sqrt{v_u^2 + v_d^2} = 246$ GeV, and β is defined through the usual MSSM relationship $\tan \beta \equiv v_u / v_d$. With this result, the first of Eqs. (3.3) uniquely fixes $\hat{g}_2$ and $\hat{g}_3$ in terms of $\tan \beta$, while the second one reduces to

$$\frac{1}{g_Y^2}(1 - \epsilon) = \frac{1}{\hat{g}_H^2} + \frac{1}{\hat{g}_V^2}, \tag{3.9}$$

where

$$\epsilon = \frac{g_Y^2}{15 \hat{g}_5^2} \approx \frac{8 \cdot 10^{-3}}{1 + \tan^2 \beta}. \tag{3.10}$$

Thus, requiring that the model reproduce the SM gauge couplings and the top Yukawa leaves only two independent parameters in the gauge sector: $\tan \beta$ and the $U(1)$-sector mixing angle

$$\theta = \arctan \left(\frac{\hat{g}_V}{\hat{g}_H} \right). \tag{3.11}$$

3.2.2 Gauge Boson Spectrum

The model contains several additional gauge bosons, which will be especially important for the analysis of this paper for two reasons. First, as already mentioned, one of them, the swan $\vec{Q}$, is largely responsible for canceling the quadratically divergent contribution of the SM top loop to the Higgs mass. Second, the extra $U(1)$ gauge bosons are responsible for the strongest experimental constraints on the model parameter space. The swan mass is given by

$$m_{\vec{Q}}^2 = \hat{g}_5^2 \left(\tilde{f}_2^2 + \tilde{f}_3^2 \right), \tag{3.12}$$
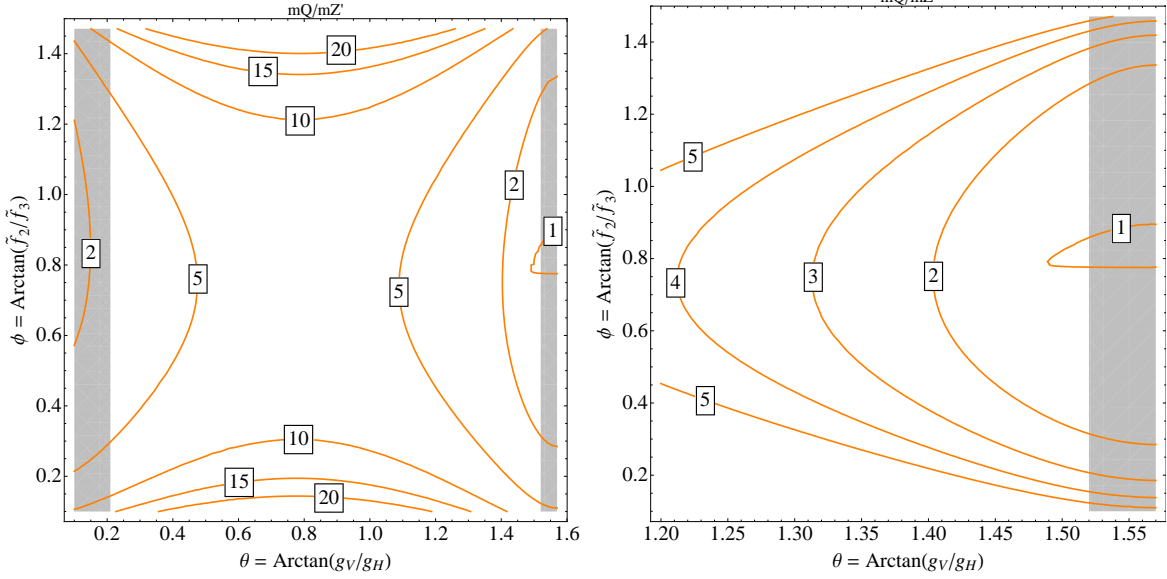
Figure 3.1: Ratio of the masses of the spin-1 top partner ("swan") and the lightest Z'. Left panel: full parameter space (gray regions indicate regions where one of the gauge couplings becomes non-perturbative). Right panel: the region where the ratio is minimized. In both plots, $\tan\beta = 0.95$; the ratio scales as $\sqrt{1 + \tan^2\beta}$.

where we defined

$$\widetilde{f}_{2,3} = \frac{f_{2,3}^2 + \bar{f}_{2,3}^2}{2}. \tag{3.13}$$

Requiring that the left-handed top quark is predominantly a gaugino requires $f_3 \ll \bar{f}_2$, as mentioned above; however, no particular hierarchy between $\bar{f}_3$ and f_2 is required, so the scales $\widetilde{f}_2$ and $\widetilde{f}_3$ are essentially independent parameters. We find it convenient to define

$$\widetilde{f} = \sqrt{\widetilde{f}_2^2 + \widetilde{f}_3^2}, \quad \phi = \arctan\frac{\widetilde{f}_2}{\widetilde{f}_3}. \tag{3.14}$$

With this notation, the swan mass is simply

$$m_{\tilde{Q}}^2 = \hat{g}_5^2 \widetilde{f}^2 \approx (1 + \tan^2\beta)\widetilde{f}^2. \tag{3.15}$$

The mass of the lightest extra $U(1)$ gauge boson, the Z', is given by

$$m_{Z'}^2 \approx 2g_Y^2 \frac{\csc^2 2\theta \sin^2 2\phi}{5 - \cos 2\phi} \, \widetilde{f}^2, \tag{3.16}$$

where corrections of order ϵ and $v^2/\widetilde{f}^2$ have been dropped. (The complete spectrum of the $U(1)$ gauge bosons is given in Appendix A.) Since $g_Y \approx 0.3$, the swan is generally significantly heavier that the Z'; see Fig. 3.1. We will see below that this results in very strong experimental lower bounds on the swan mass.

For completeness, we also list the masses of the heavy partners of the gluon and the charged W bosons:

$$m_{G'}^2 = 2\left(\hat{g}_3^2 + \hat{g}_5^2\right)\widetilde{f}_3^2 \approx \frac{2g_3^2(1 + \tan^2 \beta)\cos^2 \phi}{1 + \tan^2 \beta - g_3^3}\, \widetilde{f}^2, \tag{3.17}$$

$$m_{W'}^2 = 2\left(\hat{g}_2^2 + \hat{g}_5^2\right)\widetilde{f}_2^2 \approx \frac{2g_2^2(1 + \tan^2 \beta)\sin^2 \phi}{1 + \tan^2 \beta - g_2^3}\, \widetilde{f}^2. \tag{3.18}$$

3.2.3 Beta Functions and the Strong-Coupling Scale

The CCT model is an effective theory, since some of its gauge groups are not asymptotically free and their gauge couplings hit a Landau pole at a finite energy scale. At that scale, the model has to be either embedded into a larger structure, providing a UV completion, or else a non-perturbative description of the dynamics is required. Defining the one-loop beta function as

$$\beta_i \equiv \mu \frac{dg_i}{d\mu} = -\frac{g_i^3}{16\pi^2} b_i, \tag{3.19}$$

we find the coefficients

$$b_5 = 9 \ , b_3 = -2 \ , b_2 = -5 \ , b_H = -\frac{40}{3} \ , b_V = -\frac{3}{5} \ . \tag{3.20}$$

With the exception of $SU(5)$, all other factors in G are not asymptotically free. We estimate the strong-coupling scale Λ_i for each group with the condition $g_i(\Lambda_i) = \beta_i$, or equivalently $b_i g_i^2/(16\pi^2) = 1$; this yields

$$\Lambda_i = f_i \exp\left[\frac{2\pi}{|b_i|\alpha_i(f)} - \frac{1}{2}\right],\tag{3.21}$$

where f_i is the scale where the gauge group associated with each gauge coupling is broken.

The parameters in the gauge sector of the theory are restricted by perturbativity requirements. For the asymptotically free $SU(5)$ coupling, we demand $b_5 \hat{g}_5^2/(16\pi^2) \leq 1$ at the symmetry-breaking scale f; for the other couplings, we require $\Lambda_i/f \gtrsim 5$. This yields

$$0.8 \lesssim \tan\beta \lesssim 4.0, \quad 0.2 \lesssim \sin\theta \lesssim 0.99.\tag{3.22}$$

The bounds on $\tan\beta$ should be compared to the case of the MSSM, where the relationship analogous to Eq. (3.8) is $y_t = \frac{\sqrt{2}m_t}{v\sin\beta}$ and imposes only the much weaker constraints $0.3 \lesssim \tan\beta \lesssim 150$. The fact that $\tan\beta$ is constrained to lie close to 1 will tend to suppress the Higgs mass, since at tree-level and in the decoupling limit it is proportional to $\cos 2\beta$; this will be discussed in Section 3.5.

3.3   Precision Electroweak Constraints

As described in the previous section, the CCT model extends the SM gauge group and introduces additional R-even gauge bosons, W' and Z'. These gauge bosons generically mix with the SM Z and W, leading to deviations of their properties from the SM predictions. In addition, tree-level exchanges of W' and Z' induce effective four-fermion interactions not present in the SM. Such effects are tightly constrained by precision electroweak (PEW) measurements, which can be translated into restrictions

68
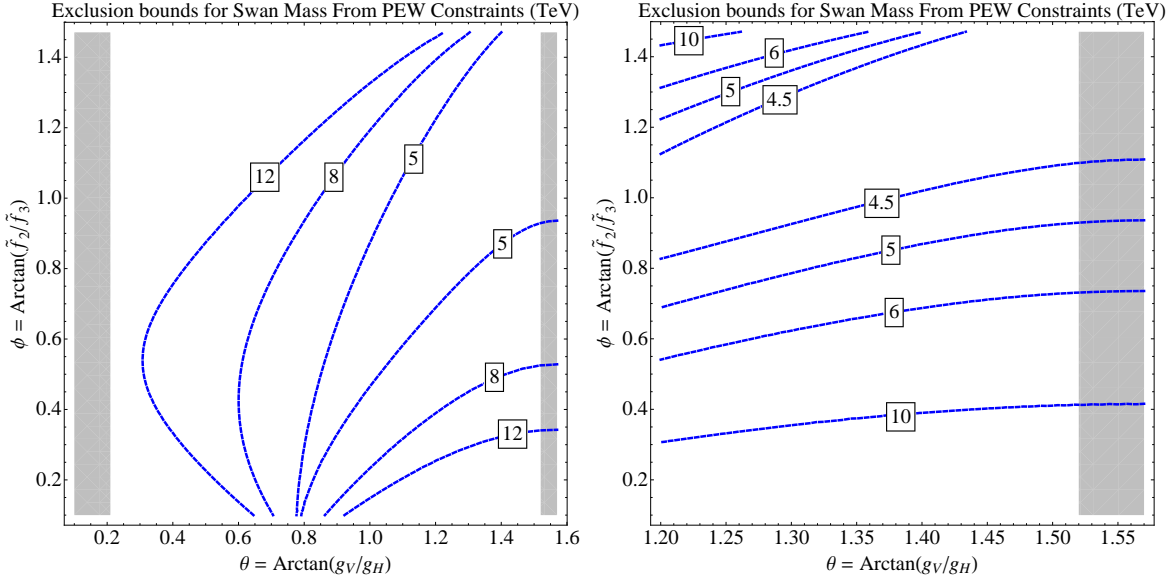
Figure 3.2: Lower bound on the swan mass (in TeV) from precision electroweak constraints. Left panel: full parameter space (gray regions indicate regions where one of the gauge couplings becomes non-perturbative). Right panel: the region where the constraint is minimized. In both plots, $\tan\beta = 0.95$; the bounds scale as $\sqrt{1 + \tan^2\beta}$.

on the parameter space of the CCT model. Before proceeding, let us note that while the CCT model predicts many new states at the TeV scale (see Table 3.2), it is easy to see that the PEW constraints are dominated by the W' and Z'. Most of the other fields do not contribute to PEW observables at tree level at all, either due to negative R-parity or, as in the case of vector-like fermions in the top sector and the heavy partner of the gluon, due to the structure of their couplings to the SM. The only states that do make a tree-level contribution are the scalars from link fields, which however only have suppressed couplings to light fermions of order v/M_F. We will ignore such contributions.

It is well known that the effect of Z' and W' bosons on PEW observables can be cast in terms of the oblique parameters S, T and U [211, 224–226]. Evaluating the

T parameter in the CCT model yields[1]

$$\alpha T = \left[\frac{3}{4} \frac{\left((1-\epsilon)\cos^2\theta + \epsilon\right)^2}{\cos^2\phi} + \frac{1}{8} \frac{\left((1-\epsilon)\cos 2\theta - 4\epsilon\right)^2}{\sin^2\phi} \right] \left(\frac{v}{\widetilde{f}}\right)^2. \qquad (3.23)$$

Both S and U parameters are not generated at order $(v/\widetilde{f})^2$. The leading contributions to these parameters, up to $\mathcal{O}(\epsilon)$ corrections, are given by

$$
\begin{aligned}
U &= \left(\frac{\cos^2\theta_W}{2\alpha}\right)\left(\frac{9\sin^2\theta\cos^6\theta}{2\cos^4\phi} + \frac{\sin^2 4\theta}{32\sin^4\phi} + \frac{3\sin^2\theta\cos 2\theta\cos^4\theta}{\sin^2\phi\cos^2\phi}\right)\left(\frac{v}{\widetilde{f}}\right)^4 ; \\
S &= -U - \frac{\sin^2\theta_W}{16\alpha}\frac{1}{\sin^4\phi}\, x\,(1+x)^{-3}\left(\frac{v}{\widetilde{f}}\right)^4 ,
\end{aligned}
\qquad (3.24)
$$

where $x = (g_2/\hat{g}_5)^2 \approx g_2^2(1+\tan^2\beta)^{-1}$.

The 95% c.l. PEW lower bound on the swan mass is shown in Figure 3.2. As expected, the bound is strongly dominated by the T parameter. (The current 95% c.l. bound on T, for $S \approx 0$, is $T \lesssim 0.12$ [228].) Here we fixed $\tan\beta = 0.95$, close to the low end of the allowed range; the bound is stronger for larger values of $\tan\beta$, scaling as $\sqrt{1+\tan^2\beta}$. We find that the lowest possible bound occurs when $\widetilde{f}_2 > \widetilde{f}_3$ and $\hat{g}_V \gg \hat{g}_H$, and it is roughly given by

$$m_{\tilde{Q}} \gtrsim 4.5\ \text{TeV}. \qquad (3.25)$$

Since swans need to be pair-produced in proton collisions due to their negative R-parity, this bound effectively puts them out of reach of the direct LHC searches. It also implies significant fine-tuning in the EWSB, as will be discussed in section 3.5.

Additional contributions to PEW observables may be generated by strongly-coupled physics in the ultraviolet (UV), and in a generic UV completion, the strong-coupling scale must be above ~ 10 TeV to avoid conflict with experiment. Bounds on the perturbative contribution to the T parameter, together with the parameter

---

[1]Oblique parameters in the CCT model have been previously computed in Ref. [227].

space constraints (3.22), ensure that such non-perturbative contributions are negligible throughout the viable parameter space, with the possible exception of the far upper-right corner of the plots in Fig. 3.2, where the $SU(3)$ gauge group may become strongly coupled below 10 TeV. Since $SU(3)$ is not part of the electroweak gauge group, this by itself does not imply additional contributions to PEW observables at the same scale; they may or may not be induced, depending on the nature of the UV completion. In any case, this caveat only affects a small corner of the parameter space, and the basic conclusions of the perturbative analysis remain valid.

3.4 Direct Searches at the LHC

Further bounds on the model parameter space come from direct searches at the LHC. Conventional SUSY searches place bounds on many of the R-odd states, which are also present in the MSSM spectrum. In the MSSM, assuming a spectrum with a weakly interacting lightest R-odd particle, and large mass gaps between this particle and colored R-odd states, current LHC bounds require $m_{\widetilde{G}} \gtrsim 1.2 - 1.4$ TeV for gluinos, $m_{\widetilde{Q}} \gtrsim 0.8$ TeV for squarks of first two generations, and $m_{\widetilde{t}} \gtrsim 0.7$ TeV for stops/sbottoms. The bounds in the CCT model can be modified due to the presence of additional states with the quantum numbers of gluinos and stops, $\widetilde{G}'$, $\widetilde{\widetilde{T}}$, and $\widetilde{\widetilde{T}}'$. These can induce additional cascade decays, strengthening the bounds somewhat; however, we do not expect a major qualitative change. It should also be noted that while the superpartner masses are generally expected to be at the scale f, the precise relation between them is model-dependent, since the details of SUSY breaking come into play. On the other hand, searches for the R-even states, in particular extra gauge bosons, in many cases have higher reach, since these states can be produced singly, and can be described in terms of just a small number of parameters, as explained in Section 3.2. With this motivation, we investigate these bounds in detail in this section.
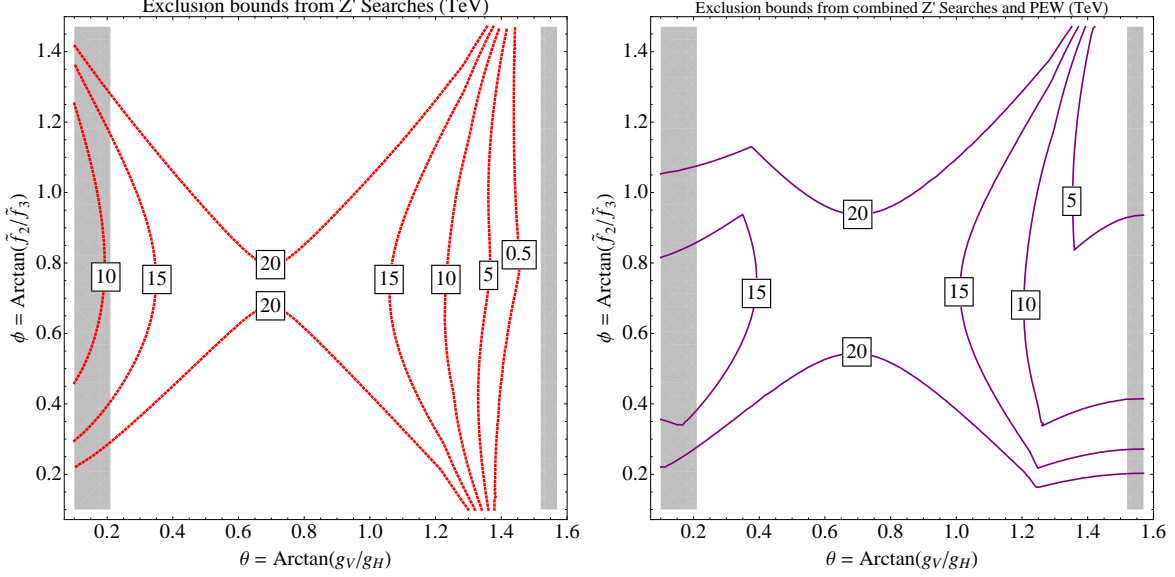
Figure 3.3: Lower bounds on the swan mass (in TeV) from direct searches for the Z' at the LHC (left panel) and the combination of direct search and precision electroweak constraint (right panel). In both plots, $\tan\beta = 0.95$; the bounds scale as $\sqrt{1 + \tan^2\beta}$.

The strongest bounds come from searches for Z' gauge bosons, in particular in the $Z' \to \mu^+\mu^-$ channel. We incorporated the relevant couplings of the CCT model (listed in Appendix 3.A) into the `MadGraph/MadEvent 5` event generator [229], and computed the cross section of the process $pp \to Z' \to \mu^+\mu^-$ at the $\sqrt{s} = 8$ TeV LHC as a function of the Z' mass. We then used the cross section bound presented by the CMS collaboration [230], based on the full 20 fb^{-1} data set collected at LHC-8, to constrain the model parameter space. The resulting bound on the swan mass, for $\tan\beta = 0.95$, is shown in Fig. 3.3 (left panel). (As for precision electroweak, the direct search bound on the swan mass scales as $\sqrt{1 + \tan^2\beta}$, so the bounds in Fig. 3.3 become stronger for larger $\tan\beta$.) Generically, the bounds on the swan mass are quite high, above 10 TeV in most of the parameter space. This is stronger than the PEW bound. However, the direct search bound is weakened significantly in the region $g_V \gg g_H$, where the Z' couplings to fermions are suppressed. In this region, the PEW constraint dominates; the combined bound from PEW and direct searches

is presented in Fig. 3.3 (right panel). Overall, the lowest bound on $m_{\tilde{Q}}$ found in the PEW analysis, about 4.5 TeV, remains unchanged.

In addition to Z', the model contains two more electrically neutral gauge bosons: Z'', the heaviest of the mass eigenstates composed of $U(1)_H$, $U(1)_V$ and T_{24} gauge bosons; and W'^3, the heavy mass eigenstate composed of the diagonal $SU(2)$ and $SU(2)' \in SU(5)$ gauge bosons. Since $\hat{g}_5$ is larger than the other gauge couplings, both Z'' and W'^3 are significantly heavier than the Z' throughout the parameter space. Furthermore, for the same reason, both Z'' and W'^3 are dominated by their $SU(5)$ components, and since light fermions are not charged under the $SU(5)$, their production cross sections are suppressed. As a result, we find that including these states in the analysis does not improve the bounds derived by considering only the lightest Z'. Likewise, massive electrically charged gauge bosons W' and color-octet gauge bosons G' do not yield relevant bounds.

3.5   Higgs Mass and EWSB Fine-Tuning

Just as in the MSSM, the superpotential of the CCT model, Eq. (3.1), does not contribute to the Higgs quartic coupling, and the D-term contribution by itself is far too small for compatibility with a 125 GeV Higgs. The quartic is enhanced by the RG evolution between the SUSY breaking scale Λ_{susy}, and the electroweak scale. To understand whether this enhancement is sufficient to produce a viable Higgs mass, we evolve the weak-scale Higgs quartic $\lambda(M_t)$, inferred from the data, up to the scale Λ_{susy}, and compare it with the SUSY prediction at that scale:[2]

$$\lambda_{\text{susy}} = \frac{g_2^2(\Lambda_{\text{susy}}) + g_Y^2(\Lambda_{\text{susy}})}{8} \cos^2 2\beta. \tag{3.26}$$

---

[2]Our normalization for λ is such that the Higgs scalar potential in $V = -m^2 H^\dagger H + \lambda(H^\dagger H)^2$, where H is the Higgs doublet field. In this normalization, $\lambda_{\text{SM}}(M_t) \approx 0.127$.
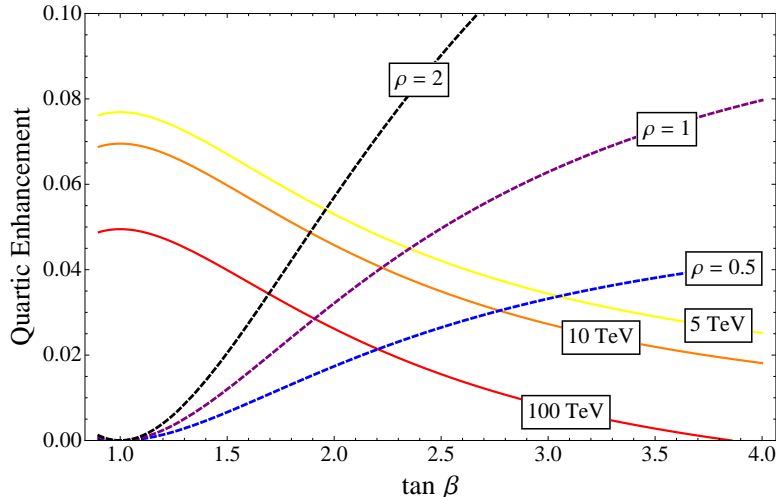
Figure 3.4: Solid lines: The difference δ between the value Higgs quartic $\lambda_{\mathrm{SM}}(\Lambda_{\mathrm{susy}})$ needed to accommodate the 125 GeV Higgs, and the value predicted by a SUSY theory with the SM gauge group. Top to bottom: $\Lambda_{\mathrm{susy}} = 5, 10, 100$ TeV. Dashed lines: The additional contribution to λ from non-decoupling D-terms possibly present in the CCT model. Top to bottom: $\rho = 2.0, 1.0, 0.5$. (For definition of ρ and other details, see Appendix 3.B.)

Assuming that all non-SM particles have masses at or above Λ_{susy}, we use the SM beta functions at two-loop order, and the values of SM couplings at the weak scale given in Ref. [231], to obtain $\lambda_{\mathrm{SM}}(\Lambda_{\mathrm{susy}})$. We find that accommodating the 125 GeV Higgs in the minimal CCT model, with no additional contributions to the quartic, requires

$$\Lambda_{\mathrm{susy}} \gtrsim 100 \text{ TeV}. \tag{3.27}$$

This is clearly a much stronger constraint than the experimental bounds considered above, and a model with such a high SUSY-breaking scale would require a very significant amount of fine-tuning: very roughly, fine-tuning can be estimated as $(v/\Lambda_{\mathrm{susy}})^2 \sim 10^{-6}$. Moreover, for $\tan\beta \approx 1.0$, which is preferred from the point of view of the PEW and direct constraints, a much higher SUSY-breaking scale is required, since λ_{susy} is suppressed.

However, simple extensions of the minimal setup can easily alleviate this tension.

For example, consider the scenario in which the gauge symmetry breaking occurs below the SUSY-breaking scale, $f_i < \Lambda_{\text{susy}}$. In this case, λ_{susy} receives additional contributions from the D-terms associated with non-SM gauge generators, the "non-decoupling D-terms" [232, 233]. The non-decoupling D-terms in the CCT model were considered in Ref. [227]. They can be obtained as follows. Introduce additional superfields $A_{2,3}$ (in the adjoint representations of $SU(2)$ and $SU(3)$, respectively) and $S_{2,3}$ (both singlets under G), with a superpotential[3]

$$W_{\text{new}} = \lambda_{S2}S_2\Phi_2\overline{\Phi}_2 + \lambda_{S3}S_3\Phi_3\overline{\Phi}_3 + \lambda_{A2}\overline{\Phi}_2 A_2^a \frac{\sigma^a}{2}\Phi_2 + \lambda_{A3}\overline{\Phi}_3 A_3^m G^m \Phi_3. \qquad (3.28)$$

When the link fields Φ and $\overline{\Phi}$ acquire vacuum expectation values, F-terms for S are generated, inducing "hard" F-term SUSY-breaking and prevent the complete decoupling of the ultraviolet D-terms. The UV value of the Higgs quartic is modified as follows:

$$\lambda_{\text{susy}}^{\text{NDDT}} = \frac{\Delta_2 g_2^2(\Lambda_{\text{susy}}) + \Delta_Y g_Y^2(\Lambda_{\text{susy}})}{8} \cos^2 2\beta, \qquad (3.29)$$

where Δ_2 and Δ_Y are order-one coefficients which can be calculated in terms of the superpotential couplings and soft SUSY-breaking terms. (For details, see Appendix 3.B.) In Fig. 3.4, we compare the size of the quartic correction required to accommodate a 125 GeV Higgs, defined as $\delta\lambda = \lambda_{\text{SM}}(\Lambda_{\text{susy}}) - \lambda_{\text{susy}}$, with the non-decoupling D-term contribution for reasonable model parameters. It is clear that the D-term contribution can easily be large enough to provide a viable model with Λ_{susy} in the $5 - 10$ TeV range. Thus, we conclude that in the presence of non-decoupling D-terms, the 125 GeV Higgs does not place constraints beyond those already known from PEW fits and direct searches. The required fine-tuning is roughly of order 10^{-3}. The only problematic region is around $\tan\beta = 1$, where all D-term contributions to quartic vanish as $\cos^2 2\beta$. In this region, either a much higher value of Λ_{susy}, or an

---

[3]Our model of the non-decoupling D-terms differs slightly from Ref. [227] in that we include soft mass terms in the scalar potential, allowing for a simpler field content and superpotential. For details, see Appendix 3.B.
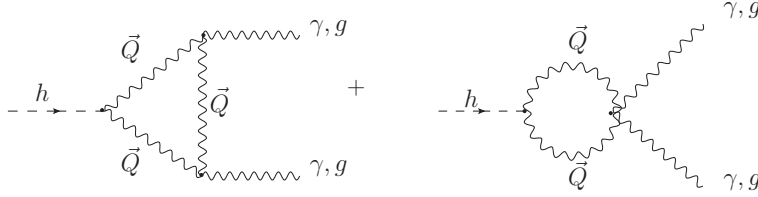
Figure 3.5: Swan contribution to Higgs couplings to gluons and photons, at the one-loop level.

alternative mechanism for raising the quartic (*e.g.* large threshold corrections), is required.

Note that the A fields introduced in this section will affect the β function coefficients, potentially shifting the location of Landau poles and modifying the constraints on the parameter space in Eq. (3.22). We find that the only effect this has is on the lower bound on $\tan \beta$, which is raised from 0.8 to 0.95. This does not have a significant effect on the precision electroweak and direct constraints on the model.

3.6   Higgs Couplings to Photons and Gluons

Following the discovery of the Higgs boson, a multi-year program to precisely measure the Higgs couplings is envisioned [234]. The upcoming LHC experiments as well as, hopefully, experiments at a next-generation electron-positron Higgs factory [235, 236], will be able to measure many Higgs couplings with precision of $\sim 1\%$ or better. It is therefore worthwhile to study deviations from the SM predicted by models of new physics at the TeV scale.

In the CCT model, the corrections to Higgs couplings are of two types. First, since the full structure of the MSSM is reproduced, the Higgs sector is extended to a two-Higgs doublet model, leading to tree-level shifts in the Higgs couplings to gauge bosons and fermions. These effects have been already comprehensively studied in the MSSM [237]. More interesting are the corrections from new particles running in loops.

In particular, it has been argued in Ref. [164, 174, 238, 239] that very generally, loops of top quark partners (*i.e.*, particles whose loops cancel the quadratic divergence in m_h^2 induced by the SM top loop) induce potentially observable shifts in the hgg and $h\gamma\gamma$ couplings.[4] The corrections from spin-0 and spin-1/2 top partners have been previously calculated. Here, we focus on the effect of the spin-1 top partner loops, shown in Fig. 3.5. We performed the calculation using the `Mathematica` implementation of the $h \to VV$ decay amplitudes for a generic gauge extension of the SM, described in [159] and available on the website `http://www.phy.syr.edu/ jhubisz/HIGGSDECAYS/`. To leading order in $(m_h/M_{\vec{Q}})^2$, we obtain the effective Lagrangian

$$\mathcal{L}_{h\gamma\gamma} = \frac{2\alpha}{9\pi v} C_\gamma h F_{\mu\nu} F^{\mu\nu}, \qquad \mathcal{L}_{hgg} = \frac{\alpha_s}{12\pi v} C_g h G^a_{\mu\nu} G^{a\mu\nu}, \qquad (3.30)$$

where F and G^a ($a = 1 \dots 8$) are the SM $U(1)$ and $SU(3)$ field strength tensors, respectively, and the Wilson coefficients are

$$C_g = C_\gamma = \frac{21}{4} \frac{\hat{g}_5^2 v^2}{m_{\vec{Q}}^2}. \qquad (3.31)$$

Here the normalization of C_g and C_γ is such that the SM top loop contribution, in the low-m_h limit, is 1. Note that, due to a large numerical coefficient, the swan induces a much larger deviation of the $hgg/h\gamma\gamma$ couplings from their SM values than either a spin-0 stop or a spin-1/2 top partner of the same mass. We find that even very strong bounds on the swan mass discussed above do not completely preclude a potentially observable deviation: a 5 TeV swan, at $\tan\beta = 1.0$, induces a fractional shift in the $hgg/h\gamma\gamma$ couplings of about 3%, which may be within a 3-sigma detection reach at the proposed e^+e^- Higgs factories.

The CCT model contains a large number of colored and/or electrically charged

---

[4]These two couplings are singled out because they are absent at tree level in the SM, making the new physics effects relatively more significant. Top partner loops may have other potentially observable effects, *e.g.* wavefunction renormalization corrections which may be measured in the $e^+e^- \to hZ$ process at Higgs factories [240].
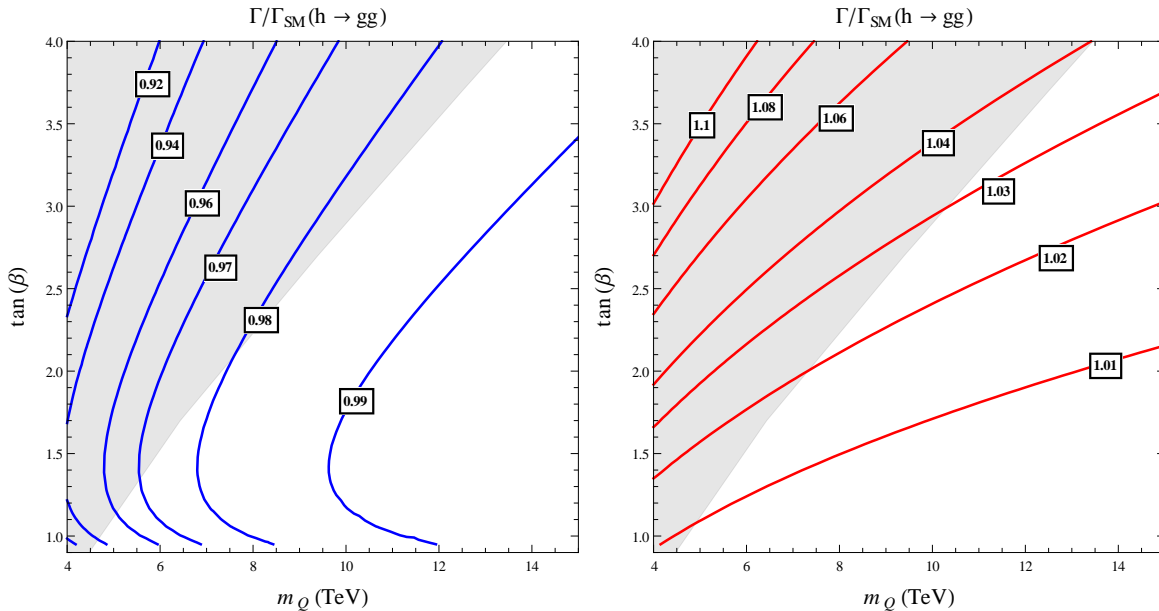
Figure 3.6: Fractional deviation in the hgg (left panel) and $h\gamma\gamma$ (right panel) couplings from the SM in the CCT model, as a function of the swan mass and $\tan\beta$. (See text for details on the values of other model parameters.) The shaded region is disfavored by precision electroweak constraints and direct LHC searches for a Z'.

states at the same mass scale as the swan, and loops of those particles will in general contribute to the coefficients C_g and C_γ, modifying the predictions (3.31). The contributions of scalars and fermions can be computed using the Higgs low energy theorems [207, 241], while the spin-1 states other than the swan can be treated using the results of [159]. A comprehensive analysis of these effects is complicated by the large dimensionality of the parameter space. We will not attempt such an analysis here; instead, we illustrate the typical size of the overall contribution to C_g and C_γ with a two-dimensional plot, Fig. 3.6, where we vary the swan mass and $\tan\beta$ and fix all other parameters. (All parameters with dimension of mass are fixed at the scale $m_{\vec{Q}}$, with mild hierarchies imposed in some cases to ensure that the conditions (3.5) are satisfied and an acceptable Higgs mass is generated through non-decoupling D-terms.) In this slice of the parameter space, we find that deviations in the hgg coupling of
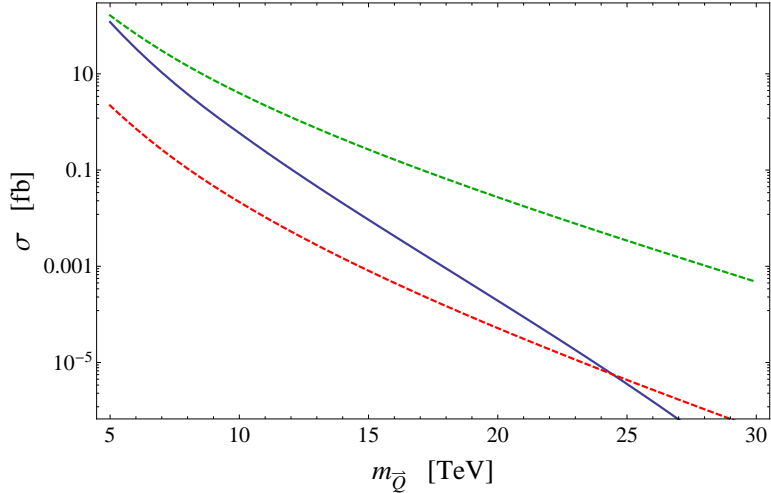
Figure 3.7: Swan production cross sections at a 100 TeV pp collider: $pp \to \vec{Q}\vec{Q}$ (blue), $\vec{Q}\widetilde{g}$ (green dashed), $\vec{Q}\widetilde{\chi}_1^0$ (red dashed).

about 5% are possible, while the maximum deviation in $h\gamma\gamma$ is about 4%. Such shifts may be within reach of the proposed e^+e^- Higgs factories.

3.7 Future Prospects for Direct Searches

Existing bounds on the swan mass, and the fact that swans must be pair-produced, preclude the possibility of direct swan production at the LHC. Of course, it may well happen that other particles in the CCT model, such as a Z' or some of the MSSM-like states, will be within the reach of the LHC-14. However, without a direct observation of the swan, it would be difficult to distinguish between this model and more conventional realizations of weak-scale supersymmetry. If a Z' is discovered, some indirect evidence can perhaps be obtained by measuring its couplings, which are predicted in the CCT model with few free parameters (see Appendix A). A much more direct and convincing test would have to await the direct discovery of the swan, and measurement of its spin. A next-generation pp collider with $\sqrt{s} = 100$ TeV, which is currently under discussion in the high-energy physics community, would

provide an opportunity for such a direct discovery. As a first step to an estimate of the potential of such a collider to search for swans, we computed the cross sections of swan pair-production, along with associated production with a gluino $\widetilde{g}$ and a neutralino $\widetilde{\chi}_1^0$. The analytic formulas for parton-level cross sections are collected in Appendix C. The cross sections for 100 TeV pp collisions are plotted in Fig. 3.7. Here we assumed $m_{\widetilde{g}} = 1$ TeV and $m_{\widetilde{\chi}_1^0} = 0.5$ TeV; the plotted associated production cross sections represent the maximum possible values, and would decrease if $m_{\widetilde{g}}/m_{\widetilde{\chi}_1^0}$ are increased. We used the NNPDF2.3 NNLO parton distribution functions [242], including top quark pdf's for associated production, and set the renormalization/factorization scale to $Q^2 = (10 \text{ TeV})^2$. It is interesting to note that the large associated production cross sections are due to appreciable b and t content in the proton at this scale.

Swans within a broad mass range will be copiously produced in 100 TeV pp collisions. For example, if 3000 fb^{-1} of data is collected (the integrated luminosity assumed in the Snowmass study [243]), we expect that $\gtrsim \mathcal{O}(100)$ swans would be produced in pair-production up to $m_{\vec{Q}} \approx 15$ TeV, and in association with gluinos up to $m_{\vec{Q}} \approx 25$ TeV (assuming $m_{\widetilde{g}} \ll m_{\vec{Q}}$). This suggests that direct reach of such an experiment for swan discovery can potentially extend into $10 - 20$ TeV domain, although the actual reach depends on the swan decay chains, which will determine relevant backgrounds, kinematic cuts, *etc.* Once a swan is produced, its spin could be determined using the techniques proposed for top partner spin determination at the LHC, see e.g. [244]. Thus, a 100 TeV collider may be capable of directly demonstrating the existence of a spin-1 top partner.

3.8 Conclusions and Outlook

In this paper, we considered the phenomenology of the Cai-Cheng-Terning (CCT) model, in which the superpartner of the (left-handed) SM top quark is the spin-1 particle, the "swan". Our main result is that existing constraints from precision

electroweak fits and direct LHC searches for a Z' place a very strong bound on the swan mass, which is required to be above at least 4.5 TeV, and in fact above 10 TeV in most of the parameter space. The primary reason for this bound is the tight relation between the swan mass and the mass of a neutral, R-even Z' boson, which is tightly constrained. The masses of the two bosons arise from the same symmetry breaking, and the structure of the gauge couplings of the CCT model induces an additional hierarchy, typically of a factor $5 - 10$, between the swan and Z' masses.

The tight bounds on the swan mass imply that the models of this type would need to be quite fine-tuned if realized in nature, making them less appealing. It also precludes the possibility of a direct swan discovery at the LHC. It is interesting to note, however, that neither conclusion would hold in a model with a spin-1 top partner *not* accompanied a Z' whose mass arises from the same symmetry breaking, or in a model where a Z' is odd under an R parity. It would be interesting to construct such models. Even if a complete model proves hard to build, a phenomenological model with these features, analogous to minimal set-ups used for the spin-0 top partner ("natural SUSY" [95, 245]) and the spin-1/2 top partner (see *e.g.* [246]), would be potentially quite useful.

Field	Spin	$SU(3)_c$	$SU(2)_L$	$U(1)_Y$	R-Parity	UV Multiplet	Mass Scale
$\Phi_{3S}, \overline{\Phi}_{3S}$ $\Phi_{2S}, \overline{\Phi}_{2S}$	0	**1**	**1**	0	+1	$\Phi_i, \overline{\Phi}_i$	f
$\Phi_{3A}, \overline{\Phi}_{3A}$	0	**Adj**	**1**	0	+1	$\Phi_3, \overline{\Phi}_3$	f
$\Phi_{2A}, \overline{\Phi}_{2A}$	0	**1**	**Adj**	0	+1	$\Phi_2, \overline{\Phi}_2$	f
$\widetilde{\overline{\Phi}}_{3t}, \widetilde{\overline{\Phi}}_{2t}$	0	**3**	**2**	1/6	-1	$\Phi_2, \overline{\Phi}_3$	f
$\widetilde{\Phi}_{3t}, \widetilde{\overline{\overline{\Phi}}}_{2t}$	0	**$\overline{3}$**	**2**	-1/6	-1	$\Phi_3, \overline{\Phi}_2$	f
$\widetilde{\Phi}_{3S}, \widetilde{\overline{\Phi}}_{3S}$ $\widetilde{\Phi}_{2S}, \widetilde{\overline{\Phi}}_{2S}$	1/2	**1**	**1**	0	-1	$\Phi_i, \overline{\Phi}_i$	f
$\widetilde{\Phi}_{3A}, \widetilde{\overline{\Phi}}_{3A}$	1/2	**Adj**	**1**	0	-1	$\Phi_3, \overline{\Phi}_3$	f
$\widetilde{\Phi}_{2A}, \widetilde{\overline{\Phi}}_{2A}$	1/2	**1**	**Adj**	0	-1	$\Phi_2, \overline{\Phi}_2$	f
$\overline{\Phi}_{3t}, \Phi_{2t}$	1/2	**3**	**2**	1/6	+1	$\Phi_2, \overline{\Phi}_3$	f
$\Phi_{3t}, \overline{\Phi}_{2t}$	1/2	**$\overline{3}$**	**2**	-1/6	+1	$\Phi_3, \overline{\Phi}_2$	f
$\widetilde{\overline{T}}$	0	**$\overline{3}$**	**1**	-2/3	-1	$\overline{H}$	f
$\widetilde{\overline{T^c}}$	0	**3**	**1**	2/3	-1	H	f
$\overline{T}$	1/2	**$\overline{3}$**	**1**	-2/3	+1	$\overline{H}$	v
$\overline{T^c}$	1/2	**3**	**1**	2/3	+1	H	f
λ	1/2	**3**	**2**	1/6	+1	$SU(5)$ gauginos	v
$\overline{\lambda}$	1/2	**$\overline{3}$**	**2**	-1/6	+1	$SU(5)$ gauginos	f
$\widetilde{W}'$	1/2	**1**	**Adj**	0	-1	$SU(2)$, $SU(5)$ gauginos	f
$\widetilde{G}'$	1/2	**Adj**	**1**	0	-1	$SU(3)$, $SU(5)$ gauginos	f
$\widetilde{B}', \widetilde{B}''$	1/2	**1**	**1**	0	-1	$U(1)_H$, $U(1)_V$, $SU(5)$ gauginos	f
W'	1	**1**	**Adj**	0	+1	$SU(2)$, $SU(5)$ gauge fields	f
G'	1	**Adj**	**1**	0	+1	$SU(3)$, $SU(5)$ gauge fields	f
Z', Z''	1	**1**	**1**	0	+1	$U(1)_H$, $U(1)_V$, $SU(5)$ gauge fields	f
$\vec{Q}$	1	**3**	**2**	1/6	-1	$SU(5)$ gauge fields	f

Table 3.2: Field content after the UV symmetry breaking; all entries with spin 0 correspond to complex scalar fields. The MSSM fields are not included in this table.

	λ	Φ_{2t}	$\overline{\Phi_{3t}}$	Q_3
$\overline{\lambda}$	M_5	$\hat{g}_5 f_2$	$\hat{g}_5 \overline{f}_3$	0
Φ_{3t}	$\hat{g}_5 f_3$	0	μ_3	$y_1 \overline{f}_2$
$\overline{\Phi}_{2t}$	$\hat{g}_5 \overline{f}_2$	μ_2	0	$y_1 f_3$

Table 3.3: Mass matrix for fermions in the $(\mathbf{3}, \mathbf{2}, 1/6)$ (and conjugate) sector.

Appendix

3.A Masses and Couplings of Z' States

Compared to the MSSM, this model possesses three additional neutral, massive gauge bosons. Two of them are linear combinations of the UV gauge fields B_H, B_V, B_{24} obtained by diagonalizing the following quadratic terms:

$$6\widetilde{f}_3^2 \left(\frac{\hat{g}_H}{6} B_H - \frac{\hat{g}_V}{10} B_V - \frac{\hat{g}_5}{\sqrt{15}} B_{24} \right)^2 + 4\widetilde{f}_2^2 \left(\frac{\hat{g}_V}{10} B_V - \frac{\sqrt{15}}{10} \hat{g}_5 B_{24} \right)^2 . \qquad (3.32)$$

The massless linear combination $B \equiv \frac{g_Y}{\hat{g}_H} B_H + \frac{g_Y}{\hat{g}_V} B_V + \frac{g_Y}{\sqrt{15}\hat{g}_5} B_{24}$ will be the gauge boson of the SM $U(1)_Y$ group; we refer to the other two eigenstates with non-vanishing masses as the Z' and Z'', in ascending order of masses. As discussed in section 3.2, it is convenient to re-express the parameters $\hat{g}_H$, $\hat{g}_V$, $\hat{g}_5$, $\widetilde{f}_2$, and $\widetilde{f}_3$ in terms of $\epsilon \equiv g_Y^2/15\hat{g}_5^2$, $\theta \equiv \arctan(\hat{g}_V/\hat{g}_H)$, $\widetilde{f}^2 \equiv \widetilde{f}_2^2 + \widetilde{f}_3^2$ and $\phi \equiv \arctan\left(\widetilde{f}_2/\widetilde{f}_3\right)$. In this parameterization, the mass of the Z' and Z'' can be written as:

$$m_{Z',Z''}^2 = \frac{m_{\widetilde{Q}}^2}{20(1-\epsilon)} \left(A(\epsilon, \theta, \phi) \mp \sqrt{B(\epsilon, \theta, \phi)} \right) , \qquad (3.33)$$

where $m_{\widetilde{Q}}^2$ is the squared mass of the swan and the A, B functions are given by:

$$A(\epsilon, \theta, \phi) \equiv 50\epsilon \csc^2 \theta \cos^2 \phi + 3\epsilon \sec^2 \theta \left(\cos 2\phi + 5 \right) - 2\left(1 - \epsilon\right)\left(\cos 2\phi - 5 \right) , \quad (3.34)$$

and,

$$
\begin{aligned}
B(\epsilon, \theta, \phi) \ \equiv \ & 2500\epsilon^2 \csc^4\theta \cos^4\phi + 9\epsilon^2 \sec^4\theta \left(\cos 2\phi + 5\right)^2 \\
+ \ & 100\epsilon \csc^2\theta \cos^2\phi \left(5\left(\epsilon + 2\right)\cos 2\phi + 5\epsilon - 2\right) \\
+ \ & 3\epsilon \sec^2\theta \left(300\epsilon \cos 2\phi + \left(27\epsilon + 98\right)\cos 4\phi + 177\epsilon - 2\right) \ . \quad (3.35)
\end{aligned}
$$

Since ϵ is typically $O(5) \times 10^{-3}$ (see Eq. (3.10)), we can obtain much simpler formulas by expanding to $O(\epsilon)$, in which case we can write the Z' mass as:

$$
m_{Z'}^2 \approx 30 m_{\tilde{Q}}^2 \epsilon \frac{\csc^2 2\theta \sin^2 2\phi}{5 - \cos 2\phi} = 2g_Y^2 \frac{\csc^2 2\theta \sin^2 2\phi}{5 - \cos 2\phi} \widetilde{f}^2, \qquad (3.36)
$$

where the second equality was obtained by using $m_{\tilde{Q}}^2 = \hat{g}_5^2 \widetilde{f}^2$ and the definition of ϵ. For the Z'', we have:

$$
m_{Z''}^2 \approx m_{\tilde{Q}}^2 \left(\frac{5 - \cos 2\phi}{5}\right) + O(\epsilon) \ . \qquad (3.37)
$$

The couplings of the Z' to the light fermions of the SM will be given by

$$
g_{Z'\bar{f}f} = \hat{g}_H \langle Z'|B_H \rangle \left(Q - T_3\right) \ , \qquad (3.38)
$$

where $\langle Z'|B_H \rangle$ is the amount of B_H contained in the Z' mass eigenstates. The couplings of the Z'' follows an analogous formula, with the replacement of $\langle Z'|B_H \rangle$ by $\langle Z''|B_H \rangle$. While explicit formulas for these coefficients are straightforward to compute, they are cumbersome and unenlightening. We note, however, that $\hat{g}_H \langle Z'|B_H \rangle = \frac{|g_Y \tan^{-1}\theta|}{\sqrt{15}} + O(\epsilon)$, which indicates that the Z' decouples from the light SM fermions in the large $\tan\theta$ region; this explains why the bounds on the Z' mass are weakest in this region of Fig. 3.3. The couplings of the Z' and Z'' to the third generation quarks will be different from Eq. (3.38) because these fermions are charged differently under

the UV gauge group[5]. The coupling to the right-handed top is

$$g_{Z'\bar{t}_R t_R} = \frac{1}{2}\hat{g}_H \langle Z'|B_H \rangle - \frac{1}{10}\hat{g}_V \langle Z'|B_V \rangle - \frac{1}{\sqrt{15}}\hat{g}_5 \langle Z'|B_{24} \rangle \ , \qquad (3.39)$$

while the coupling to the third generation doublet of the SM, $Q_L^3 = (t_L, b_L)$ is

$$g_{Z'\bar{Q}_L^3 Q_L^3} = \sqrt{\frac{5}{12}}\hat{g}_5 \langle Z'|B_{24} \rangle \ . \qquad (3.40)$$

The couplings of the Z'' can once again be obtained by replacing $\langle Z'|B_i \rangle$ by $\langle Z''|B_i \rangle$ in the above.

3.B   Non-Decoupling D-Terms

The non-decoupling D-terms coefficients Δ_2 and Δ_Y were introduced in Section 3.5 as a way of enhancing the tree-level quartic of the Higgs at the scale Λ_{susy} to obtain the observed Higgs mass. (Non-decoupling D-terms in the CCT model were previously discussed in Ref. [227].) Here we outline the derivation of these coefficients.

Combining the superpotential terms of Eqs. 3.1 and 3.28 to the usual soft SUSY breaking terms, we obtain the following potential for the link fields:

$$\begin{aligned}
V_{link} &= \left(\mu_2^2 + m_2^2\right)\Phi_2\Phi_2^* + \left(\mu_2^2 + \overline{m}_2^2\right)\overline{\Phi}_2\overline{\Phi}_2^* + \left(\mu_3^2 + m_3^2\right)\Phi_3\Phi_3^* + \left(\mu_3^2 + \overline{m}_3^2\right)\overline{\Phi}_3\overline{\Phi}_3^* \\
&- b_2\left(\Phi_2\overline{\Phi}_2 + c.c.\right) - b_3\left(\Phi_3\overline{\Phi}_3 + c.c.\right) + y_1^2|\Phi_3\overline{\Phi}_2|^2 + \lambda_{S2}^2|\Phi_2\overline{\Phi}_2|^2 + \lambda_{S3}^2|\Phi_3\overline{\Phi}_3|^2 \\
&+ \lambda_{A2}^2|\overline{\Phi}_2^a\frac{\sigma^a}{2}\Phi_2|^2 + \lambda_{A3}^2|\overline{\Phi}_3^m G^m \Phi_3|^2 + (\text{D} - \text{terms}) \ .
\end{aligned} \qquad (3.41)$$

Though the soft SUSY-breaking masses m_i^2 and $\overline{m}_i^2$ can in principle be independent from one another, we will make the simplifying assumption that they are identical. Note however that while this assumption greatly simplifies the following analysis, the theory possesses no symmetry that could make this equality exact and stable under

---

[5]The exception is the right-handed bottom quark b_R, whose coupling to the Z' follows Eq. (3.38)

radiative corrections, even if it is approximately realized at the messenger scale. Under this assumption then, we can derive simple formulas for the vevs from Eq. (3.41):

$$f_2^2 = \bar{f}_2^2 = \frac{b_2 - (\mu_2^2 + m_2^2)}{2\lambda_{S2}^2} \ ,$$
$$f_3^2 = \bar{f}_3^2 = \frac{b_3 - (\mu_3^2 + m_3^2)}{3\lambda_{S3}^2} \ . \tag{3.42}$$

We can shift the link fields by these vevs in Eq. (3.41) and compute the mass spectrum for the scalar components of the link sector. It is convenient to invert the formulas for the masses to express the parameters of the potential in terms of more physical quantities: the vevs f_2 and f_3, the masses of the two CP-odd singlets $m_{O_{2,3}}^2$, and the masses of the two CP-even singlets $m_{E_{2,3}}^2$. The relationship between the masses and the parameters of the potential in Eq. (3.41) is:

$$m_{O_{2,3}}^2 = 2b_{2,3} \ , \tag{3.43}$$
$$m_{E_2}^2 = 4f_2^2\lambda_{S2}^2 \ , \tag{3.44}$$
$$m_{E_3}^2 = 6f_3^2\lambda_{S3}^2 \ . \tag{3.45}$$

The effect of the aforementioned non-decoupling D-terms on the low-energy Higgs potential can be obtained by integrating out at tree-level the scalar fields that possess trilinear coupling to the Higgs bilinears. This will effectively modify the low-energy Higgs potential through the substitutions $g_Y \to \Delta_Y g_Y$, $g_2 \to \Delta_2 g_2$, where:

$$\Delta_2 = \left(1 + \frac{\rho_2}{2\hat{g}_2^2}\right) \times \left(1 + \frac{\rho_2}{2\left(\hat{g}_5^2 + \hat{g}_2^2\right)}\right)^{-1} \ ,$$
$$\Delta_Y = \frac{1 + N_2\rho_2 + N_3\rho_3 + N_{23}\rho_2\rho_3}{1 + D_2\rho_2 + D_3\rho_3 + D_{23}\rho_2\rho_3} \ , \tag{3.46}$$

with

$$\rho_2 \equiv \frac{m_{O2}^2 - m_{E2}^2}{f_2^2} = 2\left(\frac{m_2^2 + \mu_2^2}{f_2^2}\right) , \qquad \rho_3 \equiv \frac{m_{O3}^2 - m_{E3}^2}{f_3^2} = 2\left(\frac{m_3^2 + \mu_3^2}{f_3^2}\right) , \tag{3.47}$$

and the various $N_i(\theta, \epsilon)$, $D_i(\theta, \epsilon)$ coefficient functions are:

$$
\begin{aligned}
N_2(\theta, \epsilon) &\equiv \left(\frac{1 + 15\epsilon}{2g_Y^2} \right) , \\
N_3(\theta, \epsilon) &\equiv 3 \left(\frac{\epsilon \sin^2 \theta + \cos^2 \theta}{g_Y^2} \right) , \\
N_{23}(\theta, \epsilon) &\equiv 3 \left(\frac{(1 - \epsilon) \sin^2 \theta \cos^2 \theta \left(1 + \epsilon \tan^2 \theta + 25\epsilon \csc^2 \theta\right)}{2g_Y^4} \right) , \\
D_2(\theta, \epsilon) &\equiv \left(\frac{(1 - \epsilon)(1 + 33\epsilon + 16\epsilon \cos 2\theta - (1 - \epsilon) \cos 4\theta)}{4g_Y^2} \right) , \\
D_3(\theta, \epsilon) &\equiv \left(\frac{3(1 - \epsilon) \sin^2 2\theta \left(1 + \epsilon \tan^2 \theta\right)}{4g_Y^2} \right) , \\
D_{23}(\theta, \epsilon) &\equiv \left(\frac{75(1 - \epsilon)^2 \epsilon \sin^2 2\theta}{8g_Y^4} \right) .
\end{aligned}
\tag{3.48}
$$

3.C   Parton-Level Cross Sections for Swan Production

In this Appendix, we list the formulas for parton-level cross sections of swan production in pp collisions. For swan pair-production, we find

$$
\begin{aligned}
\frac{d\sigma(gg \to \vec{Q}\bar{\vec{Q}})}{d\cos(\theta)} = \ &\frac{g_3^4}{16\pi s} \sqrt{1 - \frac{4m_{\vec{Q}}^2}{s}} \Bigg[4 + \frac{9\left(m_{\vec{Q}}^4 + m_{\vec{Q}}^2 s - tu\right)}{4s^2} + \frac{6m_{\vec{Q}}^4 + 2s^2}{3\left(t - m_{\vec{Q}}^2\right)^2} \\
&+ \frac{6m_{\vec{Q}}^4 + 2s^2}{3\left(u - m_{\vec{Q}}^2\right)^2} - \frac{\left(m_{\vec{Q}}^2 + s\right)\left(m_{\vec{Q}}^2 + 3s\right)}{2s\left(m_{\vec{Q}}^2 - u\right)} - \frac{\left(m_{\vec{Q}}^2 + s\right)\left(m_{\vec{Q}}^2 + 3s\right)}{2s\left(t - m_{\vec{Q}}^2\right)} \Bigg]
\end{aligned}
\tag{3.49}
$$

The quark-initiated contribution to swan pair-production is negligibly small in the relevant swan mass range. The associated swan-gluino production cross section is

$$
\frac{d\sigma(g t_L \to \vec{Q}\widetilde{G})}{d\cos(\theta)} = \frac{g_3^2 \hat{g}_5^2 \cos(\theta_{\widetilde{G}})^2}{16\pi s^2} \sqrt{\left(s - m_{\widetilde{G}}^2 - m_{\vec{Q}}^2\right)^2 - 4m_{\widetilde{G}}^2 m_{\vec{Q}}^2} \left[\frac{4m_{\vec{Q}}^4 - m_{\widetilde{G}}^4 - u\left(m_{\widetilde{G}}^2 + 2m_{\vec{Q}}^2\right)}{9m_{\vec{Q}}^2 s} \right.
$$
$$
+ \frac{4s^2 + 4m_{\vec{Q}}^4 - 2m_{\widetilde{G}}^4 - 2m_{\widetilde{G}}^2 m_{\vec{Q}}^2}{9\left(t - m_{\vec{Q}}^2\right)^2} + \frac{2m_{\widetilde{G}}^2 m_{\vec{Q}}^4 - m_{\widetilde{G}}^6 - m_{\widetilde{G}}^4 m_{\vec{Q}}^2}{2m_{\vec{Q}}^2\left(u - m_{\widetilde{G}}^2\right)^2} - \frac{1}{18} - \frac{m_{\widetilde{G}}^2}{4m_{\vec{Q}}^2}
$$
$$
- \frac{2m_{\vec{Q}}^2 s^2 - 4s\left(2m_{\vec{Q}}^4 - m_{\widetilde{G}}^4 - m_{\widetilde{G}}^2 m_{\vec{Q}}^2\right) - 4m_{\widetilde{G}}^6 - 9m_{\widetilde{G}}^4 m_{\vec{Q}}^2 + 3m_{\widetilde{G}}^2 m_{\vec{Q}}^4 + 10m_{\vec{Q}}^6}{18m_{\vec{Q}}^2 s\left(t - m_{\vec{Q}}^2\right)}
$$
$$
\left. + \frac{\left(m_{\widetilde{G}}^2 + 2m_{\vec{Q}}^2\right)\left(s^2 - 2s\left(m_{\vec{Q}}^2 - m_{\widetilde{G}}^2\right) - 2m_{\widetilde{G}}^2 m_{\vec{Q}}^2 + 2m_{\vec{Q}}^4\right)}{4m_{\vec{Q}}^2 s\left(m_{\widetilde{G}}^2 - u\right)} \right], \tag{3.50}
$$

where $\cos(\theta_{\widetilde{G}})$ is the overlap of the gaugino being produced with the $SU(5)$ gaugino. (In Fig. 3.7, we assumed that the mixing angle for gauginos and corresponding gauge bosons are aligned.) Finally, the associated swan-neutralino production cross section is

$$
\frac{d\sigma(g t_L \to \vec{Q}\widetilde{N})}{d\cos(\theta)} = \frac{g_3^2 \hat{g}_5^2 \cos(\theta_{\widetilde{N}})^2}{16\pi s^2} \sqrt{\left(s - m_{\widetilde{N}}^2 - m_{\vec{Q}}^2\right)^2 - 4m_{\widetilde{N}}^2 m_{\vec{Q}}^2} \left[\frac{1}{4} + \frac{m_{\widetilde{N}}^2}{24m_{\vec{Q}}^2} + \right.
$$
$$
+ \frac{t\left(m_{\widetilde{N}}^2 + 2m_{\vec{Q}}^2\right) - 3m_{\widetilde{N}}^2 m_{\vec{Q}}^2 + 2m_{\vec{Q}}^4 - 2m_{\widetilde{N}}^4}{24m_{\vec{Q}}^2 s} + \frac{2s^2 + 2m_{\vec{Q}}^4 - m_{\widetilde{N}}^4 - m_{\widetilde{N}}^2 m_{\vec{Q}}^2}{12\left(t - m_{\vec{Q}}^2\right)^2}
$$
$$
\left. + \frac{4m_{\vec{Q}}^2 s^2 + s\left(2m_{\vec{Q}}^4 - m_{\widetilde{N}}^4 - m_{\widetilde{N}}^2 m_{\vec{Q}}^2\right) - 3m_{\widetilde{N}}^2 m_{\vec{Q}}^4 + 2m_{\vec{Q}}^6 + m_{\widetilde{N}}^6}{12m_{\vec{Q}}^2 s\left(t - m_{\vec{Q}}^2\right)} \right]. \tag{3.51}
$$

Chapter 4

Split SUSY in context of High Scale Inflation

4.1 Introduction

Supersymmetry (SUSY) has long been a favorite theoretical framework of physics beyond the Standard Model (SM). However, given the current null results of all SUSY searches, if SUSY is realized in Nature, it is unclear at what scale it will manifest itself. At the moment, theoretical studies of SUSY fall into two broad catalogues: one direction is to still focus on weak-scale natural SUSY and design non-trivial structures of flavor and Higgs sectors to evade the direct search constraints and explain the observed Higgs mass. The other direction is take seriously high-scale fine-tuned SUSY, in particular, split SUSY, with scalars heavier than gauginos. The virtues of this approach include simplicity, automatic amelioration of SUSY flavor and CP problems, preservation of gauge coupling unification and the lightest neutralino being a dark matter (DM) candidate. The idea of split SUSY, in particular, mini-split with scalars one-loop factor heavier than gauginos, was actually predicted a while ago by the simplest version of anomaly mediation [247, 248] (and later by a wide variety of moduli mediation scenarios [249–254]). Since 2003, split SUSY has

started to be taken as a viable possibility despite the presence of a fine-tuned EWSB and gained more attention recently given the increasing tension between data and naturalness [98–101, 253–261].

In split SUSY, the high SUSY breaking scale could naturally lead to a heavy unstable gravitino. In the mini-split scenario based on anomaly mediation, there is a loop factor separating the gravitino and gaugino mass scales with gravitino at about $(10^2 - 10^3)$ TeV and gaugino at the TeV scale. In this scenario, the neutralino DM particles produced by late-time gravitino decays could not annihilate efficiently and thus inherit the number density of the gravitinos which adds to its thermal number density. During the reheating era, the thermal scattering of the SM superpartners contributes (at least part of) the gravitino primordial relic abundance, which is approximately proportional to the reheating temperature T_R. Consequently the requirement that the neutralino DM does not overclose the Universe sets an interesting upper bound on T_R as a function of DM mass. This upper bound could be tightened if wino is (a component of) DM. Indirect detection looking for excesses in the photon continuum spectrum or a monochromatic photon line sets a strong bound on allowed wino DM relic abundance for the whole mass range assuming NFW or Einasto DM profiles [262, 263]. The bound could be relaxed if the Milky Way DM distribution near the galactic center deviates considerably from the standard DM-only N-body simulation predications. However, the bound does not necessarily disappear entirely. For example, even if the Milky Way DM profile has a significant core with a radius of 1 kpc, light non-thermal wino with mass below 400 GeV as a single-component DM is excluded [263]. We will present the derivation of the upper bound on T_R from the constraints of the relic abundance of neutralino DM, in particular, wino DM in Sec. 4.2 and Sec. 4.3.

On the other hand, the we have the combined BiCEP/Keck Arrary and Planck analysis [264]. The observation could be fit by a lensed ΛCDM plus tensor model with a tensor-to-scalar ratio $r < 0.1(95\%CL.)$. Such a large r prefers large field inflation

with a heavy inflaton and very likely a high reheating temperature. We will present estimates of inflaton mass scale and reheating temperature in Sec. 4.4.

We find that in the mini-split scenario based on anomaly mediation, T_R is bounded to be at or below $10^9 - 10^{10}$ GeV while the Planck-BICEP2 joint data analysis prefers T_R to be around or above 10^9 GeV. Thus comological observations has some tension with the mini-split scenario with a heavy gravitino. In other words, the Planck-BICEP result favors a splitting between gravitinos and gauginos larger than the loop factor predicted by anomaly mediation. Intriguingly, if SUSY breaking is tied up with gravity, e.g., through the Scherk-Schwarz mechanism, gravitinos could be as heavy as 10^{13} GeV, which is the same mass scale of the inflaton inferred from the Planck-BICEP result while gauginos could still be light at the TeV scale. The implications for SUSY scales will be discussed in Sec. 4.5.

We conclude in Sec. 4.6 and present a discussion of gravitinos from inflaton decays in the appendix.

4.2 Gravitino and Wino Relic Abundance

In this section, we first review different mechanisms generating the primordial gravitino relic abundance in the early Universe. Then we discuss the relic abundance of wino DM from gravitino decays. Notice that most of the discussions also apply to other neutralino DM scenarios such as higgsino DM. The main point we want to emphasize is that: for gravitinos at or below the PeV scale, the neutralino DM relic abundance has an irreducible non-thermal contribution which scales linearly with the inflaton reheating temperature T_R; **in particular, requiring DM relic abundance not overclose the Universe restricts the reheating temperature to be below** $(10^{10} - 10^9)$ **GeV for DM mass in the range (100 GeV - 1 TeV)**; for gravitino above the PeV scale, the neutralino DM relic abundance is almost UV insensitive, meaning that it is almost independent of T_R.

4.2.1 Primordial Gravitino Relic Abundance

As a superpartner of the graviton, the gravitino couples to all supermultiplets with gravitational interaction strength. In an R-parity conserving scenario, an unstable gravitino always decays to a particle and its superpartner. Decay of a gravitino will always produce a lightest superparticle (LSP) as all the other produced superparticles will cascade down to the LSP. The decay width of an unstable gravitino is given by

$$\Gamma_{3/2} \approx 2.0 \times 10^{-23} \, \text{GeV} \left(\frac{N_G}{12} \right) \left(\frac{m_{3/2}}{100 \, \text{TeV}} \right)^3, \tag{4.1}$$

where $m_{3/2}$ is the gravitino mass and N_G is the number of degrees of freedom gravitino decays to. In the split SUSY scenarios with all gauginos lighter than the gravitino and the squarks heavier than the gravitino, $N_G = 12$.[1]

There could be several different origins of the primordial gravitino relic abundance, $\Omega_{3/2}h^2$. One comes from scattering processes of MSSM particles in the thermal bath [265, 266]. This contribution approximately scales linearly with the inflaton reheating temperature T_R. The higher T_R is, the larger the gravitino relic abundance is. We will use the following approximate formula for the gravitino yield:

$$Y_{3/2}^{UV} \approx \sum_{i=1}^{3} y_i g_i^2(T_R) \ln \left(\frac{k_i}{g_i(T_R)} \right) \left(\frac{T_R}{10^9 \, \text{GeV}} \right), \tag{4.2}$$

where $y_{1,2,3} = (0.653, 1.604, 4.276) \times 10^{-13}$, $k_{1,2,3} = 1.266, 1.312, 1.271$ and $g_{1,2,3}(T_R)$ are gauge couplings of SM gauge group $U(1)_Y, SU(2)_W, SU(3)_c$ evaluated at T_R respectively [265]. The small y's originate from T_R/M_p with M_p the reduced Planck scale. Compared to the formula given in [265], we neglected a contribution at the order of $(M_i^2/m_{3/2}^2)$ with M_i the gaugino masses. The yield given in (4.2) leads to a

---

[1]The squarks could be lighter than the gravitino in the split SUSY scenarios and then N_G is larger. However, it will not change much our discussions and results.

gravitino relic abundance

$$\Omega_{3/2}^{UV}h^2 \approx 5.1 \times 10^{-2} \left(\frac{m_{3/2}}{1\,\mathrm{TeV}}\right)\left(\frac{T_R}{10^9\,\mathrm{GeV}}\right), \tag{4.3}$$

where we evaluated temperature dependent variables in Eq. (4.2) at $T_R = 10^9\,\mathrm{GeV}$. In the numerical evaluation in Sec. 4.3, we include the full temperature dependence.

Another potential important contribution to the gravitino relic abundance comes from the decays of superpartners that are still in thermal equilibrium with the post-inflationary thermal bath [267].[2] When the temperature of the primordial plasma drops around the SUSY scalar masses, which we will take to be around the same scale, decays of the scalars to gravitinos could also generate a potentially non-negligible contribution to the gravitino relic abundance. This is the "freeze-in" mechanism [268]. When the temperature drops below the scalar masses, the number density of SUSY scalars is suppressed exponentially, $e^{-m_s/T}$ and freeze-in stops. The freeze-in contribution is independent of the UV physics, particularly the reheating temperature T_R [269]. The gravitino yield from freeze-in is

$$
\begin{aligned}
Y_{3/2}^{FI} &\simeq \frac{405}{4\pi^4}\sqrt{\frac{5}{2}}\frac{M_p}{g_*^{3/2}}\sum_i g_i\frac{\Gamma_i}{m_i^2}, \\
&\approx 1.6 \times 10^{-16}\left(\frac{200}{g_*}\right)^{3/2}\left(\frac{100\,\mathrm{TeV}}{m_{3/2}}\right)^2\sum_i g_i\left(\frac{m_i}{1000\,\mathrm{TeV}}\right)^3,
\end{aligned}
\tag{4.4}
$$

where we approximated $g_*(m_i) \simeq g_{S*}(m_i)$ and $\Gamma_i = (1/48\pi)(m_i^5/(m_{3/2}^2 M_p^2))$ as the partial decay width of scalar i to the gravitino. Here, g_i denotes degrees of freedom of SUSY scalar i with mass m_i. The yield in Eq. (4.4) leads to a gravitino relic abundance

$$\Omega_{3/2}^{FI}h^2 \approx 1.1 \times 10^{-2}\left(\frac{100\,\mathrm{TeV}}{m_{3/2}}\right)\sum_i g_i\left(\frac{m_i}{1000\,\mathrm{TeV}}\right)^3. \tag{4.5}$$

---

[2]This contribution exists only when $m_s > m_{3/2}$, where m_s denotes the SUSY scalar mass. Besides, the thermal equilibrium requires reheating temperature to be $T_R > m_s$.

It is clear that the gravitino relic abundance $\Omega_{3/2}h^2$ from the freeze-in contribution is highly sensitive to the scalar superpartner masses m_i as it scales as $\sim m_i^3$.

The total gravitino abundance is just a sum of the thermal scattering (Eq. (4.3)) and freeze-in (Eq. (4.5)) contributions

$$\Omega_{3/2}h^2 = \Omega_{3/2}^{UV}h^2 + \Omega_{3/2}^{FI}h^2. \tag{4.6}$$

Before ending this section, we want to mention that there could be other model-dependent sources of primordial gravitino relic abundance. For example, decay of inflaton itself could also produce a sizable gravitino relic abundance. The contribution to gravitino relic abundance from inflaton decays depends on the structure of the dynamical SUSY breaking sector and could be problematic [270, 271]. However, as discussed in [272, 273], gravitino production from inflaton decay can be suppressed if there exists a hierarchy between the mass scales of the inflaton and the field whose F-term VEV breaks SUSY spontaneously. In the discussions below, we will not include this model dependent contribution. We refer the reader to the Appendix A for more details of gravitinos from inflaton decays.

4.2.2 Wino Relic Abundance from Gravitino Decays

In this section, we will specify the neutralino DM to be wino yet the discussions hold for other neutralino DM such as higgsino DM. We will also focus on gravitino with mass above 10 TeV so that its lifetime is shorter than a second and its decays do not spoil the successful Big Bang Nucleosynthesis [274].

The relic abundance of wino DM is a sum of the thermal contribution and the non-thermal contribution from gravitino decays. The non-thermal contribution could be computed numerically by solving the Boltzmann equations Eq. (2.1) - (2.3) in Ref [275]. The primordial gravitino relic abundance in Eq. (4.2) and (4.4) discussed in the previous section is an input to the Boltzmann equations. In solving the Boltzmann

equations, we took $g_*(T)$ and $g_{*,s}(T)$ from a table in the DarkSUSY code [276].[3] As the Sommerfeld effect becomes important for heavy winos [275, 277, 278], we computed the temperature-dependent value of $\langle \sigma_{\rm eff} v \rangle$ from a preliminary version 1.1 of the DarkSE code [279], taking into account not only the Sommerfeld effect but also co-annihilation among different wino species.[4] As an input to this code, we used the two-loop splitting between the neutral and charged winos from Ref. [280]. For wino masses of about a TeV and temperatures around a GeV, the Sommerfeld enhancement can be as large as a factor of 3 in $\langle \sigma_{\rm eff} v \rangle$.

The non-thermal contribution to wino relic abundance from gravitino decays changes parametrically when the gravitino mass $m_{3/2}$ increases. For large gravitino mass, the wino LSP produced from the gravitino decays can annihilate effectively due to the high temperature of the plasma at the time of gravitino decay. More specifically, we find that DM annihilation is efficient for $m_{3/2} \gtrsim 10^4$ TeV. This can be seen by estimating the "decay temperature" as in [275]

$$T_{3/2} \equiv \left(\frac{10}{g_*(T_{3/2})\pi^2} M_{\rm pl}^2 \Gamma_{3/2}^2 \right)^{1/4} \approx 2.2 \, {\rm GeV} \left(\frac{75.75}{g_*(T_{3/2})} \right)^{1/4} \sqrt{\frac{N_G}{12}} \left(\frac{m_{3/2}}{10^4 \, {\rm TeV}} \right)^{3/2} \quad (4.7)$$

At such high temperature, winos produced from the gravitino decays annihilate rapidly, reducing the number density $n_{\widetilde{W}}$ down to a critical value $n_{c,\widetilde{W}} \simeq 3H/\langle \sigma_{\rm eff} v \rangle \, |_{T=T_{3/2}}$ at which winos can no longer annihilate. This critical value $n_{c,\widetilde{W}}$ behaves as an attractor in determining relic abundance of wino LSP, making it independent of the primordial gravitino relic abundance. In this case, the wino relic abundance is given as

$$\Omega_{\widetilde{W}}^{(ann)} h^2 \approx m_{\widetilde{W}} \frac{3H}{\langle \sigma_{\rm eff} v \rangle \, s} \bigg|_{T=T_{3/2}} \left(\frac{h^2}{\rho_{c,0}/s_0} \right), \quad (4.8)$$

$$\approx 0.12 \left(\frac{75.75}{g_*(T_{3/2})} \right)^{1/4} \left(\frac{m_{\widetilde{W}}}{1 \, {\rm TeV}} \right) \left(\frac{1.2 \times 10^{-7} \, {\rm GeV}}{\langle \sigma_{\rm eff} v \rangle \, (T_{3/2})} \right) \left(\frac{m_{3/2}}{10^4 {\rm TeV}} \right)^{-3/2} \quad (4.9)$$

---

[3]We keep factors involving $\partial \log g_{*(s)}(T)/\partial \log T$ in the Boltzmann equation for $\rho_{\rm rad}$.

[4]This version was kindly provided by Andrzej Hryczuk to JF in a previous project.

where we used Hubble parameter $H(T) = \sqrt{g_*(T)\pi^2/90}T^2/M_p$, entropy density $s(T) = 2\pi^2 g_{*,s}(T)T^3/45$. We also assumed $g_* \simeq g_{s,*}$ for the temperature of interest. We will present a more precise numerical evaluation in the following section.

For a lighter gravitino within the mass range, $10 \text{ TeV} < m_{3/2} < 10^4 \text{ TeV}$, the gravitino starts to decay at such a low temperature that the annihilation of wino DM is ineffective. In this case, almost all the winos produced from gravitino decays survive and hence, its relic abundance is proportional to the total gravitino abundance.

$$
\begin{aligned}
\Omega_{\widetilde{W}}^{(no-ann)}h^2 &= \frac{m_{\widetilde{W}}}{m_{3/2}}\left(\Omega_{3/2}^{UV}h^2 + \Omega_{3/2}^{FI}h^2\right) \\
&\approx 0.12\left(\frac{m_{\widetilde{W}}}{1\,\text{TeV}}\right)\left[\left(\frac{T_R}{2\times 10^9\,\text{GeV}}\right) + 10^{-3}\left(\frac{100\,\text{TeV}}{m_{3/2}}\right)^2\sum_i g_i\left(\frac{m_i}{1000\,\text{TeV}}\right)^3\right]
\end{aligned}
\tag{4.10}
$$

where the first(second) term in the square brackets in the second line originates from decays of gravitino produced by the thermal scattering (freeze-in). We want to caution the reader that there is no sharp boundary point in $m_{3/2}$ that separates the two cases with "effective" and "ineffective" wino annihilations in Eq. (4.8) and Eq. (4.10). In Sec. 4.3, we will derive more precise bounds by solving the Boltzmann equations numerically.

From Eq. (4.10), we could see that for gravitino at or below PeV scale as in the mini-split scenario, to avoid overproduction of DM from gravitino decays, the reheating temperature has to be below

$$
T_R \lesssim 2 \times 10^9\,\text{GeV}\left(\frac{1\,\text{TeV}}{m_{\widetilde{W}}}\right),
\tag{4.11}
$$

assuming a negligible contribution from freeze-in. This upper bound would only be pushed even lower if the freeze-in contribution is comparable to or even dominate over the thermal scattering contribution. Similarly, one could obtain an upper bound

on the scalar soft mass

$$m_s \lesssim 10^4 \, \text{TeV} \left(\frac{m_{3/2}}{100 \, \text{TeV}} \right)^{2/3} \left(\frac{1 \, \text{TeV}}{m_{\widetilde{W}}} \right)^{1/3}. \tag{4.12}$$

4.3   Indirect Detection Constraints

As wino DM has a large annihilation rate, there are strong constraints on its relic abundance from indirect detection searches looking for its annihilation products [281–285]. Thus in the wino DM case, one could obtain a stronger upper bound on the reheating temperature compared to Eq. (4.11) which holds for generic neutralino DM. In this section, we present a numerical evaluation of the constraints on the reheating temperature and SUSY scalar mass scale in the scenario with wino as (a component of) DM.

There are multiple indirect search channels for wino DM [286]. In general DM indirect detection searches for decay and annihilation products of DM in fluxes of cosmic rays containing charged particles or photons or neutrinos. We focus on searches looking for excesses in the photon continuum spectrum of satellite dwarf galaxies [281, 285], or our galactic center [287] and monochromatic photon line [283, 288].[5] A continuum photon spectrum is generated from either the bremsstrahlung of charged particles or the hadronic fragmentation of the decay products of W/Z's in the final state of tree-level processes $\chi^0 \chi^0 \to W^+ W^- / ZZ$. The gamma ray lines are generated from DM annihilation into $\gamma\gamma/\gamma Z$. Each photon in the final state carries away energy about the DM mass.

As demonstrated by Fig. 4 in Ref. [263], the thermal wino relic abundance (computed in [277, 289]) is ruled out by the indirect constraint for $m_{\widetilde{W}}$ above 1.5 TeV assuming standard cuspy (NFW and Einasto) DM halo profiles. Since the wino relic abundance is a sum of the thermal contribution and the non-thermal contribution from gravitino decays, there is room for a non-thermal relic abundance only for wino

---

[5]The first paper on the HESS search constraint for wino DM is Ref. [289].

with mass below 1.5 TeV.[6]

We express the constraints on allowed non-thermal $\Omega_{\widetilde{W}}h^2$ as an upper bound on the inflaton reheating temperature T_R as a function of wino mass for $m_{3/2} = 100$ TeV and 10^4 TeV in Fig. 4.1. In this figure, we assumed that freeze-in contribution to the primordial gravitino relic abundance is negligible. As mentioned at the end of last section, taking into account of the freeze-in contribution will only make the upper bound stronger.

Figure 4.1: Upper bounds on inflaton reheating temperature T_R as a function of wino mass for $m_{3/2} = 100$ TeV (left) and $m_{3/2} = 10^4$ TeV (right). The blue, purple, green curves with bands around them correspond to constraints from Fermi galactic center continuum, Fermi line search and HESS line search respectively. The bands are derived by varying parameters of NFW (Einasto) dark matter profiles in the 2σ range [5]. The burgundy dot-dashed line corresponds to the upper bound derived from requiring $\Omega_{\widetilde{W}}h^2 = 0.12$.

The left panel of Fig. 4.1 stays almost unmodified for 10 TeV $< m_{3/2} < 10^4$ TeV as the wino annihilation is ineffective and the relic abundance is independent of $m_{3/2}$ as can be seen from the first term in Eq. (4.10). The reheating temperature is bounded to be below 3×10^9 GeV for the whole wino mass range. For wino mass close to 1.5 TeV, the HESS constraint pushes the reheating temperature to be even lower to about a few times 10^8 GeV.

In the right panel of Fig. 4.1, the gravitino mass is set to be 10^4 TeV. In this case,

---

[6]There could be different non-thermal scenario such as moduli scenario [290]. The implications of indirect detection for moduli scenario have been discussed in [263, 291, 292].

for light wino with mass below 300 GeV, wino annihilation becomes effective and its relic abundance is insensitive to the reheating temperature as shown in Eq. (4.8). Therefore, the upper bound on the inflaton reheating temperature is lifted up entirely. For heavier wino, the annihilation rate drops with the increasing mass and the wino relic abundance interpolates between Eq. (4.8) and Eq. (4.10). In the whole wino mass range, the upper bound on T_R is above 10^9 GeV. For even heavier gravitino, the bound on T_R becomes even weaker.

One could also consider upper bound on the SUSY scalar masses, m_s, which is depicted in Fig. 4.2. In the left panel, we took $m_{3/2} = 100$ TeV and $T_R = 10^8$ GeV so that the thermal scattering contribution is negligible. Increasing the reheating temperature will only make the bound even stronger. In this case, indirect detection constraints restrict the scalar mass to be below $(2-3) \times 10^3$ TeV for the whole wino mass range. In the right panel, we set $m_{3/2} = 10^4$ TeV and $T_R = 2 \times 10^9$ GeV. Since this is the case where wino annihilation becomes more effective, the upper bounds on the SUSY scalar mass depends less on T_R and are reduced significantly compared to the case with a lighter gravitino. More specifically, for wino above 300 GeV, indirect detection constraints restrict scalar masses to be below $10^4 - 10^6$ TeV. For wino below 300 GeV, the upper bound is almost lifted up entirely.

4.4 Implications of the Planck-BICEP2 Analysis

Recently the Planck 2015 analysis [264] for the results on contraints on inflation was concluded. The implications for cosmic inflation of the Planck measurements of the cosmic microwave background (CMB) anisotropies in both temperature and polarization based on the full Planck survey were presented. The upper bound on the tensor-to-scalar ratio is $r_{0.002} < 0.11(95\%CL)$. This upper limit is consistent with the B-mode polarization constraint $r < 0.12(95\%CL)$ obtained from a joint analysis of the BICEP2/Keck Array and Planck data [293]. Such a large tensor-to-scalar
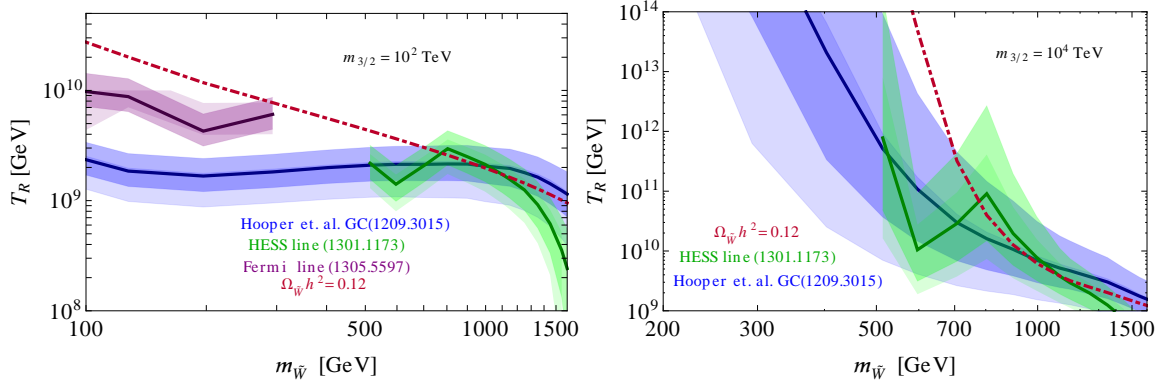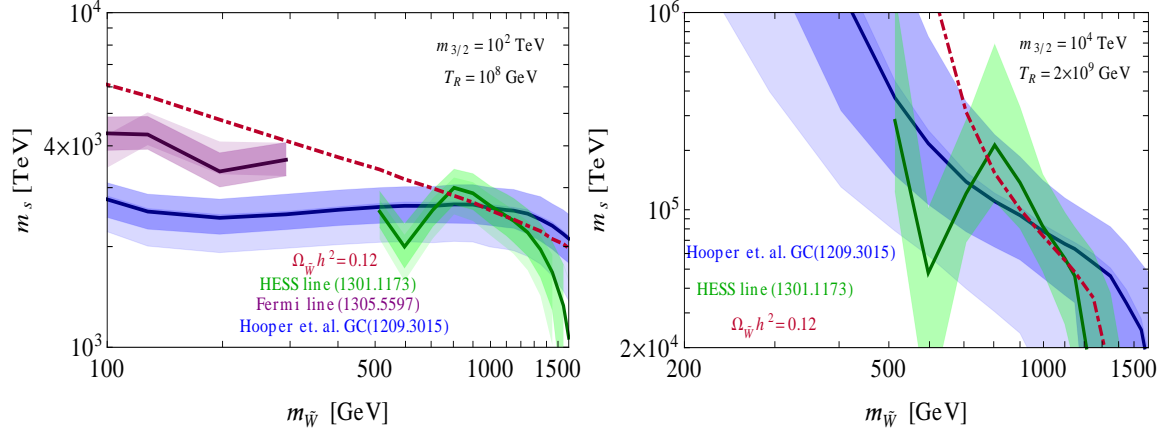
Figure 4.2: Upper bounds on scalar mass m_s as a function of wino mass for $m_{3/2} = 100$ TeV(left) and $m_{3/2} = 10^4$ TeV (right). The blue, purple, green curves with bands around them correspond to constraints from Fermi galactic center continuum, Fermi line search and HESS line search respectively. The bands are derived by varying parameters of NFW (Einasto) dark matter profiles in the 2σ range [5]. The burgundy dot-dashed line corresponds to the upper bound derived from requiring $\Omega_{\widetilde{W}} h^2 = 0.12$.

ratio has a profound implication for the inflation paradigm. We will first review the basics of tensor-to-scalar ratio in the slow-roll inflation paradigm for completeness in Sec. 4.4.1. Readers who are familiar with this topic could skip this section. Then we will discuss the implications of the recent result for the inflation mass scale and reheating temperature in Sec. 4.4.2.

4.4.1 Basics of Tensor-to-Scalar Ratio

We will follow closely Lecture 2 in Ref. [294] in this brief review. In slow-roll inflation models, the metric perturbation during the inflation period could be decomposed into scalar and tensor modes, which result in density and gravitational wave fluctuations respectively. Each mode could be characterized by a fluctuation amplitude

squared [295, 296]

$$\Delta_s^2(k) = \frac{H^4}{4\pi^2 \dot{\phi}^2} = \frac{1}{12\pi^2 M_p^6} \frac{V^3}{V'^2} \quad \text{scalar} \tag{4.13}$$

$$\Delta_t^2(k) = \frac{2H^2}{\pi^2 M_p^2} = \frac{2}{3\pi^2} \frac{V}{M_p^4}, \quad \text{tensor} \tag{4.14}$$

where the reduced Planck scale is $M_p = 2.4 \times 10^{18}$ GeV. It should be understood that all the physical quantities above are evaluated at horizon crossing $k = aH$ at which the relevant comoving scales for the CMB exits the Hubble radius. $\dot{\phi}$ is the time derivative of the inflaton field ϕ and V' is the derivative of the inflaton potential with respect to ϕ. In deriving the second expression of the amplitude squared in each line, we used equation of motion for the inflaton $H^2 \approx V/(3M_p^2)$ and $\dot{\phi} \approx -V'/(3H)$.[7]

Normalizing the scalar spectrum to the COBE [298] or WMAP [299] anisotropy measurement gives $\Delta_s^2(k) \approx 2.2 \times 10^{-9}$. Then one could define tensor-to-scalar ratio $r \equiv \Delta_t^2(k)/\Delta_s^2(k)$, which directly measures the inflation energy scale

$$V \approx (1.8 \times 10^{16} \, \text{GeV})^4 \left(\frac{r}{0.1}\right). \tag{4.15}$$

r also relates directly to the evolution of the inflaton as

$$r = \frac{8}{M_p^2} \left(\frac{d\phi}{dN}\right)^2, \tag{4.16}$$

where differential e-folds $dN = Hdt$. Then one could write the field displacement between the time when CMB fluctuations exited the horizon at N_{cmb} and the end of

---

[7]One easy way to understand the appearance of $\dot{\phi}^2$ in the scalar perturbation amplitude squared is through effective field theory (EFT) [297]. The key insight of inflation EFT is that the inflaton spontaneously breaks time translation invariance and results in a Goldstone mode "eaten" by the graviton to appear in the scalar modes. Compared to the tensor mode, the kinetic term for the Goldstone (scalar) mode has an additional factor of $\dot{H}$ in the kinetic term, which signals the break down of EFT in the limit of pure de Sitter space $\dot{H} = 0$. By equation of motion, $\dot{H}$ is proportional to $\dot{\phi}^2$ and consequently $\dot{\phi}^2$ appear in the denominator of scalar fluctuation amplitude squared.

inflation at N_{end} in terms of an integral

$$\frac{\Delta\phi}{M_p} = \int_{N_{\text{end}}}^{N_{\text{cmb}}} dN \sqrt{\frac{r}{8}}. \tag{4.17}$$

Setting $N_{\text{end}} = 0$ and given that $N_{\text{cmb}} \approx (40 - 60)$ and r is approximately constant during the inflation era, one obtains the famous Lyth bound [300]

$$\frac{\Delta\phi}{M_p} \approx 6.7 \left(\frac{N_{\text{cmb}}}{60}\right) \sqrt{\frac{r}{0.1}}. \tag{4.18}$$

Inspecting Eq. (4.15) and (4.18), one could see immediately that the BICEP2 result points towards a large field displacement of order Planck scale during inflation or in other words, large field inflation. Existing examples of large-field inflation include chaotic inflation where a single power term dominates the potential [301, 302]

$$V(\phi) = \lambda_p \phi^p, \tag{4.19}$$

and natural inflation with a periodic potential resulting from a shift symmetry the inflaton enjoys [303]

$$V(\phi) = V_0 \left(1 + \cos\left(\frac{\phi}{f}\right)\right). \tag{4.20}$$

4.4.2 Implication for Reheating Temperature

Now we want to estimate the inflaton mass scale. We start with a toy model of large field inflation $V = m_\phi^2 \phi^2$. In this model, the scalar fluctuation amplitude squared is

$$\Delta_s^2(k) = \frac{m_\phi^2}{M_p^2} \frac{N_{\text{cmb}}^2}{3\pi^2}, \tag{4.21}$$

where $N_{\text{cmb}} = \phi_{\text{cmb}}^2/(4M_p^2)$. Given the normalization to the CMB measurement, $\Delta_s^2(k) \approx 2.2 \times 10^{-9}$, the inflaton mass is

$$m_\phi \approx 10^{13}\,\text{GeV}\left(\frac{60}{N_{\text{cmb}}}\right)^2. \tag{4.22}$$

One could check in more realistic models such as chaotic inflation and natural inflation that the inflaton mass scale is around 10^{13} GeV [304–306]. One crude estimate of the inflaton mass in all these large-field inflation model is

$$m_\phi^2 \sim \frac{V}{(\Delta\phi)^2} \approx \left(2 \times 10^{13}\,\text{GeV}\right)^2, \tag{4.23}$$

where we used Eq. (4.15) and (4.18) assuming $N_{\text{cmb}} = 60$.

After inflation ends, inflaton starts to oscillate around the minimal of the potential. Its coupling to other particles induce conversion of the inflationary energy into the SM degrees of freedom. The reheating temperature is then determined by the inflaton decay width Γ_ϕ as

$$T_R = \left(\frac{10}{g_*(T_R)\pi^2}\right)^{1/4}\sqrt{\Gamma_\phi M_p} \approx 0.3\sqrt{\Gamma_\phi M_p}, \tag{4.24}$$

where we took $g_*(T_R) \approx 200$. The simplest possibility is that inflatons decay through renormalizable couplings to lighter degrees of freedom. For example, the decay width is $\Gamma_\phi = y^2 m_\phi/(8\pi)$ for inflaton coupling to fermions with a Yukawa coupling y. Then the reheating temperature is

$$T_R \approx 3 \times 10^{11}\,\text{GeV}\left(\frac{y}{10^{-3}}\right)\sqrt{\frac{m_\phi}{10^{13}\,\text{GeV}}}. \tag{4.25}$$

Notice that Yukawa coupling larger than 10^{-5} only makes sense in supersymmetric scenarios where the one-loop quantum correction does not modify the inflaton potential much due to a cancelation between fermionic and bosonic contributions.

If the renormalizable couplings of inflaton to lighter particles are negligible (e.g., $y < 10^{-5}$), it would always decay through Planck-scale suppressed operators. At the leading order, the inflaton decay width and the corresponding reheating temperature are

$$\Gamma_\phi = \frac{c m_\phi^3}{M_p^2}, \quad T_R \approx 5 \times 10^9 \, \text{GeV} \sqrt{c} \left(\frac{m_\phi}{10^{13} \, \text{GeV}} \right)^{3/2}, \tag{4.26}$$

where c is some order one number determined by quantum gravity. From the point of view of operator analysis, this decay is induced by dimension five operators such as $\phi F \widetilde{F} / M_p$ with F the field strength of SM gauge interaction. In other words, the BICEP2 results imply a minimal reheating temperature at or above 10^9 GeV!

One should worry about the caveats of the very simple estimate above. One question is whether the leading order gravitational couplings through dimension five operators could be suppressed and the reheating temperature could be even lower. This could be true if the inflaton is charged under a gauge symmetry (global symmetry is not respected by quantum gravity) and then dimension five operators are forbidden. This is an interesting possibility but we will not explore it here further but leave it for future work. Another concern is that since reheating is a very complicated process (for a review, see [307]), our simple estimate of a minimal reheating temperature might be misleading. In particular, there could exist a preheating era in which particles coupled to the inflaton are resonantly produced by parametric resonance and the temperature of the plasma could be higher than the reheating temperature. Yet preheating might make the tension between the upper bound on T_R derived in Sec. 4.2 and Sec. 4.3 and the lower bound on T_R derived in this section even worse. The reason is that gravitinos could be over-produced non-thermally during the preheating era [308–312].[8] Nonetheless, it is interesting and important to carry out a thorough study of preheating/reheating in sound (stringy) inflation models.

---

[8]In certain supergravity models, the non-thermal production could be suppressed [313, 314].

4.5 Implications for SUSY

So far we have demonstrated a (mild) tension between mini-split SUSY with a heavy unstable gravitino at around the PeV scale and the Planck-2015 result. In mini-split SUSY, the reheating temperature has to be below 10^9 GeV to avoid overproduction of DM particles from gravitino decay while Planck-2015 result prefers large-field inflation with a reheating temperature above 10^9 GeV. In other words, the Planck-2015 results favor a larger splitting between the gravitino and the gauginos than the one-loop factor if the gauginos are fixed at around the TeV scale. Interestingly, **the requirement that gaugino mass does not exceed the TeV scale constrains the gravitino mass to be around or below 10^{13} GeV, which is also the mass scale of the inflaton implied by Planck-2015 !** Below we will review the derivation of this statement by operator analysis following Refs. [98, 256].

In supergravity, the easiest way to cancel the positive vacuum energy from SUSY breaking contribution is to have a non-zero VEV of the superpotential. As the superpotential W carries R-charge 2, its VEV W_0 breaks $U(1)_R$ symmetry spontaneously. It also gives a gravitino mass

$$m_{3/2} \approx \frac{W_0}{M_p^2} \approx \frac{|F_X|}{\sqrt{3}M_p}, \tag{4.27}$$

where F_X is the F-term VEV of the SUSY breaking spurion X. A non-zero gaugino mass is generated only when both $U(1)_R$ and SUSY are broken. The lowest dimensional operator built out of SUSY breaking spurion X, $U(1)_R$ breaking spurion W and MSSM superfields arise in the Kähler potential

$$\int d^2\theta d^2\bar{\theta} \frac{X^\dagger X W W_\alpha W^\alpha}{M_*^6}, \tag{4.28}$$

where W_α denotes the MSSM gauge supermultiplet. This operator could be generated by gravitational loops where $M_* \sim M_p$ and gives a minimal contribution to the

gaugino mass

$$m_{1/2} \gtrsim \frac{|F_X|^2 \, W_0}{M_p^6} \approx \frac{3 m_{3/2}^3}{M_p^2}. \tag{4.29}$$

Requiring $m_{1/2}$ at or below TeV leads to $m_{3/2} \lesssim 10^{13}$ GeV! This large hierarchy between gravitino and gaugino could be realized in no-scale supergravity which could arise from the Scherk-Schwarz mechanism [315, 316].

4.6 Conclusions and Outlook

In this chapter, we study the implication of DM indirect detection and Planck-BICEP2 in the split SUSY scenario with a heavy unstable gravitino. In the mini-split spectrum with scalars/gravitinos only one-loop factor above the TeV-scale gauginos, the reheating temperature has to be low to avoid overproduction of DM particles from gravitino decays. In particular, we demonstrate that indirect detection requires the reheating temperature to be below about 10^9 GeV if the wino is (a component of) DM. On the other hand, the large tensor-to-scalar ratio observed by BICEP2 favors large-field-inflation with a reheating temperature around or above 10^9 GeV. Given this mild tension and the phenomenological upper bound on the gravitino mass derived by requiring the gauginos to be at the TeV scale, it is tempting to think more seriously of the (highly) split SUSY scenario in which inflaton/gravitino are at around 10^{13} TeV and gauginos are still at the TeV scale with lightest neutralino being (part of) DM.[9] Indeed this picture has recently been discussed in the framework of Intermediate Scale SUSY [317].

In general, given the Planck result, it is very interesting to use the scale of inflation to probe the full range of split SUSY scenarios through observables such as equilateral non-gaussianity [318]. It will also be of interest to study the implications of the Planck result for baryogenesis. For example, thermal leptogenesis works for a reheating

---

[9]Axion could be the dominant DM component.

temperature above 2×10^9 GeV [319], which fits well with the Planck result.

Appendix

4.A Gravitino from Inflaton Decay

In this appendix, we review non-thermal gravitino production from inflaton decays. In general, decays of inflaton can overproduce gravitinos which subsequent decays can induce LSP overproduction [270, 271]. Consider the following simple model of SUSY breaking and inflation [273],

$$K \;=\; |\phi|^2 + |X|^2 + |z|^2 - \frac{|z|^4}{\widetilde{\Lambda}^2}, \tag{4.30}$$

$$W \;=\; X\left(g\frac{\phi^n}{M_p^{n-2}} - v^2\right) + \mu^2 z + W_0, \tag{4.31}$$

where z is the SUSY breaking spurion and $\widetilde{\Lambda}$ is the QCD scale of the dynamical SUSY breaking sector. Here, μ is the SUSY breaking scale related to the F-term VEV of z through $F_z \simeq -\mu^2 \simeq \sqrt{3}m_{3/2}M_p$ and W_0 is the constant term introduced in order to cancel the positive vacuum energy from SUSY breaking in order to obtain a vanishing cosmological constant.

The scalar potential in supergravity is given by

$$V = e^{K/M_{pl}^2}\left[K_{i\bar{j}}^{-1}(D_iW)(D_{\bar{j}}W) - 3\frac{|W|^2}{M_p^2}\right], \tag{4.32}$$

where D_i is the covariant derivative with respect to field i. There is a mass mixing

between X and z arising from the following terms in the scalar potential above (4.32),

$$V \supset \left| \frac{Xng\phi^{n-1}}{M_p^{n-2}} + \frac{\phi^\dagger W}{M_p^2} \right|^2 \approx \frac{m_\phi \langle \phi \rangle \mu^2}{M_p^2} X z^\dagger + h.c, \tag{4.33}$$

where $m_\phi = ng\langle \phi \rangle^{n-1}/M_p^{n-2}$.

The operator $|z|^4/\widetilde{\Lambda}$ in the Kähler potential induces z decaying into the goldstino pair $(\widetilde{z})$ via

$$\mathcal{L} \supset \int d^2\theta d^2\bar{\theta} K \sim -2 \frac{F_z^\dagger}{\widetilde{\Lambda}^2} z^\dagger \widetilde{z}\widetilde{z} + h.c, \tag{4.34}$$

where the decay rate is given by

$$\Gamma_{z \to \widetilde{z}\widetilde{z}} \simeq \frac{1}{96\pi} \frac{m_z^5}{m_{3/2}^2 M_p^2}. \tag{4.35}$$

Since the goldstino is "eaten" by the gravitino via the super-Higgs mechanism, the decay rate above can be expressed as the decay rate of the inflaton into a pair of gravitinos via the mass mixing with z:

$$\begin{aligned} \Gamma_{\phi \to \widetilde{z}\widetilde{z}} &\sim \left(\frac{\theta}{\sqrt{2}} \right)^2 \frac{m_\phi}{m_z} \, \Gamma_{z \to \widetilde{z}\widetilde{z}}, \\ &\sim \left(\frac{\theta}{\sqrt{2}} \right)^2 \left(\frac{m_z}{m_\phi} \right)^4 \frac{m_\phi^5}{m_{3/2}^2 M_p^2} \end{aligned} \tag{4.36}$$

where the mixing angle between inflaton ϕ and z, θ, is given by $\sqrt{3}(m_{3/2}\langle \phi \rangle)/(m_\phi M_p)$ for $m_\phi \gg m_z$, $\sqrt{3}(m_{3/2}m_\phi\langle \phi \rangle)/(m_z^2 M_p)$ for $m_\phi \ll m_z$. Therefore, in the case that $m_\phi \gg m_z$, the decay rate (4.36) of inflaton into a pair of gravitino is suppressed by $(m_z/m_\phi)^4$.

If z is only charged under some global symmetry, one could not forbid operators such as $|\phi|^2 z$ and $|\phi|^2 zz$ in the Kähler potential (4.30). These operators will always be induced by Planck scale physics as it only respects local symmetries [320]. These operators are dangerous as they would enhance the decay rate of inflaton to gravitinos

by $m_\phi^2/m_{3/2}^2$. Thus in addition to the hierarchy $m_{3/2} \ll m_z \ll m_\phi$, the SUSY breaking spurion cannot be a gauge singlet!

Chapter 5

Holographic Phase Transitions

5.1 Introduction

Randall-Sundrum models [135, 136] offer an attractive solution to the hierarchy problem, and put the cosmological constant problem into a new perspective [321–323]. The warping of AdS space geometrically generates large hierarchies, and the low energy value of the cosmological constant is in this case a *sum* of terms involving the bulk 5D cosmological constant, and two brane tensions associated with the UV and IR branes. The tiny observed value of the cosmological constant is then obtained by separately tuning the UV brane tension against the bulk cosmological constant, and the IR brane tension against the same bulk cosmological constant.

This "double" fine-tuning in the 5D theory is necessary to force a flat direction for the location of the branes, for which the potential would otherwise cause either collapse of the geometry or a run-away. The Goldberger-Wise stabilization mechanism offers a solution to this tuning problem, with a 5D bulk scalar field developing a vacuum expectation value in the bulk of the extra dimension, and leading to a non-trivial potential for the location of the IR brane [153]. However, this solution relied upon the mistune in the brane tensions being small to begin with, so that the bulk scalar field vev did not deform the geometry very far from AdS.

In terms of the AdS/CFT correspondence, the double tuning of RS in the absence of a stabilization mechanism has a natural interpretation [158, 324–327]. The tuning of the UV brane tension against the bulk cosmological constant is viewed as a tuning of the bare cosmological constant in a non-supersymmetry CFT to zero. This is required as such a curvature term would explicitly break conformal invariance. The second tuning of the IR brane tension is interpreted as a tuning associated with the scale invariant quartic associated with an order parameter for the CFT. The flat direction for the "radion" degree of freedom in RS appears as a tuning of this allowed parameter in the CFT to zero. If non-zero, such a quartic coupling would forbid the generation of a condensate that spontaneously breaks the CFT [328]. A solution to this problem appears if one allows a deformation of the CFT, i.e. by the introduction of a near- marginal operator. The effect of such a deformation would be to give the order parameters for the CFT a non-trivial running. This scale dependence effectively deforms the quartic to a more generic potential that may have non-trivial minima away from the origin.

The Goldberger-Wise solution ameliorates this second tuning to some degree, but the requirement that the backreaction of the scalar field on the geometry remain small meant that only slight mistunes in the brane tensions could be accommodated. Thus a degree of tuning remained, as naive dimensional analysis suggests that the mistune be parametrically larger in strongly coupled scale invariant theories, with natural values for the scale invariant quartic being $\lambda \sim \mathcal{O}\left[(4\pi)^2\right]$.

Relaxing this tuning means that the GW scalar field value will continue to grow, and higher order terms in the scalar potential (i.e. ϕ^3 and higher powers) will come to be important. In addition, the backreaction on the geometry will induce a growing curvature, and higher order curvature terms generated by quantum corrections will come to be of the same order as the terms in the Einstein-Hilbert action.

If, however, the scalar potential has only a soft dependence on ϕ, with the coefficients of the higher order interaction terms in the GW bulk potential being small,

then the scalar field enters a large backreaction regime before the higher curvature terms come to dominate and perturbative control is lost. This ansatz for the bulk scalar potential is equivalent, via the AdS/CFT dictionary, to having a beta function in the CFT that remains small even in the regime of large coupling. With this type of presumed dynamics, the coupling is permitted to explore a larger range of values, and the scale invariant quartic could potentially find a zero, permitting a dynamical condensate that spontaneously breaks the approximate conformal invariance without fine tuning [154–157, 329, 330]. Holographic studies of this scenario show that the dilaton mass in such models is suppressed relative to the breaking scale, and the cosmological constant is also small [331].

In this work, we show that in these holographic realizations, a soft-wall breaking of conformal symmetry is generic, with the gap being set by a continuous changeover in the 5D geometry rather than the IR brane. The brane in this case serves primarily as a cutoff of large curvature effects, and the low energy dynamics is relatively insensitive to its position. We begin studies of the phenomenology of this different class of holographic realization of spontaneously broken scale invariance. In particular, we analyze the finite temperature behavior of such theories as it pertains to a cosmological phase transition. A potential issue with such models is that a finite-time phase transition is not generic, with eternal inflation inhibiting the phase transition for a large range of parameters. **We show that this class of model does not experience this issue. The primary reason for this difference is a parametrically smaller hierarchy between the critical temperature for the phase transition and the breaking scale.**

The organization of this paper is as follows. In Section 5.2, we review the calculation of the zero-temperature holographic dilaton effective theory for various 5D scalar bulk potentials. We give particular attention to the soft-wall phenomenon which is of primary interest in this paper. We work out in detail the constant potential case as it can be studied exactly, and then give analytic expressions for more generic bulk

scalar potentials. In Section 5.3, we analyze the finite temperature behavior of conformal theories at finite temperature, and study the holographic finite temperature dilaton potential. In Section 5.4, we study the properties of the finite temperature cosmological phase transition. As it is a first order phase transition, we calculate the bubble nucleation rate to determine the phenomenological viability of the models under study. If the rate is slow relative the the expansion of the universe, bubbles will not form, and the universe will instead inflate eternally.

5.2 Zero-Temperature Dilaton Effective Theory

We consider classical solutions to a real coupled $5D$ scalar and Einstein field equations in the presence of non-trivial scalar-field vacuum expectation value. The bulk action is given by

$$S = \int d^5x \sqrt{g} \left[\frac{1}{2} \left(\partial_M \phi \right)^2 - V(\phi) - \frac{1}{2\kappa^2} R \right] \tag{5.1}$$

where $\kappa^{-2} \equiv 2M_*^3$, with M_* being the 5D planck scale. We consider metric solutions with flat $4D$ slices, or $SO(4,1)$ symmetry. Such metrics are of the form

$$ds^2 = e^{-2A(\widetilde{y})} \eta_{\mu\nu} dx^\mu dx^\nu - d\widetilde{y}^2 \tag{5.2}$$

or can equivalently be expressed in convenient coordinates $y = A(\widetilde{y})$ ("RG-gauge")[1] as:

$$ds^2 = e^{-2y} \eta_{\mu\nu} dx^\mu dx^\nu - \frac{dy^2}{G(y)} \tag{5.3}$$

where $G(y) = [A'(\widetilde{y}(y))]^2$.

In these coordinates, utilizing "dot" to represent derivatives with respect to y, the

---

[1] This is a convenient choice of coordinate as the warp factor, $A(\widetilde{y})$ via AdS/CFT is equivalent to the renormalization scale, μ. So, in this coordinate choice its easier to work in the language of field theory. Though it should be noted that when the backreaction effects on geometry are large then with the departure from AdS we many no longer be able to use A(y) to play the role of the RG scale, μ

Einstein and scalar field equations can be written as:

$$G = \frac{\frac{-\kappa^2}{6} V(\phi)}{1 - \frac{\kappa^2}{12} \dot{\phi}^2} \tag{5.4}$$

$$\frac{\dot{G}}{G} = \frac{2\kappa^2}{3} \dot{\phi}^2 \tag{5.5}$$

$$\ddot{\phi} = \left(4 - \frac{1}{2} \frac{\dot{G}}{G} \right) \dot{\phi} + \frac{1}{G} \frac{\partial V}{\partial \phi}. \tag{5.6}$$

G can then be eliminated in the scalar field equation of motion, which becomes

$$\ddot{\phi} = 4 \left(\dot{\phi} - \frac{3}{2\kappa^2} \frac{\partial \log V(\phi)}{\partial \phi} \right) \left(1 - \frac{\kappa^2}{12} \dot{\phi}^2 \right). \tag{5.7}$$

The total value of the classical action can be expressed as a pure boundary term. In particular, after substituting for the kinetic and potential terms for ϕ using the Einstein field equations, and taking into account contributions from singular terms in the scalar curvature at the orbifold fixed points, the resulting effective 4D potential is given by [331]

$$V_{\text{eff}} = e^{-4y_0} \left[V_0(\phi(y_0)) - \frac{6}{\kappa^2} \sqrt{G(y_0)} \right] + e^{-4y_1} \left[V_1(\phi(y_1)) + \frac{6}{\kappa^2} \sqrt{G(y_1)} \right] \tag{5.8}$$

The coordinates y_0 and y_1 are the positions of the UV and IR branes, respectively, and V_0 and V_1 are brane-localized scalar field potentials. This in particular means that the asymptotics for ϕ are what is most relevant for the effective potential. By choosing a form for the brane localized potentials and imposing the boundary conditions for ϕ, we can further simplify the expression for the effective potential.

We take the brane localized potentials to each contain a brane tension along with a mass term:

$$V_{0,1}(\phi) = \Lambda_{0,1} + \frac{1}{2} \gamma_{0,1} (\phi - v_{0,1})^2. \tag{5.9}$$

115

Extremizing the action with respect to ϕ yields the boundary conditions

$$\frac{\partial V_{0,1}}{\partial \phi}(\phi(y_{0,1})) = \pm\sqrt{G(y_{0,1})}\dot{\phi}(y_{0,1}) = \pm\sqrt{\frac{3}{2\kappa^2}}\dot{G}(y_{0,1}) \qquad (5.10)$$

where the Einstein equations have been used in the second equality.

Plugging this condition into the effective potential gives

$$V_{\text{eff}} = e^{-4y_0}\left[\Lambda_0 + \frac{3}{4\kappa^2\gamma_0}\dot{G}(y_0) - \frac{6}{\kappa^2}\sqrt{G(y_0)}\right]$$
$$+ e^{-4y_1}\left[\Lambda_1 + \frac{3}{4\kappa^2\gamma_1}\dot{G}(y_1) + \frac{6}{\kappa^2}\sqrt{G(y_1)}\right]. \qquad (5.11)$$

Note that different forms for the brane localized potentials will modify this last expression, although the general character of our later results is not especially sensitive to this.

In the next two subsections we discuss the application of these results first to the case of constant bulk potential $V(\phi) = -\frac{6k^2}{\kappa^2}$, and then to more general potentials. The constant potential case corresponds via AdS/CFT to an undeformed CFT. In the section on general potentials, we add a term to the 5D action that corresponds to sourcing a marginally relevant operator that stabilizes the pure scale-invariant dilaton quartic coupling typical for conformal field theories.

5.2.1 Constant Potential

The case of constant potential can be solved analytically, and the result for ϕ is given by

$$\phi = \phi_0 \pm \frac{1}{4}\sqrt{\frac{12}{\kappa^2}}\log\left[e^{4(y-y_c)}\left(1 + \sqrt{1 + e^{8(y_c-y)}}\right)\right] \qquad (5.12)$$

The integration constant y_c is chosen so as to correspond to the value of y for which the behavior of ϕ changes qualitatively from $\phi \approx$ constant to a behavior that is linear in y: $\phi \approx \phi_0 \pm \left(\log 2 + \sqrt{\frac{12}{\kappa^2}}(y - y_c)\right)$. Defining $\mu_0 \equiv ke^{-y_0}$, $f \equiv ke^{-y_c}$, and

$\mu_1 \equiv k e^{-y_1}$ the asymptotics of ϕ are given by:

$$\phi \approx \begin{cases} \phi_0 \pm \frac{1}{4}\sqrt{\frac{12}{\kappa^2}}\left(\frac{f}{\mu_0}\right)^4 + \mathcal{O}\left(\left(\frac{f}{\mu_0}\right)^{12}\right) & \mu_0 \gg f \\ \phi_0 \pm \frac{1}{4}\sqrt{\frac{12}{\kappa^2}}\left[\log\left(2\left(\frac{f}{\mu_1}\right)^4\right)\right] & \mu_1 \ll f \end{cases} \tag{5.13}$$

We can also evaluate the expression for $G(y)$ exactly. In terms of f and $\mu \equiv k e^{-y}$, and taking $V = -\frac{6k^2}{\kappa^2}$, we have

$$G = k^2 \left[1 + \left(\frac{f}{\mu}\right)^8\right] \tag{5.14}$$

$$G = k^2 \begin{cases} 1 + \mathcal{O}\left(\left(\frac{f}{\mu}\right)^8\right) & \mu \gg f \\ \left(\frac{f}{\mu_1}\right)^8 + \mathcal{O}\left(\left(\frac{\mu}{f}\right)^4\right) & \mu \ll f \end{cases} \tag{5.15}$$

With the above information we can extract the dilaton potential:

$$V_{\text{eff}} = \left(\frac{\mu_0}{k}\right)^4\left[\Lambda_0 + \frac{12k^2}{\kappa^2\gamma_0}\left(\frac{f}{\mu_0}\right)^8 - \frac{6k}{\kappa^2}\sqrt{1 + \left(\frac{f}{\mu_0}\right)^8}\right]$$
$$+ \left(\frac{\mu_1}{k}\right)^4\left[\Lambda_1 + \frac{12k^2}{\kappa^2\gamma_1}\left(\frac{f}{\mu_1}\right)^8 + \frac{6k}{\kappa^2}\sqrt{1 + \left(\frac{f}{\mu_1}\right)^8}\right]. \tag{5.16}$$

Our next step is to determine whether or not, for fixed f, there is a minimum of the potential as a function of μ_1. Typically, in the large γ_i limit (often referred to as the stiff wall limit), we expect that $f \gg \mu_1$ if there is a hierarchy between ϕ_0 and ϕ_1. To obtain this hierarchy, we minimize the above potential with respect to μ_1. The minimization condition is given by

$$\left[\frac{2k}{\gamma_1}\left(\frac{f}{\mu_1}\right)^8 - \frac{\kappa^2\Lambda_1}{6k}\right]\left(\frac{f}{\mu_1}\right)^4\sqrt{1 + \left(\frac{\mu_1}{f}\right)^8} - 1 = 0 \tag{5.17}$$

117

There is typically a non-trivial minimum when the IR brane tension is positive, and has a size commensurate with naive dimensional analysis. The minimum is at

$$\left(\frac{f}{\mu_1}\right)^8 \approx \frac{\kappa^2 \Lambda_1 \gamma_1}{12 k^2}. \tag{5.18}$$

For the small curvatures that are necessary for perturbativity of the 5D gravity theory, we have $k^3 \kappa^2 \ll 1$, and if the other parameters of the 5D theory are taken to be close to their NDA inspired values, this hierarchy is large. In particular, the stiff wall limit $\gamma_1 \to \infty$ drives the hierarchy to infinity, decoupling the IR brane completely. Note, however, that in this limit, higher curvature terms induced by quantum effects will become sizable in the IR region, and the form of the action we use is not expected to remain valid throughout the entire bulk.

Neglecting terms of order $(f/\mu_0)^8$ induced by the explicit breaking of conformal invariance associated with sourcing 4D gravity at the scale μ_0, the effective potential as a function of f can be written as

$$V_{\text{eff}} = \left(\frac{\mu_0}{k}\right)^4 \left[\Lambda_0 - \frac{6k}{\kappa^2}\right] + \left(\frac{f}{k}\right)^4 \frac{6k}{\kappa^2} \left[1 + \sqrt{\frac{4\kappa^2 \Lambda_1}{3\gamma_1}}\right]. \tag{5.19}$$

The first term in this expression is the contribution to the bare cosmological constant. This is expected to be either tuned to zero by choosing $\Lambda_0 = \frac{6k}{\kappa^2}$, or made vanishing by the introduction of additional UV symmetries (i.e. supersymmetry). The second is the contribution to the cosmological constant via the spontaneous breaking of conformal symmetry, or in other words, the dilaton quartic. Note that this term is always positive when the IR brane tension is positive and the soft-wall solution dominates. Note that we expect higher curvature operators that are expected to be induced by quantum corrections to give corrections to the dilaton potential, but the form should still be that of a scale invariant quartic unless a non-trivial scalar potential is included [332, 333].

The interpretation of this result is that even in the absence of an IR brane, there

is a notion of a breaking scale of conformal symmetry given by $f \equiv ke^{-y_c}$. This scale corresponds in 5D to a position in the extra dimension at which the leading behavior of the curvature (or scalar field evolution) makes a transition from one behavior to another, from constant in y to linear in y. The effective potential for f is precisely what is expected for an approximately conformal theory with explicit breaking manifest in the form of a bare CC, and from the introduction of the Planck brane itself, making the position of this turnover of the 5D behavior of the scalar-gravity background a candidate for the dilaton. This identification is further established by identifying a zero mode in the scalar-gravity system which couples to the divergence of the dilatation current with strength set by f. In the Appendix 5.B, we derive the wave-function and a kinetic term for a massless dilaton in this background.

This "soft-wall dilaton" is massless but unstable. We have demonstrated that in cases where the soft-wall precedes the IR brane, the quartic coupling is large and positive. This drives f to zero in the absence of a stabilization mechanism. This means that the effective potential is minimized when the conformal symmetry is unbroken (or instead when breaking manifests in the form of a finely tuned IR brane, as is the case in unstabilized Randall-Sundrum models). Further, the ansatz of flat 4D metric slices is only valid in the case that the bare cosmological constant vanishes, or when the two terms in the first contribution to the potential are arranged so as to exactly cancel each other. The tuning of the bare CC, and the tuning of the dilaton quartic are precisely the two tunings that are required in two-brane RS models.

That there is a lack of stability of the constant potential case comes as little surprise. Typical conformal theories without a supersymmetry do not support spontaneous conformal breaking due to the presence of the scale invariant quartic (in other words, the lack of scalar flat directions). A deformation of the CFT, or in other words a departure from conformality, is typically required to stabilize such potentials. The decoupling of the IR brane in favor of the soft-wall has taken away our dial for fine tuning this quartic away. In the next sub-section, we demonstrate how deforma-

tions of the CFT (introduced in the AdS dual by considering a nontrivial bulk scalar potential) can stabilize the soft-wall dilaton.

5.2.2 More General Potentials

To stabilize the soft-wall dilaton, we consider adding a deformation to the bulk scalar potential:

$$V(\phi) = -\frac{6k^2}{\kappa^2}\left(1 + \epsilon f(\phi)\right) \tag{5.20}$$

where ϵ is a small parameter controlling the explicit breaking of shift symmetry, [156]. We will take $f(\phi)$ as a quadratic in ϕ.

$$V(\phi) = -\frac{6k^2}{\kappa^2}\left(1 + \frac{\kappa^2}{3}\epsilon\phi^2\right) \tag{5.21}$$

The mass term for ϕ corresponds via AdS/CFT to a non-trivial quantum scaling dimension for the CFT operator that corresponds to ϕ. If ϕ takes a non-trivial value on the boundary of AdS, then this operator is sourced in the theory, contributing as an explicit violation of conformal invariance. In the constant potential limit, this operator is precisely marginal, and does not deform the CFT. When ϵ is positive, which is the ansatz we will take in our work, the scalar field is tachyonic, and tends to grow with increasing y. This is dual to sourcing a near-marginal relevant deformation of the CFT.

In general, the equations of motion cannot be solved exactly. As we have emphasized, the asymptotics for the behavior of ϕ are of greatest importance in determining the effective dilaton potential. In the UV, where $y \ll y_c$, we can neglect the backreaction terms in the equations of motion, and we can write the approximate solution for ϕ as

$$\phi_{\text{UV}}(y) = \phi_0 e^{\epsilon(y-y_0)} + \sqrt{\frac{3}{4\kappa^2}}e^{(4-\epsilon)(y-y_c)}. \tag{5.22}$$

Here, ϕ_0 and y_c are constants of integration. In obtaining this expression, the exponents have been expanded in small ϵ. Also, for all potentials, so long as ϕ is reasonably small in the UV [2] then we can write the UV asymptotics of $\partial \log V / \partial \phi$ as

$$\frac{\partial \log V}{\partial \phi} \sim \frac{2\kappa^2}{3} \epsilon \phi \tag{5.23}$$

For the determination of G in the UV, we use the equations of motion, and Taylor expand in small $e^{(y-y_c)}$ to obtain

$$G_{\text{UV}}(y) \approx k^2 \left(1 + \sqrt{\frac{4\kappa^2}{3}} \epsilon \phi_0 e^{(4-\epsilon)(y-y_c)} \right). \tag{5.24}$$

Note that we have left out y_c independent terms that are suppressed by ϵ. These can be absorbed into the definition of k here. We can now evaluate the UV contribution to the dilaton effective potential by plugging these expressions into the general equation, Eq. (5.11):

$$V_{\text{UV}} = \left(\frac{\mu_0}{k}\right)^4 \left[\Lambda_0 - \frac{6k}{\kappa^2} \right] - \epsilon k \phi_0 \sqrt{\frac{12}{\kappa^2}} \left(\frac{\mu_0}{k}\right)^\epsilon \left[1 - \frac{2k}{\gamma_0} \right] \left(\frac{f}{k}\right)^{4-\epsilon}. \tag{5.25}$$

For small k and NDA values for γ_0, this is a negative contribution to a nearly marginal but relevant operator. It now remains to identify the IR contribution to the effective potential.

In the IR region, we can use the following asymptotic form for $\dot{\phi}$:

$$\dot{\phi} = \sqrt{\frac{12}{\kappa^2}} \left(1 - \delta v_{\text{IR}} \right). \tag{5.26}$$

So long as the UV $y \ll y_c$ behavior is as described above, and well-approximated by the AdS geometry, this IR behavior is universal and gives a good approximation for the behavior of ϕ for $y \gg y_c$ independent of the form of $V(\phi)$. In this limit, the scalar

---

[2]Note that it can be made small by redefinition of the bulk potential

equation of motion can be re-written as

$$\dot{\delta v}_{\rm IR} = -8\left(1 - \frac{1}{8}\frac{d}{dy}\log V(\phi)\right)\delta v_{\rm IR}, \tag{5.27}$$

where we have kept only the leading linear terms in $\delta v_{\rm IR}$. This equation is integrable, yielding the following relation between $\delta v_{\rm IR}$ and the scalar bulk potential:

$$\delta v_{\rm IR} = \frac{1}{2\widetilde{\lambda}^2}\frac{V(\phi(y))}{V(\phi(y_c))}e^{-8(y-y_c)}. \tag{5.28}$$

Here, $\widetilde{\lambda}$ is an integration constant, and the y_c dependence has been factored out such that $\delta v_{\rm IR} \sim \mathcal{O}(1)$ when $y = y_c$. Full numerical solutions indicate that it is appropriate to take $\widetilde{\lambda} \approx 1 - \epsilon + \mathcal{O}(\epsilon^2)$. This expression is independent of the form of the bulk potential, and assumes only that the trajectory for ϕ ends up on the condensate branch, which appears generic for all trajectories that lead to near-AdS geometry in the $y \to -\infty$ limit. Plugging this into Eq. (5.4), we obtain a simple expression for $G(y)$ in the IR:

$$G_{\rm IR}(y) = -\frac{\kappa^2\widetilde{\lambda}^2}{6}V(\phi(y_c))e^{8(y-y_c)} \tag{5.29}$$

with the dependence on the deep IR behavior of $V(\phi)$ dropping out.

Using this relation, we find the IR contribution to the effective dilaton potential for arbitrary $V(\phi)$:

$$V_{\rm IR} = \frac{6\widetilde{\lambda}}{\kappa^2}\left(\frac{f}{k}\right)^4\sqrt{-\frac{\kappa^2}{6}V(\phi(y_c))}\left[1 + \sqrt{\frac{4\kappa^2\Lambda_1}{3\gamma_1}}\right]$$

$$\approx \frac{6k}{\kappa^2}\left(\frac{f}{k}\right)^4\left[1 + \epsilon\phi_0\sqrt{\frac{\kappa^2}{12}}\left(\frac{f}{\mu_0}\right)^{-\epsilon}\right]\left[1 + \sqrt{\frac{4\kappa^2\Lambda_1}{3\gamma_1}}\right] \tag{5.30}$$

In this relation, we have already minimized over μ_1, given that the conditions for a large $(f/\mu_1)^8$ hierarchy are met.

Summing up all the contributions, and neglecting the bare CC term, we find that

the dilaton potential [3] can be written as

$$V_{\text{dilaton}} = -\epsilon \lambda_\epsilon \mu_0^\epsilon f^{4-\epsilon} + \lambda_4 f^4, \tag{5.31}$$

where we have defined $\lambda_\epsilon = \frac{\phi_0}{k^3} \sqrt{\frac{3}{\kappa^2}} \left[1 - \frac{4k}{\gamma_0} - \sqrt{\frac{16\kappa^2 \Lambda_1}{3\gamma_1}} \right]$, and $\lambda_4 = \frac{6}{\kappa^2 k^3} \left[1 + \sqrt{\frac{4\kappa^2 \Lambda_1}{3\gamma_1}} \right]$.
The potential has a global minimum at

$$\frac{f}{\mu_0} \approx \left(\frac{(4-\epsilon)\epsilon \lambda_\epsilon}{4\lambda_4} \right)^{1/\epsilon}, \tag{5.32}$$

and the contribution to the vacuum energy from the condensate f at the minimum
is given by:

$$V_{\text{min}} \approx -\frac{\epsilon \lambda_4 f^4}{4}. \tag{5.33}$$

In the case of large $\gamma_{0,1}$, we can neglect the effects of the brane localized potentials
on λ_ϵ and λ_4, and we have

$$\left(\frac{f}{\mu_0} \right) \approx \left(\epsilon \phi_0 \sqrt{\frac{\kappa^2}{12}} \right)^{1/\epsilon}, \text{ and } V_{\text{min}} \approx -\frac{3\epsilon}{2k^3 \kappa^2} f^4. \tag{5.34}$$

There are two points which deserve special attention. First, the near-marginal
operator has a coefficient which is suppressed by a factor of ϵ, in contrast with models
where the IR brane plays the role of the dilaton. This means that large hierarchies
are more typical in Eq. (5.32) for a given set of parameters of the theory in soft-wall
scenarios. In hard wall models, the term in the numerator could easily dominate,
driving the condensate up to the Planck scale. Second, the value of the potential at
the minimum is suppressed by a single power of ϵ. This is in contrast to the typical
Goldberger-Wise scenario, in which the minimum scales as $\epsilon^{3/2}$ [334, 335].

---

[3]Here, the form of the dilaton potential has been computed using asymptotic solutions, under
the assumption that there is no significant backreaction near y_c and the UV solution can be used to
estimate, $G(y)_{IR}$. We are currently analyzing the coefficients of the effective potential numerically,
however this will be presented in a future work.

5.3 Finite Temperature

There are many reasons to consider the behavior of this class of theories at finite temperature. The cosmology of such models is of particular interest. Studies of the RS1 phase transition indicate that it is strongly first order, with a critical temperature well below the scale of the condensate [334, 336]. This is due to the presence of a near flat direction at the minimum of the dilaton potential. It is this which allows for the light dilaton, and also for a suppression in the contribution of condensates to the effective IR value of the cosmological constant. At finite temperature, such non-compact flat directions are lifted, sending the dilaton field value to the origin, thus evaporating the condensate.

In order to study the theory at finite temperature, the class of geometries we study is opened up to include the possibility of a horizon (or "black brane") at some point $y = y_h$ in the 5D coordinate. In AdS space, the hawking radiation from such a black hole allows the black hole to reach equilibrium with the thermal bath. The partition function associated with these classical solutions corresponds to the thermodynamical free energy of the system. The geometry we study has metric function

$$ds^2 = e^{-2y} \left[h(y)dt^2 + d\vec{x}^2 \right] + \frac{1}{h(y)} \frac{dy^2}{G(y)}. \tag{5.35}$$

The presence of a horizon is associated with a zero in the horizon function $h(y)$ at position y_h. As we are considering a thermal partition function, we work in Euclidean metric signature, with the time coordinate compactified on a circle: $t \in [0, 1/T)$.

The equations of motion for the metric functions h and G, and for the scalar field

ϕ are given by [4]

$$\frac{\ddot{h}}{h} = 4 - \frac{1}{2}\frac{\dot{G}}{G} \tag{5.36}$$

$$\frac{\dot{G}}{G} = \frac{2\kappa^2}{3}\dot{\phi}^2$$

$$G = -\frac{\frac{\kappa^2}{6}\frac{V(\phi)}{h}}{1 - \frac{1}{4}\frac{\dot{h}}{h} - \frac{\kappa^2}{12}\dot{\phi}^2} \tag{5.37}$$

$$\ddot{\phi} = 4\left(\dot{\phi} - \frac{3}{2\kappa^2}\frac{\partial\log V}{\partial\phi}\right)\left(1 - \frac{1}{4}\frac{\dot{h}}{h} - \frac{\kappa^2}{12}\dot{\phi}^2\right). \tag{5.38}$$

The effective potential is still given by a pure boundary term, although the singular terms due to orbifold boundary conditions at a putative black hole horizon require special treatment, as we discuss later in this section.

The bulk contribution to the effective potential arises from using the equations of motion to express the bulk action as a total 5-derivative:

$$V_{\text{bulk}} = -\frac{2}{\kappa^2}\int dy \partial_5\left[e^{-4y}\sqrt{G}h\right] = \frac{2}{\kappa^2}\left[e^{-4y_0}h(y_0)\sqrt{G(y_0)} - e^{-4y_1}h(y_1)\sqrt{G(y_1)}h(y_1)\right]. \tag{5.39}$$

The curvature tensor has singularities at the orbifold fixed points that give additional contributions to the effective action. Integrating the action over these singularities at the UV and IR branes gives the following contribution to the effective potential:

$$V_{\text{sing}} = -\frac{1}{\kappa^2}\left[e^{-4y_0}\sqrt{G(y_0)}\left(8h(y_0) - \dot{h}(y_0)\right) - e^{-4y_1}\sqrt{G(y_1)}\left(8h(y_1) - \dot{h}(y_1)\right)\right] \tag{5.40}$$

Note that the equation of motion for h enforces an exact cancellation between the two $\dot{h}$ terms.

In summary, adding together the contributions to the potential when there is no black hole horizon, including the two brane localized potentials which each contribute

---

[4]While it is not of immediately practical value in this work, it seems worth noting that combining the first and third of these equations yields a rather peculiar and suggestive relationship between h and the bulk scalar potential: $\frac{d}{dy}\log V = 8 - \frac{d}{dy}\log h - 2\frac{d}{dy}\log\frac{d}{dy}\log h + \frac{d}{dy}\log\frac{d}{dy}\log\frac{d}{dy}\log h$.

$\sqrt{g_{\mathrm{ind}}(y_i)}V_i$, are:

$$V_{\mathrm{dilaton}} = e^{-4y_0}\left[\sqrt{h(y_0)}V_0(\phi(y_0)) - \frac{6}{\kappa^2}h(y_0)\sqrt{G(y_0)}\right]$$
$$+ e^{-4y_1}\left[\sqrt{h(y_1)}V_1(\phi(y_1)) + \frac{6}{\kappa^2}h(y_1)\sqrt{G(y_1)}\right] \tag{5.41}$$

Our goal is to replace the IR brane at y_1 with a black hole horizon at y_h, such that $h(y_h) = 0$ [326], however due to the structure of the manifold near the horizon, one cannot simply take $h(y_h) = 0$ in the above equation. The reason for this is that the manifold near the horizon is typically singular, with a cone feature appearing in a given $t - y$ slice of the geometry, as shown in Figure (5.1).
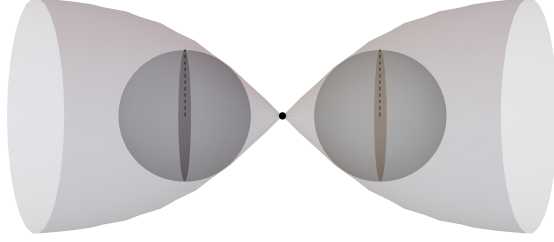
Figure 5.1: This figure displays the conical singularity appearing in the t-y slice of the geometry. A spherical cap of small radius, r is put to regularize the singularity.

In order to study such a horizon for generic bulk scalar potential, we presume that the horizon function has a zero for some finite $y = y_h$. We further presume that $h(y)$ is analytic, such that it has a Taylor expansion in the vicinity of the horizon. In this case, we have $\frac{\dot{h}}{h} \approx \frac{1}{y-y_h}$, with the sign determined by the fact that h is positive in the physical region $y < y_h$, and that it is passing through zero.

This behavior of the horizon function determines a boundary condition for ϕ that arises from taking the near-horizon limit of the scalar field equation of motion:

$$\dot{\phi}\bigg|_{y_h} = \frac{3}{2\kappa^2}\frac{\partial \log V}{\partial \phi}\bigg|_{y_h}. \tag{5.42}$$

This boundary condition enforces regularity of the solution for ϕ at the horizon -

without this condition, ϕ diverges in the approach to the horizon [337].

To compute the effective potential when the IR is screened by a black hole horizon, we need to pay closer attention to the treatment of singular terms at the orbifold fixed points at $y = y_0$ and $y = y_h$. The scalar curvature is singular in both places. In the UV, the singular terms can be treated as before, yielding a contribution to the effective potential that is given by

$$V_{\text{UV}}^{\text{BH}} = -\frac{1}{\kappa^2}e^{-4y_0}\sqrt{G(y_0)}\left[8h(y_0) - \dot{h}(y_0)\right].$$ (5.43)

The IR contribution is calculated via a proper regularization of the 2D conical singularity. There is a conically singular geometry near the black hole horizon corresponding to a system that is out-of-equilibrium. Quantum effects will generally cause the singularity to emit radiation until it reaches equilibrium with the surrounding thermal bath, at the minimum of the free energy of the thermodynamical system.

If a theory admits solutions to the h function which vanish at some finite value of y_h, then we can study such systems in the near-horizon limit. Considering the near-horizon limit of the metric, where $h \approx \dot{h}(y_h)(y - y_h)$, we have (displaying only the dt and dy components of the metric):

$$ds^2 \approx e^{-2y_h}\dot{h}(y_h)(y - y_h)dt^2 + \frac{dy^2}{\dot{h}(y_h)(y - y_h)G(y_h)}.$$ (5.44)

We now go to "good" coordinates, $(y - y_h) = \frac{\widetilde{y}^2}{4}\dot{h}(y_h)G(y_h)$, $t = \frac{\theta}{2\pi T}$ where the metric is manifestly that of a cone:

$$ds^2 = e^{-2y_h}\dot{h}^2(y_h)G(y_h)\frac{\widetilde{y}^2}{4(2\pi T)^2}d\theta^2 + d\widetilde{y}^2.$$ (5.45)

The opening angle of the cone is given by

$$\sin\alpha = -e^{-y_h}\frac{\dot{h}(y_h)\sqrt{G(y_h)}}{4\pi T},$$ (5.46)

with the overall minus sign ensuring positivity of the angle since $\dot{h}$ is negative at the horizon. By capping the cone with a sphere of radius r, which has constant curvature $2/r^2$, the contribution to the action is rendered finite and r independent, allowing a sensible $r \to 0$ limit:

$$\Delta S_{\text{IR}} = \int d^3x \frac{4\pi}{\kappa^2} \left(1 - \sin\alpha\right) e^{-3y_h} = \int d^3x \left[\frac{4\pi}{\kappa^2} e^{-3y_h} + \frac{1}{T\kappa^2} e^{-4y_h} \dot{h}(y_h)\sqrt{G(y_h)}\right]. \tag{5.47}$$

Note that a factor of two has been included as the integral is over the entire S_1 space in the S_1/Z_2 orbifold, leading to a double-copy of the spherical cap, one on each side of the orbifold fixed point. The singular IR contribution to the 4D effective potential energy is then given by

$$V_{\text{sing}}^{\text{IR}} = -\left[\frac{1}{\kappa^2} e^{-4y_h} \dot{h}(y_h)\sqrt{G(y_h)} + \frac{4\pi}{\kappa^2} e^{-3y_h} T\right]. \tag{5.48}$$

The first term cancels exactly the corresponding UV term, and we can write the complete effective potential in the presence of the black hole horizon as

$$F = e^{-4y_0}\left[\sqrt{h(y_0)}V_0(\phi(y_0)) - \frac{6}{\kappa^2}h(y_0)\sqrt{G(y_0)}\right] - \frac{4\pi T}{\kappa^2} e^{-3y_h}. \tag{5.49}$$

This expression for the free energy, $F = U - TS$ separates into an energetic component U that is completely localized on the UV brane and an entropic component $-TS$ arising from the Bekenstein-Hawking entropy of the black hole.

The value of y_h that minimizes the free energy as a function of the horizon location is obtained by inverting the following relation:

$$T = -\frac{\kappa^2}{12\pi}\frac{dU}{dy_h}e^{3y_h}. \tag{5.50}$$

The right hand side of this equation for arbitrary y_h could be interpreted as the

temperature of the black hole. The value of the free energy at the minimum is

$$V_{\min} = U + \frac{1}{3}\frac{dU}{dy_h}. \tag{5.51}$$

Up to terms that violate conformal invariance due to the introduction of the Planck brane or the Goldberger-Wise potential, the equilibrium temperature that minimizes the effective potential as a function of y_h is associated with the value of y_h that removes the conical singularity. We can use the h equation of motion to express this equilibrium temperature in terms of the near AdS-Schwarzchild UV behavior of h and G: $\dot{h}(y_0) \approx -4e^{4(y_0-\widetilde{y}_h)}$ and $G(y_0) \approx k^2$. Note that $\widetilde{y}_h$ is the position where the horizon would be if there were no deformation of the geometry due to the varying ϕ field. In the absence of scalar backreaction, $\widetilde{y}_h = y_h$. From the equations of motion one finds that the presence of the back-reaction delays the onset of the horizon, establishing the inequality $\widetilde{y}_h \leq y_h$.

$$T_{\mathrm{eq}} = T_h = \frac{k}{\pi}e^{-y_h}e^{4(y_h-\widetilde{y}_h)}. \tag{5.52}$$

As the position of the horizon, y_h, is greater than $\widetilde{y}_h$, the equilibrium temperature is larger than it would be in the absence of scalar backreaction. This is potentially problematic, as this would mean that the temperature is not necessarily a monatonic function of the position of the horizon. The temperature would in fact grow when the backreaction becomes sizable, causing a deviation between y_h and $\widetilde{y}_h$. We see that the temperature grows with increasing y_h when $\frac{dy_h}{d\widetilde{y}_h} > 4/3$. Note however, that the Bekenstein-Hawking entropy $S = \frac{4\pi}{\kappa^2}e^{-3y_h}$ is monotonically decreasing with increasing y_h. These high temperature solutions with low entropy will be disfavored relative to those of equal temperature but small y_h and thus larger entropy.

5.3.1 Constant Bulk Potential at Finite Temperature

In the case of $V(\phi) = -\frac{6k^2}{\kappa^2}$, with no dependence on ϕ, the scalar field equation of motion has a significantly simplified relationship to h:

$$\frac{d}{dy} \log \dot{\phi} = \frac{d}{dy} \log \frac{\dot{h}}{h} \tag{5.53}$$

This scalar field equation of motion is integrable, and we find that the solution is given by:

$$\phi = \phi_0 + C_l \log h, \tag{5.54}$$

where C_l is an integration constant. We note that this equation immediately excludes the case of constant bulk potential as a candidate for a spontaneously broken CFT at finite temperature, or where $h = 0$ for some finite y in a non-trivial scalar field configuration. Clearly, if h is vanishing, but C_l is finite then ϕ must be divergent at the position of the horizon, and the horizon boundary condition Eq. (5.42) cannot be satisfied. However, it will be beneficial to discuss this case a little further.

The equations can be satisfied for one particular value of C_l, however. Taking $C_l = 0$, or $\phi = $ constant, we go on to solve the Einstein field equations with the result that $h = 1 - e^{4(y_h - y)}$ and $G(y) = k^2$, corresponding to the AdS-Schwarzchild geometry. Via AdS/CFT, this configuration is dual to an *unbroken* CFT at finite temperature.

5.3.2 Generic Potential at Finite Temperature

At high temperatures the theory is expected to be in a near-conformal hot plasma phase, with finite temperature corresponding to an explicit breaking of conformal invariance. In this region, if we assume that the scalar backreaction on the geometry is small, and the non-linear terms $\frac{\kappa^2}{12} \dot{\phi}^2$ can be neglected throughout the entire bulk of the extra dimension. In this case, the solutions to the equations can be worked

out analytically, resulting in a scalar field profile that is given by the sum of hypergeometric functions. In Appendix 5.A, we give a derivation of the approximate zero-backreaction scalar field profile in the AdS-Schwarzchild background derived above for the constant potential case:

$$\phi_T(y) \approx \phi_h \left[e^{\epsilon(y-y_h)} + \frac{\epsilon}{8} e^{(4+\epsilon)(y-y_h)} - \frac{\epsilon}{8} e^{(4-\epsilon)(y-y_h)} \right]$$
$$= \phi_0 e^{\epsilon(y-y_0)} \left[1 + \frac{\epsilon}{8} e^{4(y-y_h)} - \frac{\epsilon}{8} e^{(4-2\epsilon)(y-y_h)} \right]. \tag{5.55}$$

Note that ϕ_h is the value of the scalar field evaluated at the position of the horizon. On the second line, we have absorbed the y_h dependence into the new constant ϕ_0, so that the UV limit behavior of the finite temperature and zero temperature solutions are identical. Thus the decoupling of the finite temperature corrections is manifest in the expression for ϕ.

We now ask at what temperature this solution grows to the point where large backreaction effects can dominate the solution. The figure of merit in this calculation is the quantity $l^2 = \frac{\kappa^2}{12}\dot{\phi}^2$. Evaluated on the horizon, we have the approximate result

$$l^2 \approx \frac{\kappa^2}{12} \epsilon^2 \phi_0^2 e^{2\epsilon(y_h - y_0)} = \frac{\kappa^2}{12} \epsilon^2 \phi_0^2 \left(\frac{\pi T_h}{\mu_0} \right)^{-2\epsilon}. \tag{5.56}$$

Taking $l^2 \sim 0.1$ as a threshold for when backreaction effects should be included for an appropriate finite temperature description, we find that we require

$$T_h \gtrsim \frac{\mu_0}{\pi} \left(\sqrt{\frac{10\kappa^2}{12}} \epsilon \phi_0 \right)^{1/\epsilon} \tag{5.57}$$

From zero temperature analiysis, we have a relation for μ_0 in terms of f. Using eq. 5.34 in the above inequality we see that, back reaction effects can be neglected iff $T_h \gg f$.

Now, in order to make use of the free energy formula in Eq. 5.49, we consider

the far-UV behavior of the function h. In the deep UV, the backreaction is small, and the solution for h can be written as $h \approx 1 - e^{4(y - \widetilde{y}_h)}$. If the backreaction were negligible throughout the entire bulk, then this formula would suffice, and there would be a horizon at $y = \widetilde{y}_h$. However, as we just discussed this is not always a good approximation, in which case there is an integral formula for h:

$$h = 1 - 4k \int_{-\infty}^{y} \frac{e^{4(y' - \widetilde{y}_h)}}{\sqrt{G(y')}} dy'. \tag{5.58}$$

The second term is typically very small in the near-AdS region for low temperatures. The actual position of the horizon is given by the value $y = y_h$ that corresponds to a zero of h. Due to the fact that G is monotonically increasing as a function of y, there is an inequality $y_h > \widetilde{y}_h$. Note that a zero is not guaranteed for all $\widetilde{y}_h$, but if there is one, Eq. (5.58) provides an integral relation between $\widetilde{y}_h$ and y_h.

The free energy for the finite temperature solutions can then be written in terms of the Hawking temperature, T_h as

$$F = e^{-4y_0} \left[V_0(\phi(y_0)) - \frac{6}{\kappa^2} \sqrt{G(y_0)} \right] + \frac{\pi^4}{k^3 \kappa^2} T_h^4 \Sigma(y_h)^3 \left[\frac{6}{k} \sqrt{G(y_0)} - \frac{\kappa^2}{2k} V_0(\phi_0) \right] - \frac{4\pi^4}{k^3 \kappa^2} T \Sigma(y_h)^3 T_h^3 \tag{5.59}$$

Here we have defined the quantity which encodes the deviations from the AdS-S solution in terms of

$$\Sigma(y_h) = e^{4(\widetilde{y}_h - y_h)}$$
$$= 4k \int_{-\infty}^{y_h} \frac{e^{4(y' - y_h)}}{\sqrt{G(y')}} dy' \tag{5.60}$$

Now, the Hawking temperature given in Eq. 5.52, can be rewritten as,

$$T_h = \frac{k}{\pi} \frac{e^{-y_h}}{\Sigma(y_h)}. \tag{5.61}$$

The first term in the expression for free energy of this deformed AdS-S solution,

contains the contribution to the bare cosmological constant which can be set to zero as was done in the previous sections of zero temperature analysis. The second term is the energetic component, the quantity inside the square brackets has a correction coming from the solution for the scalar field and geometry near the UV brane. However, these contributions from the Goldberger-Wise scalar field would be ϵ suppressed, and hence we can safely neglect it for the purposes of comparison with the zero temperature solution. The last term is usual entropic component.

Neglecting the bare CC term and the small contributions from the GW field, the total free energy for the finite temperature phase is given by

$$F = \frac{3\pi^4}{k^3\kappa^2}T_h^4 \ \Sigma(y_h)^3 - \frac{4\pi^4}{k^3\kappa^2}T \ \Sigma(y_h)^3 \ T_h^3 \tag{5.62}$$

where we can think of the Hawking temperature, T_h as the scalar field parameterizing the effective distance between the horizon and the UV brane and T as the temperature of the system.

If we neglect the back reaction, then at $T_h = T$, F acquires a minimum value of

$$F_{min} = -\frac{\pi^4}{\kappa^3 k^2} \ T^4 \tag{5.63}$$

However, in general the temperature at which F attains a minimum is different from the temperature at which the conical singularity is resolved.

We now consider specific forms of the bulk potential, with the aim of studying their finite temperature behavior. The bulk potentials of interest are:

$$V(\phi) = -\frac{6k^2}{\kappa^2} \exp[\kappa^2\epsilon\phi^2/3] \quad \text{and} \quad V(\phi) = -\frac{6k^2}{\kappa^2}(1 + \kappa^2\epsilon\phi^2/3)$$

The potential dependence enters the free energy equation 5.62, via the sigma function and the Hawking temperature. We solve the equations of motion 5.38 numerically and calculate $\Sigma(y_h)$ and T_h. These functions are then used to compute the free energy

of the system. We numerically examine the behaviour of the free energy keeping the explicit CFT breaking term, $\epsilon = 0.1$, and we work in units of κ choosing $k = 0.1$. The normalized free energy, V/T^4 for both the quadratic and exponential potentials are plotted in Fig. 5.2. We plot the free energy as a function of the proper distance between the UV brane and the horizon position, given by [5]

$$\int_{-\infty}^{y_h} \frac{kdy}{\sqrt{G(y)}}. \tag{5.64}$$

For backreaction effects to be significant, the black brane needs to be sufficiently far from the UV brane, thus we focus on free energy curves with inter-brane distance, $\Delta y > 8$. Each color corresponds to finite temperature phase at a unique temperature, and temperature of the system increases as we move rightward, from blue to red curves. If the backreaction effects were neglected then functional form of the free energy is same as that for a AdS-S geometry [334].

$$F = \frac{3\pi^4}{k^3\kappa^2}T_h^4 - \frac{4\pi^4}{k^3\kappa^2}T\ T_h^3 \tag{5.65}$$

The dot-dashed curves correspond to the case when $y_h = \widetilde{y_h}$ and when the geometry deviates from AdS-S we get free energy behaviour as shown in the solid curved of Fig. 5.2. This means that phase transition is likely to proceed at higher temperatures than in the case where there is no backreaction, as the finite temperature potential well is not as deep at a given temperature, T. One can see that backreaction is a crucial element that assists phase transition. The finite temperature behavior of both the quadratic and the exponential potential are very similar, in both cases backreaction effects are significant as can be seen in Figures. 5.2a and 5.2b respectively.

---

[5]When backreaction effects are included then in RG units, $\text{Log}\left(\frac{\mu_0}{f}\right) = \int_{-\infty}^{y_h} \frac{kdy}{\sqrt{G(y)}}$
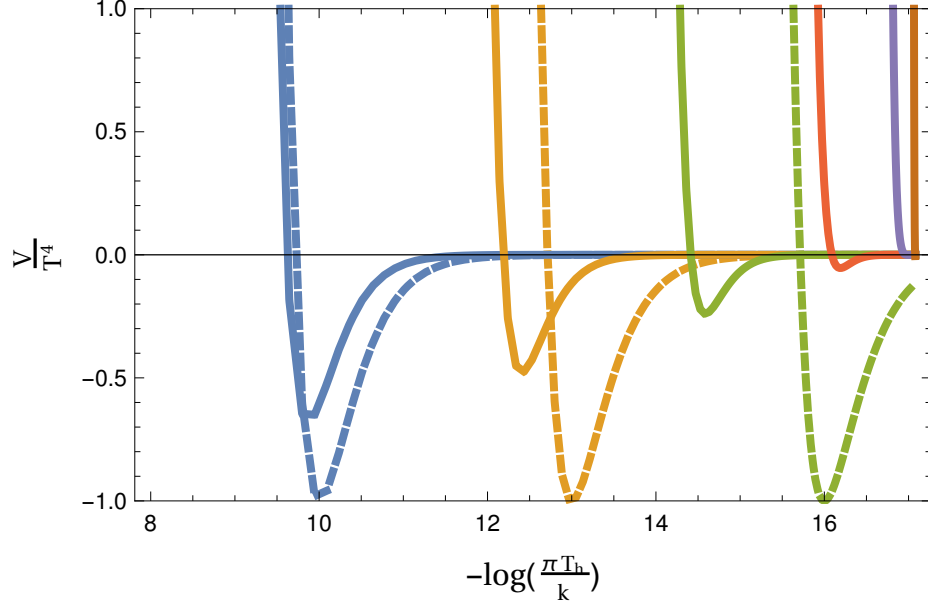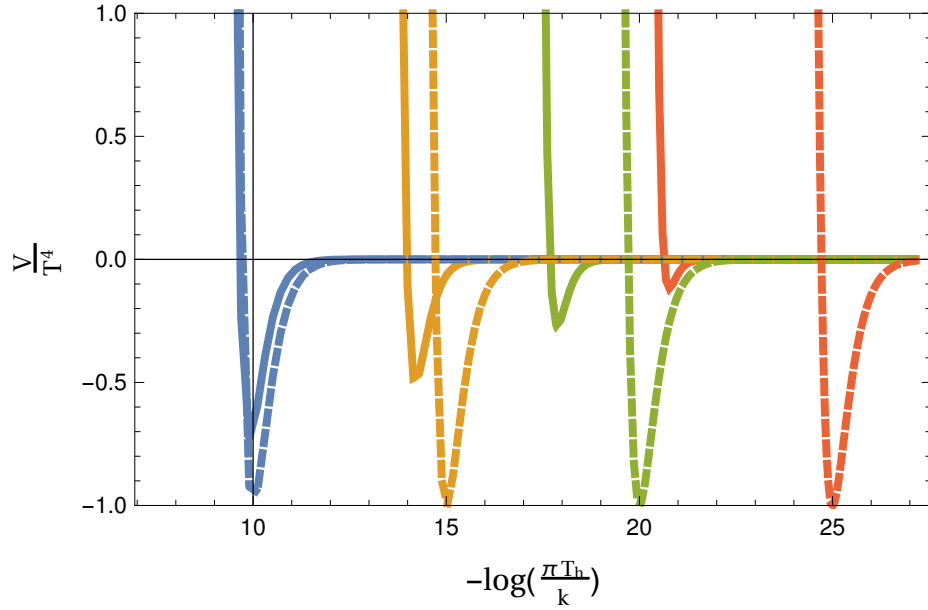
Figure 5.2: This figure displays the normalized free energy, V/T^4 as a function of the proper distance between the UV brane and the horizon position. The dot-dashed curves correspond to the case when back-reaction effects are neglected, while the solid curves include back-reaction effects. Each color corresponds to finite temperature phase at a unique temperature, T, which is decreasing from left to right. In the two plots, we have taken $\epsilon = 0.1, \kappa = 1, k = 0.1$. The bulk potential is exponential, $V(\phi) = -\frac{6k^2}{\kappa^2} \exp[\kappa^2 \epsilon \phi^2/3]$ (left) and quadratic $V(\phi) = -\frac{6k^2}{\kappa^2}(1 + \kappa^2 \epsilon \phi^2/3)$ (right).

5.4 Phase Transitions

We wish to further explore the finite temperature behavior of these holographic soft-wall models of conformal symmetry breaking. It has been extensively investigated in [334, 338], that there are two gravity solutions relevant at finite temperature. At low temperatures, there exists a warped extra dimensional solution with time compactified and no black hole horizon while at high temperatures, a near-AdS-Schwarzchild solution (AdS-S) with horizon is seen. We are interested in understanding the dynamics of the phase transition between these two different geometries in the soft wall models we have been studying. Comparison of the minimum total free energy for each geometry identifies the preferred vacuum at various temperatures, and the structure of the potential that interpolates between the AdS-S minimum and the conformal breaking minimum specifies the dynamics that interpolates between the two phases. Our analysis parallels earlier work on conformal phase transitions [334, 336], but with emphasis on the particulars of the soft-wall light dilaton construction .

5.4.1 Transition temperature

We compare the effective dilaton potential at zero and finite temperatures as computed in Eq. (5.31) with that from the effect of the scalar potential in the AdS-S background, alongwith the contribution of the black hole, Eq. (5.62). The contribution from the bare cosmological constant term, $\left(\frac{\mu_0}{k}\right)^4 \left[V(\phi_0) - \frac{6k}{\kappa^2}\right]$ is present in both the solutions and hence cancels out, and it is anyways tuned to zero to ensure curvature does not explicitly break conformal symmetry. Thus, it is safe to neglect the bare cosmological constant term.

At high temperatures, the effective potential is chiefly described by the free energy of the black hole, see Eq. (5.62). At the critical temperature T_c, the values of the minimum of the effective potentials at zero and finite temperatures should be equal , i.e

$$V_0^{min} = V_T^{min} \qquad \Rightarrow \qquad -\frac{\epsilon \lambda_4 f^4}{4} = -\frac{\pi^4}{k^3 \kappa^2} T_c^4. \qquad (5.66)$$

Using this information we estimate the critical temperature, T_c at which a first order phase transition takes place. Note that all analysis from henceforth is valid only when backreaction effects are negligible, i.e for a low temperature phase transition. In this case the critical temperature is given by:

$$T_c = f \left(\frac{2\epsilon \lambda_4}{\pi^2} \right)^{1/4} \frac{1}{\sqrt{N}}. \qquad (5.67)$$

As the temperature drops , the effective potential takes the following form:

$$V_0 = -\epsilon \lambda_\epsilon \mu_0^\epsilon f^{4-\epsilon} + \lambda_4 f^4 \qquad (5.68)$$

Here we have used the holographic interpretation for the minima of the free energy of the black hole which is equivalent to the free energy of a strongly coupled large N CFT. This gives us the following relationship, $N^2 \sim 16\pi^2 (ML)^3 \sim 8\pi^2/\kappa^3 k^2$ [337]. Now, $\lambda_4 = \frac{3N^2}{4\pi^2} \left[1 + \sqrt{\frac{4\kappa^2 \Lambda_1}{3\gamma_1}} \right]$ which tells us that $T_c < f$.

We conclude that at low temperatures, $T < T_c$ the system is dominated by the condensate and then at T_c a first order phase transition occurs. This is in agreement with the results of Creminelli et. al [334].

5.4.2 Phase transition via nucleation of brane bubbles

In 4-dimensional picture, we expect that a first order phase transition between the two gravity solutions proceeds bubble nucleation as the universe approaches the true vacuum. In 5-dimensions, we can imagine that spherical brane patches of the new phase (true vacuum) form on the horizon, which would expand until the old phase (false vacuum) disappears. The completion of the phase transition would be marked by formation of the complete 3-brane.

For a successful phase transition [339, 340], the bubble nucleation rate needs to greater that the rate at which the universe expands. To be more precise, the probability to nucleate a bubble per horizon time and horizon volume $\sim T^4 e^{-S_E}/H^4$ is greater than one. In other words, $S_E \lesssim 4 \ln(m_{\mathrm{Pl}}/T_{\mathrm{n}})$, where S_E is the bubble action As we are focussing on electroweak scales, this corresponds to, $T_n \sim 10^2 - 10^3 GeV$ and so $S_E \lesssim 140$.

To calculate the exact bounce solutions we need a complete solution fo the Einsteins equations decribing the bubble. However, it is not possible to know the explicit form of the contribution to the action from the "black hole" region of the instanton. This issue was briefly discussed in Creminelli et. al [334]. We use the same assumtion of [334], where at leading order in N we can estimate the action S neglecting the contribution from the AdS-S over that from the warped solution. We will therefore integrate over the warped solution from 0 to f. This approximation is reasonable owing to the hierarchy $f > T_c$ which allows for dilaton to contribute to the action.

We will now list the various quantities which will be needed for computing the bubble action.

The magnitude of the difference in the energy density between the 2 minima is given by,

$$
\Delta V = V_{T=0} + \frac{\pi^2 N^2 T^4}{8} = \begin{cases} \dfrac{\epsilon \lambda_4 f^4}{4} \left[\dfrac{4 V_{T=0}}{\epsilon \lambda_\epsilon f^4} - \left(\dfrac{T}{T_c} \right)^4 \right] & , V_{T=0} \neq \dfrac{\epsilon \lambda_\epsilon f^4}{4} \\ \dfrac{\epsilon \lambda_4 f^4}{4} \left[1 - \left(\dfrac{T}{T_c} \right)^4 \right] & \text{otherwise.} \end{cases} \tag{5.69}
$$

The phase transition takes place by bubble nucleation of the true vacuum bubbles. The free energy of a true- vacuum bubble is [341]

$$
F = \int d^3x \left[\frac{1}{2} (\nabla \mu)^2 + V(\mu, T) \right] \tag{5.70}
$$

There are two contributions to the bubble action: a surface term, F_S from the

derivative terms of Eq. 5.70. The second constribution is the volume term, F_V coming from the difference in the free energy inside and outside the bubble.

The probability of bubble nucleation per unit volume per unit time is given by [342]

$$\Gamma = A \exp\left(-S_E\right), \tag{5.71}$$

where S_E is the Euclidean action. The prefactor, A has the dimensions of $1/\text{length}^4$, and is of the same order as f^4. At high temperatures, where the bubble radius, R is larger than the time radius, $1/T$, instanton has a $O(3)$ symmetry and bubble action reduces to S_3/T, where

$$S_3 = 4\pi \int r^2 dr \left[\frac{1}{2}\left(\frac{\partial\mu}{\partial r}\right)^2 + \Delta V\left(\mu\right)\right]. \tag{5.72}$$

At low temperatures, instanton respects $O(4)$ symmetry and bubble action is given by,

$$S_4 = 2\pi^2 \int r^3 dr \left[\frac{1}{2}\left(\frac{\partial\mu}{\partial r}\right)^2 + \Delta V\left(\mu\right)\right]. \tag{5.73}$$

There are two posible limiting cases for estimates of the bubble action for both $O(4)$ and $O(3)$ symmetric cases: the thin-wall [342] and thick-wall approximation [341]. In this cosmological phase transition, there is a potential barrier separating the high temperature symmetric minimum to the low temperature, symmetry breaking minima. This barrier is overcome via tunneling, which happens at nucleation temperature, T_n. Initially when the temperatures are high and very close to T_c, the two minimas are almost degenerate. In other words, the difference in the energies between the metastable and the true vacua are small in comparison with the height of the barrier. In this situation, the bubbles formed fit the thin wall approximation. However as the temperature drops, ΔV increases and becomes larger than the barrier. Then, the thickness of the bubble wall is of the same order as the size of the bubble and the surface term can be minimized. This is when we need to work with the thick

wall approximation. It was shown in [336] that the phase transition occurs mostly in the thick wall regime.

When temperatures are high, and in the regime where $T \sim T_c$, the two minima's of the two phases are are almost degenerate. Then the bubble is described by the action of the thermal bounce, [6]. Using thin wall approximation, we get

$$S_3^{thin} = \left(\frac{3N^2}{4\pi^2}\right)^{3/2} \frac{16\pi}{3} \frac{S_1^3}{(\Delta V)^2} \sim \left(\frac{3N^2}{4\pi^2}\right)^{3/2} \frac{16\pi 2^{3/2} f^3}{3\sqrt{V_{min}}\left(1-\left(\frac{T}{T_c}\right)^4\right)^2} \qquad (5.74)$$

where $S_1 = \int_0^f d\mu \sqrt{\Delta V}$ is coming from the surface tension of the thin wall and can be approximated to $-\int_0^f \sqrt{-2V_{min}}$, where $V_{min} = -\epsilon\lambda_4 f^4/4$. The factor $\left(\frac{3N^2}{4\pi^2}\right)$ comes from the canonical normalised kinetic energy term for μ [152, 158, 327] :

$$\mathcal{L}_{kin} = -\frac{12N^2}{16\pi^2}\sqrt{-g}(\partial\mu)^2 \qquad (5.75)$$

This leads to,

$$\begin{aligned} \frac{S_3}{T} &= 2.96\frac{N^{7/2}}{(\epsilon\lambda_4)^{3/4}}\frac{T_c/T}{\left(1-\left(\frac{T}{T_c}\right)^4\right)^2} \\ &\simeq 20.45\left(\frac{N^2}{\epsilon^{3/4}}\right)\frac{T_c/T}{\left(1-\left(\frac{T}{T_c}\right)^4\right)^2} \end{aligned} \qquad (5.76)$$

Now, to make some estimates to see whether a succesful phase transition can occur or not, we assume that the T dependent factor is $\mathcal{O}(1)$. [7]

Using, bubble nucleation condition, $S_3/T \lesssim 140$, and keeping ϵ as small as $1/20$,

---

[6]The bubble action is a factor 8 larger than computed in [334]

[7]The T dependent factor blows up as T approaches T_c. This factor becomes order one as T decreases. It reaches a minima at $T = T_c/3^{1/2}$ and grows again. It is safe to assume that bubble nucleation would occur when this factor is near its minimum, for which it is $\sim \mathcal{O}(1)$. This happens when $T_c/3^{1/2} < T < 0.9T_c$.

we finally get:

$$N \lesssim 0.85 \tag{5.77}$$

This bound shows that a model with large N [8] cannot have a sensible high temperature cosmology. Thus, thin wall bubbles gave us an action which is too big to allow for nucleation. However, as the potential is very shallow, thick-wall bubbles dominate. Again, we can use the zero temperature dilaton potential to estimate the tunneling action. The action for thick-walled bubble is given by,

$$S_3 = 2\pi R f^2 - 4\pi R^3 \frac{\Delta V}{3}, \tag{5.78}$$

where R is the bubble radius given by

$$
\begin{aligned}
R &= \left(\frac{3N^2}{4\pi^2}\right)^{1/2} \frac{f}{\sqrt{2\Delta V}} \\
&\sim \frac{0.4N}{f\sqrt{\epsilon\lambda_4}\left(1 - \left(\frac{T}{T_c}\right)^4\right)^{1/2}} \\
&\sim \frac{1.4}{f\sqrt{\epsilon}\left(1 - \left(\frac{T}{T_c}\right)^4\right)^{1/2}}
\end{aligned} \tag{5.79}
$$

The minimal value of the action associated with this bubble radius is,

$$S_3^{thick} = \frac{4\pi}{3}\left(\frac{3N^2}{4\pi^2}\right)^{3/2} \frac{f^3}{\sqrt{2\Delta V}} \sim \frac{4\pi}{3}\left(\frac{3N^2}{4\pi^2}\right)^{3/2} \frac{f^3}{\sqrt{2V_{min}\left(1 - \left(\frac{T}{T_c}\right)^4\right)}} \tag{5.80}$$

The thick wall bubble action is a factor of 16 smaller than the thin walled action

---

[8] This is necessary condition in the 5D picture when we can neglect the quantum gravity effects in the AdS solution

and hence

$$\begin{aligned}
\frac{S_3}{T} &= 0.18\frac{N^{7/2}}{(\epsilon\lambda_4)^{3/4}}\frac{T_c/T}{\left(1-\left(\frac{T}{T_c}\right)^4\right)^2} \\
&\simeq 1.28N^2\epsilon^{-3/4}\frac{T_c/T}{\left(1-\left(\frac{T}{T_c}\right)^4\right)^2}
\end{aligned} \tag{5.81}$$

Using bubble nucleation criteria we get that

$$N \lesssim 3.4 \tag{5.82}$$

The high T cosmology for these class of models is still in tension with the large N requirement.

The other possibility is the the $O(4)$ symmetric solutions. These would dominate if the phase transition is at zero temperature, moreover $T_n < 2R_{bubble}^{-1} \sim f\sqrt{\epsilon}(1-\left(\frac{T}{T_C}\right)^4)$, or in other words nucleation does not take place via thermal bubbles. The thin-wall action is,

$$\begin{aligned}
S_4^{thin} &= 27\pi^2\left(\frac{3N^2}{4\pi^2}\right)^2\frac{S_1^4}{2(\Delta V)^3} \\
&\simeq \frac{12.31N^2}{\left(1-\left(\frac{T}{T_c}\right)^4\right)^2\epsilon}
\end{aligned} \tag{5.83}$$

Using the bubble nucleation condition, $S_E \lesssim 140$, we get an upper bound as $N \lesssim 0.21$, whereas, the thick wall action at it's minimal value is given by,

$$
\begin{aligned}
S_4^{thick} &= \pi^2 \left(\frac{3N^2}{4\pi^2} \right)^2 \frac{f^4}{2(\Delta V)} \\
&\simeq \frac{1.5N^2}{\left(1 - \left(\frac{T}{T_c} \right)^4 \right)^2 \epsilon}
\end{aligned}
\tag{5.84}
$$

which puts an upper bound on N as 2.16.

Here, again we have used $\epsilon \sim 1/20$. The constraints put on N, still do not seem sufficient for a viable early universe picture in these models.

In the above computations we have ignored the effects of the scalar field on the horizon function. We expect that the constrains on N will weaken when we take backreaction effects for finite temperature into account. Also, one needs to have more precise estimates for the coefficients entering the zero temperature, effective dilaton potential 5.31. Moreover, it would be interesting to study the effects of the inclusion of the improved radion normalisation terms as discussed in detail in Appexdix 5.B.

5.5   Conclusions

In this chapter we have analyzed the hologrpahic phase transitions for extradimensional models with a soft-wall background. In the holographic description, there is a single operator $\mathcal{O}$ that is responsible for explicitly breaking the conformal symmetry and generating a condensate $\langle \mathcal{O} \rangle$. The fluctuations about the condensate $\langle \mathcal{O} \rangle$ are then identified with the dilaton. The soft-wall framework is more realistic than the Goldberger-Wise stabilized Randall Sundrum model, as it makes the hierarchy between plank scale and low energy physics even more natural. Our main focus has been to study the finite temperature properties for soft-wall models using holography. This would help us in understanding the early cosmology of the model, specifically when the temperature of the universe is close to the electroweak breaking scale. This

could help in parsing out the role played by spontaneous breaking of scale invariance. We find that presence of nearly marginal deformation in the bulk is vital for the model to exist in two different phases at low and high temperatures. For general bulk potential, which leads to SBSI, the model exhibits two distinct phases. We find that a first order phase transition occurs at a temperature T_c. Low temperature physics is dominated by the dilaton in a soft-wall background. At high temperatures, SBSI is screened by the thermal effects.

A very crucial role is played by the backreaction of the bulk stabilizing scalar field. We found that potential well at finite temperature changes rapidly when backreaction on the geometry is taken into account. Inclusion of backreaction effects both at finite and zero temperature would have interesting effect on the hight T cosmology of these models. We have partially addressed this issue and would like to probe it in detail in future.

Appendix

5.A High Temperature

At high temperatures, a horizon develops before the back-reaction of ϕ on the metric becomes important. In this case, the solution for the horizon function h is well approximated by

$$h = 1 - e^{4(y - y_h)}. \tag{5.1}$$

The differential equation for ϕ is then linear, assuming small ϕ. Taking the usual template bulk potential function, $V(\phi) = \Lambda_5 e^{\frac{\kappa^2}{3}\phi^2}$, and again neglecting $\frac{\kappa^2}{12}\dot{\phi}^2$ terms, the equation for ϕ is approximately

$$\ddot{\phi}\left(1 - e^{4(y-y_h)}\right) = 4\left(\dot{\phi} - \epsilon\phi\right). \tag{5.2}$$

The most general solutions to this equation are hypergeometric functions:

$$
\begin{aligned}
\phi(y) =&\, \phi_1 e^{2(1-\beta)(y-y_h)} \,_2F_1\left[\frac{1-\beta}{2}, \frac{1-\beta}{2}; 1-\beta; e^{4(y-y_h)}\right] \\
&+ \phi_2 e^{2(1+\beta)(y-y_h)} \,_2F_1\left[\frac{1+\beta}{2}, \frac{1+\beta}{2}; 1+\beta; e^{4(y-y_h)}\right].
\end{aligned}
\tag{5.3}
$$

where $\beta \equiv \sqrt{1-\epsilon}$. In the UV near-AdS region, these solutions can be expanded in small epsilon and small $e^{4(y-\widetilde{y}_h)}$. The resulting expression for the ϕ fields is given by

$$\phi \approx \phi_0 e^{\epsilon(y-y_0)}\left[1 + \frac{\epsilon}{8}\left(e^{4(y-\widetilde{y}_h)} + \lambda(y_h)e^{(4-2\epsilon)(y-\widetilde{y}_h)}\right)\right]. \tag{5.4}$$

Here, $\widetilde{y}_h$ is the integration constant in h that appears in the UV region, and y_h is the placement of the actual horizon.

Note that in the case where a transition to significant back-reaction occurs before the onset of the horizon, this solution is still valid in the UV region with the replacement $y_h \to \widetilde{y}_h$. However, the following discussion does not apply, since the regularity condition at the horizon occurs in the region with large backreaction, where Eq. (5.3) is invalid.

In the case where the horizon lies in the near-AdS-S region, $y_h \approx \widetilde{y}_h$, and both of these hypergeometric functions diverge at the horizon, $y = y_h$. Requiring regularity at the horizon, we obtain the full solution for ϕ throughout the bulk of the geometry:

$$\phi(y) = \phi_0 \left\{ \frac{\Gamma(1+\beta)}{\Gamma^2\left(\frac{1+\beta}{2}\right)} e^{2(1-\beta)(y-y_h)} \,_2F_1 \left[\frac{1-\beta}{2}, \frac{1-\beta}{2}; 1-\beta; e^{4(y-y_h)} \right] \right.$$
$$\left. - \frac{\Gamma(1+\beta)}{\Gamma^2\left(\frac{1+\beta}{2}\right)} e^{2(1+\beta)(y-y_h)} \,_2F_1 \left[\frac{1+\beta}{2}, \frac{1+\beta}{2}; 1+\beta; e^{4(y-y_h)} \right] \right\}. \tag{5.5}$$

Since we only require the asymptotics of the solution at the UV brane in the case of a scenario with a horizon, we now get the UV behavior at $y \ll y_h$ by expanding the proceeding hypergeometric functions in terms of small argument, and by expanding all coefficients and exponents in terms of small ϵ:

$$\phi^{\text{UV}}_{T_{\text{hot}}}(y) \approx \phi_0 \left[e^{\epsilon(y-y_h)} + \frac{\epsilon}{8} e^{(4+\epsilon)(y-y_h)} - \frac{\epsilon}{8} e^{(4-\epsilon)(y-y_h)} \right]. \tag{5.6}$$

This result is an excellent approximation to the full formula so long as epsilon is small, but of course this expression requires that we neglect backreaction effects.

5.B Radion Normalization

In this section we compute the normalization of the radian wavefunction. The normalization is relevant as it sets the scale for the physical mass upon wavefuction

renormalization.

The equation of motion for the radian was derived in [172] in the $\widetilde{y}$-coordinates defined by $z = k^{-1}e^{A(\widetilde{y})}$ with the result

$$F'' - 2\left(A' + \frac{\phi''}{\phi'}\right)F' + 4\left(-A'' + A'\frac{\phi''}{\phi'}\right)F = e^{2A}\Box F \tag{5.1}$$

where ϕ is the background scalar field living in AdS. We are interested in the normalization of the approximately massless zero-mode so we set the right side to zero. Switching to coordinates $y \equiv A(\widetilde{y})$ and using the relation $A'' = \frac{\kappa^2\phi'^2}{3}$ we obtain

$$F'' - \left(2 + \frac{\kappa^2}{3}\phi'^2 + 2\frac{\phi''}{\phi'}\right)F' + \frac{4\phi''}{\phi'}F = 0 \tag{5.2}$$

where now the prime is with respect to the coordinate y. In order to solve this equation we make the approximation to ignore the back reaction of F on the ϕ and plug in the solution in the y coordinates given by

$$\phi = \phi_0 + \frac{\sqrt{3}}{2\kappa}\log\left(e^{4(y-y_c)} + \sqrt{1 + e^{8(y-y_c)}}\right). \tag{5.3}$$

This equation is solved to obtain

$$F_0 = N_F\left(C_1 e^{2y}\sqrt{e^{8y} + e^{8y_c}} + C_2 e^{8(y-y_c)}\left(3 - (1 + e^{8(y-y_c)})\,_2F_1(1, 5/4, 7/4, -e^{8(y-y_c)}))\right)\right) \tag{5.4}$$

where $_2F_1$ is the hypergeometric function, N_F is the normalization to be calculated and C_1 and C_2 are constants fully determined by the boundary conditions. We choose the constants as follows. In the limit $y \gg y_c$ we obtain

$$F_0 \approx \widetilde{C}_1 e^{6y} + \text{const} \tag{5.5}$$

and hence we choose $\widetilde{C}_1 = 0$ to eliminate the exponentially growing solution. In the

limit $y \ll y_c$ we obtain

$$F_0 \approx N_F \widetilde{C}_2 e^{2y} \tag{5.6}$$

and we choose $\widetilde{C}_2 = 1$ so that we obtain the RS normalization in this limit in order to properly compare to standard results. With these choices the final expression for the radion wave function is

$$F_0 = N_F e^{-6y_c} \left(e^{2(y+y_c)} \sqrt{e^{8y} + e^{8y_c}} + \right.$$
$$\left. \frac{\sqrt{\pi}}{\Gamma(-1/4)\Gamma(7/4)} e^{8(y-y_c)} \left[3 - (1 + e^{8(y-y_c)}) \, {}_2F_1(1, 5/4, 7/4, -e^{8(y-y_c)}) \right] \right). \tag{5.7}$$

If we expand out the EH action for gravity in the 5D theory, the linearized metric fluctuations, encoded as F, have a dynamical term in the action. The fluctuations of the scalar field φ, also have a kinetic term. The portion of the action corresponding to the coupled dynamics of these scalar fields is given (in y-coordinates) by

$$S_{\text{kin}} = \int d^5 x \sqrt{g} \left[N_F^2 \frac{3}{\kappa^2} \, g^{\mu\nu} \partial_\mu F \partial_\nu F + N_\phi^2 \, g^{\mu\nu} \partial_\mu \phi \partial_\nu \phi \right]$$
$$= \int d^4 x \, dy \frac{e^{-2y}}{k\sqrt{1 + e^{8(y-y_c)}}} \left[N_F^2 \frac{3}{\kappa^2} \, \eta^{\mu\nu} \partial_\mu F \partial_\nu F + N_\phi^2 \, \eta^{\mu\nu} \partial_\mu \phi \partial_\nu \phi \right]. \tag{5.8}$$

The bulk equations of motion for F and ϕ couple the two, such that ϕ can be expressed in terms of F. The uncoupled equation of motion given above in fact arrives after such a substitution, where the relation between ϕ and F in the $\widetilde{y}$ coordinates is given by

$$N_\phi^2 \phi^2 = N_F^2 \frac{3}{\kappa^2} \frac{(F' - 2A'F)^2}{A''}. \tag{5.9}$$

In the y coordinates, this equation is given by

$$N_\phi^2 \phi^2 = -N_F^2 \frac{3}{\kappa^2} (F' - 2F)^2 \tag{5.10}$$

Differentiating the above equation and inserting it into the kinetic action yields

$$\frac{N_F^2}{3\kappa^2} \int d^4x \, dy \frac{e^{-2y}}{k\sqrt{1+e^{8(y-y_c)}}} \left[-3 \, \eta^{\mu\nu}\partial_\mu F \partial_\nu F + 12 \, \eta^{\mu\nu}\partial_\mu F \partial_\nu F' - \eta^{\mu\nu}\partial_\mu F' \partial_\nu F' \right]$$

(5.11)

hence

$$N_F^{-2} = \frac{1}{3\kappa^2} \int \, dy \frac{e^{-2y}}{k\sqrt{1+e^{8(y-y_c)}}} \left[-3F^2 + 12 \, FF' - F'^2 \right].$$

(5.12)

Exact results for the radian normalization are displayed in figures 5.B.1 and 5.B.2. In order to obtain analytical results we expand the hypergeometric function as

$$F_1\left(1,5/4,7/4,-e^{8(y-y_c)}\right) = \begin{cases} 1 & \text{for } y \ll y_c \\ 3 \, e^{4(y_c-y)} - \frac{3 \, \Gamma(3/4)^2}{\sqrt{\pi}} e^{6(y_c-y)} + \frac{1}{2}e^{12(y_c-y)} & \text{for } y \gg y_c. \end{cases}$$

(5.13)

In the limit $y_c \gg y_{IR} \gg y_{UV}$ we obtain

$$N_F \approx \kappa^{3/2}\frac{2}{3}e^{-ky_{IR}} = .82 \, \kappa^{3/2}e^{-ky_{IR}}$$

(5.14)

which is the radian normalization in a pure RS (AdS) background. In the limit $y_c \approx y_{IR} \gg y_{UV}$ we obtain

$$N_F \approx .62 \, \kappa^{3/2}e^{-ky_{IR}}$$

(5.15)

which is the same order of magnitude as the normalization in the RS (note that the normalization is not always smaller than the RS normalization as can be seen in the figures 5.B.1 and 5.B.2). Although the normalization does not deviate appreciably for $y_c \sim y_{IR}$ note that for deviations away from this value the normalization is significantly larger implying the radian's effective mass mN_F^{-1} is noticeably smaller than

the naive estimate m would imply. Although it is not of great interest phenomeno-logically, it should be noted that in the limit $y_c \approx y_{UV} \ll y_{IR}$ we have

$$N_F \approx 1.08\kappa^{3/2} \; e^{-ky_{UV}} \tag{5.16}$$

which blows up in the $y_{UV} \to -\infty$ limit.

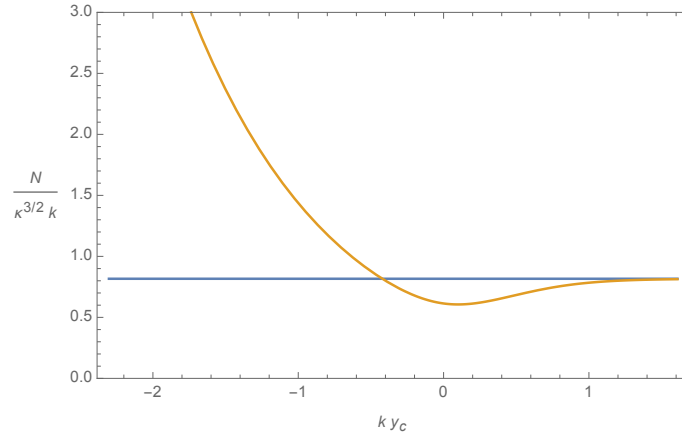Figure 5.B.1: This figure displays the radion normalization with $y_{\mathrm{IR}} = 0$ and $ky_{\mathrm{uv}} = -37$. Orange is the exact result. Blue is RS (AdS) result for comparison. Note that the normalization does not deviate appreciably for $y_c \approx y_{IR}$ but does deviate for $y_c \ll y_{IR}$.

Figure 5.B.2: This figure displays the radion normalization in the coordinates $z = k^{-1}e^{ky}$ with $z_{\mathrm{uv}}/z_{\mathrm{IR}} = 10^{-19}$. Orange is the exact result. Blue is RS (AdS) result for comparison. Note that the normalization does not deviate appreciably for $z_c \approx z_{IR}$ but does deviate for $z_c \ll z_{IR}$.
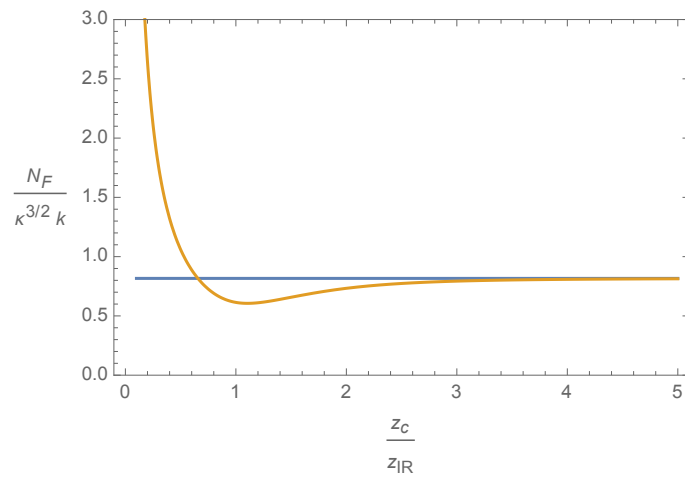
Chapter 6

Higher Curvature Gravity in Soft-Wall Models

6.1 Introduction

Holographic models, where scale invariance is spontaneously broken, provide a naturally light dilaton and a small cosmological constant [154]. However, just like the Randall-Sundrum (RS) scenario, it is straightforward to imagine that these Soft-Wall models are incomplete from either the top-down or bottom-up perspective. A possible extension of this basic model would be the existence of higher-curvature terms, in the vanilla RS models these are expected from string theory [343–346]. In this Chapter we will study how the inclusion of higher curvature gravity terms affects the nature of spontaneous breaking of scale invariance (SBSI).

As we mentioned above, SBSI is interesting as it provides an alternative way to address the question of naturalness in quantum field theory. When scale invariance is broken spontaneously by the vev of a dimensionful operator, then their exists a Nambu-Goldstone boson for scale transformations, the dilaton. However, unlike the spontaneous breaking of a (internal) global symmetry, the non-linear realization of scale symmetry allows for non-derivative quartic self coupling of the form $af^4\chi^4$.

Here, f is the scale af responsible for SBSI and χ is the dilaton field. The existence of this term is unsuited for SBSI. In the low energy effective theory, only a zero value of this constant a allows for the conformal invariance to be truly broken yielding a massless dilaton [328] [1]. However, this criteria can be relaxed to $a \ll 1$ to allow for a broken phase which is only metastable. In the language of CFT, we add an explicit breaking term to CFT, $\lambda \mathcal{O}$ with an almost marginal operator $\mathcal{O}$. This gives rise to an effective potential for the dilaton where λ is almost marginal. This prescription was suggested by Contino, Pomarol and Rattazzi (CPR) [329] and it was further investigated in the 4D effective theory in [155]. CPR suggested a simple holographic implementation which has been checked to work in [156, 331]. By holography, a near marginal deformation in CFT corresponds to introducing a nearly massless bulk scalar field. The approximately constant bulk scalar potential preserves an approximate shift symmetry which leads to a renormalisation-group flow with a small β-function. However to obtain a dilaton in the low-energy spectrum, these explicit realisations also assumed the presence of an IR brane (or hard wall) which corresponds to spontaneously breaking the conformal symmetry by another operator which has an arbitrarily large dimension. Thus by introducing two scalar operators there is a simple, although idealised way to obtain a light dilaton.

A more realistic framework to study the properties of the dilaton is to consider a soft-wall background. This corresponds to introducing a single bulk scalar field with a nontrivial bulk scalar potential. The solutions of the coupled Einstein-scalar equations of motion can then lead to a scalar profile that grows in the IR, causing a back-reaction on the metric that deviates from AdS, as was discussed in the previous Chapter 5. Thus the "soft wall" produced by the single scalar field causes the spontaneous breaking of conformal symmetry. Equivalently, in the holographic description, there is a single operator $\mathcal{O}$ which is responsible for explicitly breaking the conformal

---

[1] When $a > 0$ then then conformal invariance is unbroken (f=0) or in the language of extradimensions, IR brane is pushed to horizon. For $a < 0$ the system is destabilized i.e $f \to \infty$, the IR brane collapses and falls towards the UV brane

symmetry and generating a condensate $\langle \mathcal{O} \rangle$. The fluctuations about the condensate $\langle \mathcal{O} \rangle$ can be identified with the dilaton.

In these "Soft-Wall" models, it is assumed that the 5-dimensional gravity is well described by the Einstein-Hilbert (EH) action plus contributions from a 5D scalar. The next logical question is: would SBSI still occur if we were to surrender the above assumption? This is the discussion we would like to begin in this Chapter. We extend the EH action to include $f(R)$ gravity in the bulk (for recent review of $f(R)$ gravity see [347–354]).Higher derivative gravity and the fine-tuning problem have been discussed in [355], while studies of the cosmological aspects of the F(R) brane world were done in [356]. Some other features, such as effective Einstein equations and junction conditions for $f(R)$ brane-world, were studied in [357, 358].

6.2 Higher curvature terms

When we go beyond the EH action there are several alternatives to be examined. These modified theories include $f(R)$ theories, Gauss-Bonnet gravity, Lanczos-Lovelock models [343–345]. We consider the action to contain a general function of the scalar curvature, $f(R)$ in the bulk [2],

$$ S_{\text{grav}} = \frac{1}{2\kappa^2} \int d^5x \sqrt{g} \left(f(R) + V(\phi) \right) \tag{6.1} $$

where κ^2 is the 5D Newton constant, which is related to the 5D Planck scale via $\kappa^2 = (2M^3)^{-1}$. We take the function $f(R) = R + \frac{R^2}{\beta_2} + \frac{R^3}{\beta_3} + \cdots$, where the β_i coefficients have the appropriate dimensions. For the moment, we presume that the coefficients are independent of position, and that the higher order terms are suppressed [3]. At

---

[2]We consider this action and not more general ones which would include other higher order invariants. It is an interesting and relatively simple alternative to GR, from the study of which some useful conclusions have been derived already. That said it should be noted that it is still a toy-theory

[3]Though the $f(R)$ model contains higher derivative terms of the metric, for R = constant hypersurface all these higher derivative terms vanish [347]. Here we exclusively work on this constant

low energies or small curvature limit we expect that $f(R) \to R$ (and 5D cosmological term). We can also think of $f(R)$ as summing a number of corrections to the EH action which are suppressed by appropriate powers of κ. The usual warped metric ansatz,

$$ds^2 = e^{-2A(y)}\eta_{\mu\nu}dx^\mu dx^\nu + dy^2 \tag{6.2}$$

is considered.

We want to calculate the equations of motion to determine the background geometry, and see if the effect of the higher curvature terms destroys the interpretation of the solution as one corresponding to spontaneously broken scale invariance. If these solutions do break conformal invariance explicitly, it is important to test the degree of breaking (i.e. whether it is suppressed by $1/N$ corrections). The equations of motion (EOMs) for $f(R)$ gravity [4] are given by

$$f'(R)R_{MN} - \frac{1}{2}g_{MN}f(R) - [\nabla_M\nabla_N - g_{MN}\square] f'(R) = \kappa T_{MN} \tag{6.3}$$

where the last term on the left-hand side arises by a non-trivial surface term which vanishes for $f'(R) = 1$. Working out the Christoffel symbols, we get (for non-zero entries)

$$\Gamma^\lambda_{\mu 5} = \Gamma^\lambda_{5\mu} = -A'\delta^\lambda_\mu$$
$$\Gamma^5_{\mu\nu} = -e^{-2A}A'\eta_{\mu\nu} \tag{6.4}$$

Using this, we can write the extra term as

$$[\nabla_M\nabla_N - g_{MN}\square] f'(R) = \left[e^{-2A}\eta_{MN}\partial^2_5 - \left(3e^{-2A}\eta_{MN} - 4\delta^5_M\delta^5_N\right)A'\partial_5\right] f'(R) \tag{6.5}$$

curvature slice such that higher derivative terms do not appear

[4]There are three versions of $f(R)$ gravity, i.e different variational principles can be applied to the gravity action to derive EOMs:Metric, Palatini and metric-affine formalism [348]. Here we focus on the metric formalism.

The equations for the geometry and scalar are then given by:

$$\left(4A'^2 - A''\right) f' - \frac{1}{2}f - f''R'' + 3A'R'f'' - f'''R'^2 = \frac{\kappa^2}{2}\left(\phi'^2 + 2V(\phi)\right) \qquad (6.6)$$

$$\left(4A'' - 4A'^2\right) f' + \frac{1}{2}f - 4A'R'f'' = \frac{\kappa^2}{2}\left(\phi'^2 - 2V(\phi)\right) \qquad (6.7)$$

Here, prime $'$ on the warp factor (A), Ricci scalar (R) and scalar field (ϕ) are with respect to the extradimensional coordinate, y. The primes over $f(R)$ denote derivatives with respect to R.

At any rate, the final ϕ equation is easily integrated when $V(\phi) = $ constant. We have $\phi' = e^{4A}$. This allows us to eliminate all ϕ dependence in this case when $\epsilon = 0$. At that point we have two simultaneous equations for $A(y)$. We find that the two equations are indeed redundant when $f(R) = R$ [5].

We note that holography for the effective "dilaton" potential still holds. The bulk contribution to the free energy is given by

$$S = -\frac{1}{\kappa^2} \int d^4x \left[\sqrt{g}\left(A'f'(R) + f''R'\right)\right]\big|_{\text{UV}}^{\text{IR}} \qquad (6.8)$$

This is true independent of the form of $V(\phi)$. Note that this should allow us to capture the effect of (some) 1/N corrections to our previous dilaton potential.

The variation of the action was given by

$$\delta S = \frac{-1}{2\kappa^2} \int_{\mathcal{M}} \sqrt{g}\left[g_{MN}\left(f(R) - \kappa^2(\partial_S\phi)^2 + \kappa^2 V(\phi)\right)\delta g^{MN}\right] \qquad (6.9)$$

When we vary the EH action, there exist surface contributions which need to be canceled to keep the action stationary. Gibbons, Hawking and York proposed that if we add the trace of an extrinsic curvature of the boundary to the action the surface terms containing the variation of the metric and also variation of the derivatives of the metric are vanishes [359, 360]. We can also calculate the boundary terms that

---

[5]Higher derivatives means we can allow for more "constraints".

are generated which control the boundary conditions on the fields. Again, we need to include a generalized Gibbons-Hawking-York (GHY) term in the action to ameliorate the terms that have derivatives of the variations on the boundary [361].

The GHY terms add an additional term that makes the total "dilaton" action

$$S_{\text{dil}} = \frac{2}{\kappa^2} \int d^4x \left[\sqrt{g} \left(3A' f'(R) - f''(R)R' \right) \right]\big|_{\text{UV}}^{\text{IR}}, \tag{6.10}$$

where the GHY-like boundary term is giving by

$$S'_{GHY} = \oint_{\partial \mathcal{V}} d^3y \varepsilon \sqrt{|h|} f'(R) = \mp \frac{4}{\kappa^2} \int d^4x \sqrt{g_{0,1}} f' A', \tag{6.11}$$

with $f'(R) = df(R)/dR$ and $A' = dA/dy$. Here $\mathcal{V}$ is a hypervolume on the 5D manifold, $\partial \mathcal{V}$ its boundary, h is the determinant of the induced metric, K is the trace of the extrinsic curvature of the boundary $\partial \mathcal{V}$, and ε is $+1$ when the boundary is timelike and -1 when its spacelike. Therefore, the effective action can be still Holographically realised.

6.2.1   Background equations of motion

As we had mentioned above, for a constant bulk scalar potential, the EOMs can be exactly solved. We note that the scalar-einstein equations simplify when written in terms of $X \equiv 3A'f' - R'f''$:

$$(X' + 4A'X) - 12A'^2 f'(R) = \kappa^2 \phi'^2, \tag{6.12}$$

$$(Rf'(R) - f(R)) + (X' - 4A'X) = 2\kappa^2 V(\phi). \tag{6.13}$$

Now note that we can solve the equation for ϕ' exactly when the potential for ϕ is constant:

$$\phi'' - 4A'\phi' = \frac{\partial V(\phi)}{\partial \phi} (= 0), \tag{6.14}$$

such that

$$\phi' = \frac{\sqrt{3}}{2\kappa} e^{4A - 4A_c}, \tag{6.15}$$

where A_c is the value for A at which the "condensate" solution begins to dominate. This solution is the same as we get for the EF action [331] and as was discussed in $y \equiv A$ coordinate in the previous chapter. Thus the "soft-wall" geometry remains intact even when higher curvature terms are considered for the bulk action, alternatively SBCI still occurs.

6.3 $f(R)$ at finite temperature

We now consider the extradimensional model containing higher curvature, $f(R)$ terms at finite temperature. A rigorous analysis of the EH action coupled to scalar field was extensively discussed in the previous chapter. The finite temperature generalization of the metric is:

$$ds^2 = e^{-2A(y)} \left[h(y)dt^2 + d\vec{x}^2 \right] + \frac{dy^2}{h(y)} \tag{6.16}$$

At finite temperatures, we calculate the physical quantity of interest if the free energy of the system, and time coordinate is compactified on a circle: $t \in [0, 1/T)$. The equations of motion for the metric functions h, A and the scalar field ϕ are given by

$$\kappa^2 \phi'^2 = (X' + 4A'X) - 12A'^2 f'(R), \tag{6.17a}$$

$$2\kappa^2 V = \frac{1}{\sqrt{g}} \left(\sqrt{g} h X \right)' + \left(f'(R)R - f(R) \right), \tag{6.17b}$$

$$\phi'' = \phi' \left(4A' - \frac{h'}{h} \right) - \frac{1}{h} \frac{\partial V(\phi)}{\partial \phi}, \tag{6.17c}$$

$$\frac{h''}{h'} = 4A' + R' \frac{f''(R)}{f'(R)}, \tag{6.17d}$$

where, as before, primes denote derivatives with respect to y with the exception that derivatives on $f(R)$ are with respect to R.

The equation of motion for the horizon function, $h(y)$ takes the following form:

$$[\sqrt{g}f'(R)h']' = 0 \tag{6.18}$$

this can be used as an equation for $f'(R)$ and could possibly provide constraints on the form of $f(R)$.

6.3.1 Constant potential

A theory with constant bulk potential is the only case where it is possible to solve the EOMs analytically. Though in previous chapter we have seen that a constant bulk potential does not have a stable effective dilaton potential. When this system is studied at finite temperature then there is no notion of SBSI.

The equation for the scalar field ϕ [6.17c], for a constant bulk potential, is now slightly modified to

$$[\sqrt{g}h\phi']' = 0, \tag{6.19}$$

which can be used as an equation for h. However, when we study the behavior of the scalar field equation near the black hole horizon y_h, i.e when we take the limit $h \to 0$, then we get the following boundary condition [362]:

$$\phi'h' = -\frac{\partial V(\phi)}{\partial \phi}. \tag{6.20}$$

For a constant potential it implies that $\phi'h'|_{y_h} = 0$. For a non-trivial solution, we cannot allow for ϕ' to be zero, as we would expect that horizon forms far from the UV brane [6]. Alternatively, $h'|_{y_h} = 0$ would imply that $(df/dR)|_{y_h}$ be zero.

---

[6] The reader should recall (see for reference Chapter 5) that only in the deep UV, does the scalar field evolves slowly.

6.3.2 Free energy of the black hole solution

We want to test whether the effective 4D theory still respects holography or not. We find that the bulk contribution to the effective potential can be extracted by using the EOMs to express the bulk action as a total derivative.

$$S_{bulk} = -\frac{2}{\kappa^2} \int d^4x \left[\sqrt{g} h \left(A' f'(R) + f'' R' \right) \right]\big|_{\text{UV}}^{\text{IR}} \tag{6.21}$$

In order to have a well defined extremal action principle under metric variation, we need to include the GHY-like boundary term [7]. We would expect

$$S'_{GHY} = \mp \frac{8}{\kappa^2} \int d^4x \sqrt{g_{UV,IR}} f' A', \tag{6.22}$$

where $\sqrt{g_{UV,IR}} = \sqrt{g} \, h_{UV,IR}$, to contain the horizon function h at finite temperature. We also need to consider the effects of two brane localized potentials.

$$S_{brane} = \int d^4x \sqrt{g_{ind}} \, V_{UV}(\phi) + \int d^4x \sqrt{g_{ind}} \, V_{IR}(\phi) \tag{6.23}$$

where the induced metric, $\sqrt{g_{ind}}$ is simply given by $\sqrt{g} \, h_{UV,IR}$ for the two brane potential terms. So, we have,

$$S_{total} = S_{bulk} - S'_{GHY} - S_{brane} \tag{6.24}$$

We know that at finite temperature, the IR brane is replaced by a black-hole horizon. The UV contributions still have the same contribution as given by GHY boundary term. However, the singular term near the black-brane need to be treated more carefully, as near the horizon the manifold exhibits a conical singularity (see Fig. 5.1). We follow the same prescription as was used in the finite temperature analysis of

---

[7]This contribution gets doubled because of orbifolding.

Chapter 5, and find the complete effective potential at finite temperature to be

$$V_{dilaton} = e^{-4A(y_0)} \left[\sqrt{h(y_0)} V_0(\phi(y_0)) - \frac{2h_0}{\kappa^2} \left(3f'(R)A' - f''(R)R' \right) \right] - \frac{4\pi T}{\kappa^2} e^{-3A(y_h)} T,$$

(6.25)

which contains the usual energetic and entropic components. The Hawking temperature [340] is given by,

$$T_h = \frac{e^{-A(y_h)} h'(y_h)}{4\pi}$$

(6.26)

Therefore we see that even at finite temperature we can use the concept of holography to compute the 4D effective potential for extradimensional models which contain higher curvature terms.

6.4 Conclusions

We have obtained the equations of motion in metric formalism for extradimensional models containing $f(R)$ gravity action. We have showed that even with the inclusion of higher curvature terms the spontaneous breaking of conformal invariance occurs. There is still a notion of a "soft-wall". We expect this behaviour to still exist even with the inclusion of nearly-marginal deformations. Though this still needs to be rigorously checked.

The zero and finite temperature analyses emphasize the fact that it is possible to holographically realize these f(R) theories.

Bibliography

[1] S. L. Glashow and H. Georgi (1982), New York Times Magazine (26-09-1982).

[2] M. Baak, M. Goebel, J. Haller, A. Hoecker, D. Kennedy, et al., Eur.Phys.J. **C72**, 2205 (2012), 1209.2716.

[3] G. Aad et al. (ATLAS), Phys.Lett. **B726**, 88 (2013), 1307.1427.

[4] C. Collaboration (CMS) (2013).

[5] F. Iocco, M. Pato, G. Bertone, and P. Jetzer, JCAP **1111**, 029 (2011), 1107.5810.

[6] P. Ade et al. (Planck) (2015), 1502.01589.

[7] H. Weyl, Z.Phys. **56**, 330 (1929).

[8] C. N. Yang and R. L. Mills, Phys. Rev. **96**, 191 (1954), URL http://link.aps.org/doi/10.1103/PhysRev.96.191.

[9] S. Glashow, Nucl.Phys. **22**, 579 (1961).

[10] S. Weinberg, Phys.Rev.Lett. **19**, 1264 (1967).

[11] H. D. Politzer, Phys.Rev.Lett. **30**, 1346 (1973).

[12] D. J. Gross and F. Wilczek, Phys.Rev.Lett. **30**, 1343 (1973).

[13] D. Gross and F. Wilczek, Phys.Rev. **D8**, 3633 (1973).

[14] H. Yukawa, Proc.Phys.Math.Soc.Jap. **17**, 48 (1935).

[15] N. Cabibbo, Physical Review Letters **10**, 531 (1963).

[16] M. Kobayashi and T. Maskawa, Prog.Theor.Phys. **49**, 652 (1973).

[17] B. Pontecorvo, Sov.Phys.JETP **6**, 429 (1957).

[18] B. Pontecorvo, Sov.Phys.JETP **7**, 172 (1958).

[19] B. Pontecorvo, Sov.Phys.JETP **26**, 984 (1968).

[20] Z. Maki, M. Nakagawa, S. Sakata, and and, pp. 663–666 (1962).

[21] F. Englert and R. Brout, Phys.Rev.Lett. **13**, 321 (1964).

[22] G. Guralnik, C. Hagen, and T. Kibble, Phys.Rev.Lett. **13**, 585 (1964).

[23] P. W. Higgs, Phys.Lett. **12**, 132 (1964).

[24] P. W. Higgs, Phys.Rev.Lett. **13**, 508 (1964).

[25] P. W. Higgs, Phys.Rev. **145**, 1156 (1966).

[26] T. Kibble, Phys.Rev. **155**, 1554 (1967).

[27] R. Contino (2010), 1005.4269.

[28] G. 't Hooft and M. Veltman, Nucl.Phys. **B44**, 189 (1972).

[29] M. Gell-Mann, Phys.Lett. **8**, 214 (1964).

[30] M. E. Peskin and D. V. Schroeder, *An Introduction to quantum field theory* (1995).

[31] B. Kayser, F. Gibrat-Debu, and F. Perrier, *The Physics of massive neutrinos*, vol. 25 (1989).

[32] H. Georgi, Ann.Rev.Nucl.Part.Sci. **43**, 209 (1993).

[33] P. Sikivie, L. Susskind, M. B. Voloshin, and V. I. Zakharov, Nucl.Phys. **B173**, 189 (1980).

[34] R. S. Chivukula, M. J. Dugan, M. Golden, and E. H. Simmons, Ann.Rev.Nucl.Part.Sci. **45**, 255 (1995), `hep-ph/9503230`.

[35] R. Peccei, Lect.Notes Phys. **521**, 1 (1999), `hep-ph/9807516`.

[36] G. Lemaitre, Annales Soc.Sci.Brux.Ser.I Sci.Math.Astron.Phys. **A47**, 49 (1927).

[37] A. Friedman, Zeitschrift fr Physik **10**, 377 (1922), ISSN 0044-3328, URL `http://dx.doi.org/10.1007/BF01332580`.

[38] A. Friedmann, Zeitschrift fur Physik **21**, 326 (1924).

[39] H. P. Robertson, apj **82**, 284 (1935).

[40] H. P. Robertson, apj **83**, 187 (1936).

[41] H. P. Robertson, apj **83**, 257 (1936).

[42] A. G. Walker, Proc. London Math. Soc. pp. 90–127 (1937).

[43] E. Hubble, Proc.Nat.Acad.Sci. **15**, 168 (1929).

[44] N. A. Bahcall, L. M. Lubin, and V. Dorman, Astrophys.J. **447**, L81 (1995), `astro-ph/9506041`.

[45] I. Smail, R. S. Ellis, M. J. Fitchett, and A. C. Edge, Mon.Not.Roy.Astron.Soc. **273**, 277 (1995), `astro-ph/9402049`.

[46] A. D. Lewis, E. Ellingson, S. L. Morris, and R. Carlberg, Astrophys.J. **517**, 587 (1999), `astro-ph/9901062`.

[47] S. D. White, J. F. Navarro, A. E. Evrard, and C. S. Frenk, Nature **366**, 429 (1993).

[48] M. Fukugita, C. Hogan, and P. Peebles, Astrophys.J. **503**, 518 (1998), astro-ph/9712020.

[49] S. Dodelson, E. I. Gates, and M. S. Turner, Science **274**, 69 (1996), astro-ph/9603081.

[50] D. Spergel et al. (WMAP), Astrophys.J.Suppl. **148**, 175 (2003), astro-ph/0302209.

[51] G. Hinshaw et al. (WMAP), Astrophys.J.Suppl. **148**, 135 (2003), astro-ph/0302217.

[52] L. Verde (2003), astro-ph/0306272.

[53] S. Burles, K. Nollett, and M. S. Turner (1999), astro-ph/9903300.

[54] E. W. Kolb and M. S. Turner, *The early universe.* (1990).

[55] A. D. Linde, *The physics of elementary particles and inflationary cosmology* (1990).

[56] P. J. E. Peebles, *Principles of Physical Cosmology* (1993).

[57] G. Bertone, D. Hooper, and J. Silk, Phys.Rept. **405**, 279 (2005), hep-ph/0404175.

[58] W. Bernreuther, Lect.Notes Phys. **591**, 237 (2002), hep-ph/0205279.

[59] U. Amaldi, W. de Boer, and H. Furstenau, Phys.Lett. **B260**, 447 (1991).

[60] H. Georgi, Phys. Lett. **B169**, 231 (1986).

[61] S. Chatrchyan et al. (CMS), Phys.Lett. **B716**, 30 (2012), 1207.7235.

[62] G. Aad et al. (ATLAS), Phys.Lett. **B716**, 1 (2012), 1207.7214.

[63] J. Bernon, B. Dumont, and S. Kraml, Phys.Rev. **D90**, 071301 (2014), 1409.1588.

[64] Y. B. Zeldovich, Adv.Astron.Astrophys. **3**, 241 (1965).

[65] H.-Y. Chiu, Phys.Rev.Lett. **17**, 712 (1966).

[66] G. Steigman, Ann.Rev.Nucl.Part.Sci. **29**, 313 (1979).

[67] R. J. Scherrer and M. S. Turner, Phys.Rev. **D33**, 1585 (1986).

[68] S. Nussinov, Phys.Lett. **B165**, 55 (1985).

[69] D. B. Kaplan, Phys.Rev.Lett. **68**, 741 (1992).

[70] S. M. Barr, Phys.Rev. **D44**, 3062 (1991).

[71] D. E. Kaplan, M. A. Luty, and K. M. Zurek, Phys.Rev. **D79**, 115016 (2009), 0901.4117.

[72] R. Peccei and H. R. Quinn, Phys.Rev. **D16**, 1791 (1977).

[73] S. Weinberg, Phys.Rev.Lett. **40**, 223 (1978).

[74] F. Wilczek, Phys.Rev.Lett. **40**, 279 (1978).

[75] S. J. Asztalos, L. J. Rosenberg, K. van Bibber, P. Sikivie, and K. Zioutas, Ann.Rev.Nucl.Part.Sci. **56**, 293 (2006).

[76] S. Dodelson and L. M. Widrow, Phys.Rev.Lett. **72**, 17 (1994), hep-ph/9303287.

[77] A. Kusenko, Phys.Rept. **481**, 1 (2009), 0906.2968.

[78] K. Abazajian, M. Acero, S. Agarwalla, A. Aguilar-Arevalo, C. Albright, et al. (2012), 1204.5379.

[79] H. Georgi and S. L. Glashow, Phys. Rev. Lett. **32**, 438 (1974), URL http://link.aps.org/doi/10.1103/PhysRevLett.32.438.

[80] J. C. Pati and A. Salam, Phys. Rev. D **10**, 275 (1974), URL http://link.aps.org/doi/10.1103/PhysRevD.10.275.

[81] A. Buras, J. R. Ellis, M. Gaillard, and D. V. Nanopoulos, Nucl.Phys. **B135**, 66 (1978).

[82] D. V. Nanopoulos, p. 91 (1978).

[83] P. Langacker, Phys.Rept. **72**, 185 (1981).

[84] S. P. Martin, Adv.Ser.Direct.High Energy Phys. **21**, 1 (2010), hep-ph/9709356.

[85] R. Haag, J. T. Lopuszanski, and M. Sohnius, Nucl.Phys. **B88**, 257 (1975).

[86] S. R. Coleman and J. Mandula, Phys.Rev. **159**, 1251 (1967).

[87] J. Wess and J. Bagger., *Supersymmetry and supergravity* (Princeton University Press, Princeton, USA., 1992).

[88] J. Terning., *Modern supersymmetry: Dynamics and duality* (Oxford University Press, Oxford, United Kingdom., 2006).

[89] S. Dawson and H. Georgi, Phys.Rev.Lett. **43**, 821 (1979).

[90] M. Einhorn and D. Jones, Nucl.Phys. **B196**, 475 (1982).

[91] S. Dimopoulos and H. Georgi, Nucl.Phys. **B193**, 150 (1981).

[92] M. Dine and W. Fischler, Phys.Lett. **B110**, 227 (1982).

[93] H. E. Haber, Nucl.Phys.Proc.Suppl. **62**, 469 (1998), hep-ph/9709450.

[94] P. Bechtle, T. Plehn, and C. Sander (2015), 1506.03091.

[95] M. Papucci, J. T. Ruderman, and A. Weiler, JHEP **1209**, 035 (2012), 1110. 6926.

[96] R. Bousso and J. Polchinski, JHEP **0006**, 006 (2000), hep-th/0004134.

[97] S. Kachru, R. Kallosh, A. D. Linde, and S. P. Trivedi, Phys.Rev. **D68**, 046005 (2003), hep-th/0301240.

[98] N. Arkani-Hamed, S. Dimopoulos, G. Giudice, and A. Romanino, Nucl.Phys. **B709**, 3 (2005), hep-ph/0409232.

[99] G. Giudice and A. Romanino, Nucl.Phys. **B699**, 65 (2004), hep-ph/0406088.

[100] L. J. Hall and Y. Nomura, JHEP **1201**, 082 (2012), 1111.4519.

[101] A. Arvanitaki, N. Craig, S. Dimopoulos, and G. Villadoro, JHEP **1302**, 126 (2013), 1210.0555.

[102] S. Weinberg, Phys.Rev. **D13**, 974 (1976).

[103] L. Susskind, Phys.Rev. **D20**, 2619 (1979).

[104] C. Csaki, C. Grojean, H. Murayama, L. Pilo, and J. Terning, Phys.Rev. **D69**, 055006 (2004), hep-ph/0305237.

[105] C. Csaki, C. Grojean, L. Pilo, and J. Terning, Phys.Rev.Lett. **92**, 101802 (2004), hep-ph/0308038.

[106] C. T. Hill and E. H. Simmons, Phys.Rept. **381**, 235 (2003), hep-ph/0203079.

[107] E. Eichten and K. D. Lane, Phys.Lett. **B90**, 125 (1980).

[108] S. Dimopoulos and L. Susskind, Nucl.Phys. **B155**, 237 (1979).

[109] B. Holdom, Phys.Lett. **B150**, 301 (1985).

[110] T. W. Appelquist, D. Karabali, and L. Wijewardhana, Phys.Rev.Lett. **57**, 957 (1986).

[111] K. Yamawaki, M. Bando, and K.-i. Matumoto, Phys.Rev.Lett. **56**, 1335 (1986).

[112] T. Appelquist and L. Wijewardhana, Phys.Rev. **D35**, 774 (1987).

[113] K. D. Lane and E. Eichten, Phys.Lett. **B222**, 274 (1989).

[114] E. Eichten, K. D. Lane, and J. Womersley, Phys.Lett. **B405**, 305 (1997), hep-ph/9704455.

[115] F. Abe et al. (CDF), Phys.Rev.Lett. **74**, 2626 (1995), hep-ex/9503002.

[116] S. Abachi et al. (D0), Phys.Rev.Lett. **74**, 2632 (1995), hep-ex/9503003.

[117] A. Delgado, K. Lane, and A. Martin, Phys.Lett. **B696**, 482 (2011), 1011.0745.

[118] D. B. Kaplan, H. Georgi, and S. Dimopoulos, Phys.Lett. **B136**, 187 (1984).

[119] H. Georgi and D. B. Kaplan, Phys.Lett. **B145**, 216 (1984).

[120] B. Holdom and J. Terning, Phys.Lett. **B247**, 88 (1990).

[121] M. Golden and L. Randall, Nucl.Phys. **B361**, 3 (1991).

[122] M. E. Peskin and T. Takeuchi, Phys.Rev. **D46**, 381 (1992).

[123] N. Arkani-Hamed, A. G. Cohen, and H. Georgi, Phys.Rev.Lett. **86**, 4757 (2001), hep-th/0104005.

[124] C. T. Hill, S. Pokorski, and J. Wang, Phys.Rev. **D64**, 105005 (2001), hep-th/0104035.

[125] N. Arkani-Hamed, A. Cohen, E. Katz, and A. Nelson, JHEP **0207**, 034 (2002), hep-ph/0206021.

[126] M. Schmaltz and D. Tucker-Smith, Ann.Rev.Nucl.Part.Sci. **55**, 229 (2005), hep-ph/0502182.

[127] M. Schmaltz, JHEP **0408**, 056 (2004), hep-ph/0407143.

[128] H. Georgi and A. Pais, Phys.Rev. **D10**, 539 (1974).

[129] D. B. Kaplan and H. Georgi, Phys.Lett. **B136**, 183 (1984).

[130] N. Arkani-Hamed, A. G. Cohen, and H. Georgi, Phys.Lett. **B513**, 232 (2001), hep-ph/0105239.

[131] T. Gregoire and J. G. Wacker, JHEP **0208**, 019 (2002), hep-ph/0206023.

[132] Z. Chacko, H.-S. Goh, and R. Harnik, Phys.Rev.Lett. **96**, 231802 (2006), hep-ph/0506256.

[133] Z. Chacko, H.-S. Goh, and R. Harnik, JHEP **0601**, 108 (2006), hep-ph/0512088.

[134] D. B. Kaplan, Nucl.Phys. **B365**, 259 (1991).

[135] L. Randall and R. Sundrum, Phys.Rev.Lett. **83**, 3370 (1999), hep-ph/9905221.

[136] L. Randall and R. Sundrum, Phys.Rev.Lett. **83**, 4690 (1999), hep-th/9906064.

[137] K. Agashe, A. Delgado, M. J. May, and R. Sundrum, JHEP **0308**, 050 (2003), hep-ph/0308036.

[138] H. Davoudiasl, J. Hewett, and T. Rizzo, Phys.Lett. **B473**, 43 (2000), hep-ph/9911262.

[139] R. Contino, Y. Nomura, and A. Pomarol, Nucl.Phys. **B671**, 148 (2003), hep-ph/0306259.

[140] K. Agashe, R. Contino, and A. Pomarol, Nucl.Phys. **B719**, 165 (2005), hep-ph/0412089.

[141] Y. Hosotani, Phys.Lett. **B126**, 309 (1983).

[142] I. Antoniadis, K. Benakli, and M. Quiros, New J.Phys. **3**, 20 (2001), hep-th/0108005.

[143] H. Hatanaka, T. Inami, and C. Lim, Mod.Phys.Lett. **A13**, 2601 (1998), hep-th/9805067.

[144] G. von Gersdorff, N. Irges, and M. Quiros, Nucl.Phys. **B635**, 127 (2002), hep-th/0204223.

[145] L. J. Hall, Y. Nomura, and D. Tucker-Smith, Nucl.Phys. **B639**, 307 (2002), hep-ph/0107331.

[146] C. Csaki, C. Grojean, and H. Murayama, Phys.Rev. **D67**, 085012 (2003), hep-ph/0210133.

[147] C. A. Scrucca, M. Serone, and L. Silvestrini, Nucl.Phys. **B669**, 128 (2003), hep-ph/0304220.

[148] C. Scrucca, M. Serone, L. Silvestrini, and A. Wulzer, JHEP **0402**, 049 (2004), hep-th/0312267.

[149] G. Giudice, C. Grojean, A. Pomarol, and R. Rattazzi, JHEP **0706**, 045 (2007), hep-ph/0703164.

[150] R. Barbieri, B. Bellazzini, V. S. Rychkov, and A. Varagnolo, Phys.Rev. **D76**, 115008 (2007), 0706.0432.

[151] B. Bellazzini, C. Cski, and J. Serra, Eur.Phys.J. **C74**, 2766 (2014), 1401.2457.

[152] W. D. Goldberger and M. B. Wise, Phys.Lett. **B475**, 275 (2000), hep-ph/9911457.

[153] W. D. Goldberger and M. B. Wise, Phys.Rev.Lett. **83**, 4922 (1999), hep-ph/9907447.

[154] B. Bellazzini, C. Csaki, J. Hubisz, J. Serra, and J. Terning, Eur.Phys.J. **C73**, 2333 (2013), 1209.3299.

[155] Z. Chacko and R. K. Mishra, Phys.Rev. **D87**, 115006 (2013), 1209.3022.

[156] F. Coradeschi, P. Lodone, D. Pappadopulo, R. Rattazzi, and L. Vitale, JHEP **1311**, 057 (2013), 1306.4601.

[157] E. Megias and O. Pujolas, JHEP **1408**, 081 (2014), 1401.4998.

[158] R. Rattazzi and A. Zaffaroni, JHEP **0104**, 021 (2001), hep-th/0012248.

[159] D. Bunk, J. Hubisz, and B. Jain, Phys.Rev. **D89**, 035014 (2014), 1309.7988.

[160] H. Cai, H.-C. Cheng, and J. Terning, Phys.Rev.Lett. **101**, 171805 (2008), 0806.0386.

[161] J. Fan, B. Jain, and O. Ozsoy, JHEP **1407**, 073 (2014), 1404.1914.

[162] S. Chatrchyan et al. (CMS), Phys. Lett. **B716**, 30 (2012), 1207.7235.

[163] G. Aad et al. (ATLAS), Phys. Lett. **B716**, 1 (2012), 1207.7214.

[164] D. Carmi, A. Falkowski, E. Kuflik, and T. Volansky, JHEP **1207**, 136 (2012), 1202.3144.

[165] A. Azatov, R. Contino, and J. Galloway, JHEP **1204**, 127 (2012), 1202.3415.

[166] J. Espinosa, C. Grojean, M. Muhlleitner, and M. Trott, JHEP **1205**, 097 (2012), 1202.3697.

[167] P. P. Giardino, K. Kannike, M. Raidal, and A. Strumia, JHEP **1206**, 117 (2012), 1203.4254.

[168] J. Ellis and T. You, JHEP **1206**, 140 (2012), 1204.0464.

[169] W. D. Goldberger, B. Grinstein, and W. Skiba, Phys.Rev.Lett. **100**, 111802 (2008), 0708.1463.

[170] J. Fan, W. D. Goldberger, A. Ross, and W. Skiba, Phys.Rev. **D79**, 035017 (2009), 0803.2040.

[171] Z. Chacko, R. Franceschini, and R. K. Mishra, JHEP **1304**, 015 (2013), 1209.3259.

[172] C. Csaki, M. L. Graesser, and G. D. Kribs, Phys.Rev. **D63**, 065002 (2001), hep-th/0008151.

[173] C. Csaki, J. Hubisz, and S. J. Lee, Phys.Rev. **D76**, 125015 (2007), 0705.3844.

[174] I. Low, R. Rattazzi, and A. Vichi, JHEP **1004**, 126 (2010), 0907.5413.

[175] R. Contino, C. Grojean, M. Moretti, F. Piccinini, and R. Rattazzi, JHEP **1005**, 089 (2010), 1002.1011.

[176] R. Contino, D. Marzocca, D. Pappadopulo, and R. Rattazzi, JHEP **1110**, 081 (2011), 1109.1570.

[177] M. Farina, C. Grojean, and E. Salvioni, JHEP **1207**, 012 (2012), 1205.0011.

[178] C. H. Llewellyn Smith, Phys. Lett. B **46**, 233 (1973).

[179] D. Dicus and V. Mathur, Phys.Rev. **D7**, 3111 (1973).

[180] J. M. Cornwall, D. N. Levin, and G. Tiktopoulos, Phys.Rev.Lett. **30**, 1268 (1973).

[181] J. M. Cornwall, D. N. Levin, and G. Tiktopoulos, Phys.Rev. **D10**, 1145 (1974).

[182] B. W. Lee, C. Quigg, and H. Thacker, Phys.Rev.Lett. **38**, 883 (1977).

[183] B. W. Lee, C. Quigg, and H. Thacker, Phys.Rev. **D16**, 1519 (1977).

[184] M. S. Chanowitz and M. K. Gaillard, Nucl.Phys. **B261**, 379 (1985).

[185] M. Papucci (2004), hep-ph/0408058.

[186] R. Foadi, M. Jarvinen, and F. Sannino, Phys.Rev. **D79**, 035010 (2009), 0811. 3719.

[187] R. Barbieri, G. Isidori, V. S. Rychkov, and E. Trincherini, Phys.Rev. **D78**, 036012 (2008), 0806.1624.

[188] A. Carcamo Hernandez and R. Torre, Nucl.Phys. **B841**, 188 (2010), 1005.3809.

[189] O. Eboli, J. Gonzalez-Fraile, and M. Gonzalez-Garcia, Phys.Rev. **D85**, 055019 (2012), 1112.0316.

[190] B. Bellazzini, C. Csaki, J. Hubisz, J. Serra, and J. Terning, JHEP **1211**, 003 (2012), 1205.4032.

[191] J. Erler and P. Langacker (2008).

[192] S. R. Coleman, J. Wess, and B. Zumino, Phys.Rev. **177**, 2239 (1969).

[193] J. Callan, Curtis G., S. R. Coleman, J. Wess, and B. Zumino, Phys.Rev. **177**, 2247 (1969).

[194] M. Bando, T. Kugo, S. Uehara, K. Yamawaki, and T. Yanagida, Phys.Rev.Lett. **54**, 1215 (1985).

[195] M. Bando, T. Kugo, and K. Yamawaki, Phys.Rept. **164**, 217 (1988).

[196] H. Georgi, Nucl.Phys. **B331**, 311 (1990).

[197] R. Casalbuoni, S. De Curtis, D. Dominici, and R. Gatto, Phys.Lett. **B155**, 95 (1985).

[198] R. Casalbuoni, S. De Curtis, D. Dominici, and R. Gatto, Nucl.Phys. **B282**, 235 (1987).

[199] R. Casalbuoni, A. Deandrea, S. De Curtis, D. Dominici, F. Feruglio, et al., Phys.Lett. **B349**, 533 (1995), `hep-ph/9502247`.

[200] G. Ecker, J. Gasser, H. Leutwyler, A. Pich, and E. de Rafael, Phys.Lett. **B223**, 425 (1989).

[201] S. Chatrchyan et al. (CMS), Phys.Lett. **B726**, 587 (2013), `1307.5515`.

[202] J. S. Gainer, W.-Y. Keung, I. Low, and P. Schwaller, Phys.Rev. **D86**, 033010 (2012), `1112.1405`.

[203] R. Torre (2011), `1110.3906`.

[204] C.-W. Chiang and K. Yagyu, Phys.Rev. **D87**, 033003 (2013), `1207.1065`.

[205] H. Cai, JHEP **1404**, 052 (2014), `1306.3922`.

[206] A. Azatov, R. Contino, A. Di Iura, and J. Galloway, Phys.Rev. **D88**, 075019 (2013), `1308.2676`.

[207] M. A. Shifman, A. Vainshtein, M. Voloshin, and V. I. Zakharov, Sov.J.Nucl.Phys. **30**, 711 (1979).

[208] J. F. Gunion, H. E. Haber, G. L. Kane, and S. Dawson, Front.Phys. **80**, 1 (2000).

[209] *Higgs Decays*, `http://www.phy.syr.edu/~jhubisz/HIGGSDECAYS/RL`.

[210] R. S. Chivukula and E. H. Simmons, Phys.Rev. **D78**, 077701 (2008), `0808.2071`.

[211] R. Barbieri, A. Pomarol, R. Rattazzi, and A. Strumia, Nucl.Phys. **B703**, 127 (2004), `hep-ph/0405040`.

[212] G. Cacciapaglia, C. Csaki, G. Marandella, and A. Strumia, Phys.Rev. **D74**, 033011 (2006), hep-ph/0604111.

[213] A. Orgogozo and S. Rychkov, JHEP **1203**, 046 (2012), 1111.3534.

[214] M. Gillioz, R. Grober, C. Grojean, M. Muhlleitner, and E. Salvioni, JHEP **1210**, 004 (2012), 1206.7120.

[215] C. Grojean, E. E. Jenkins, A. V. Manohar, and M. Trott, JHEP **1304**, 016 (2013), 1301.2588.

[216] J. Kublbeck, H. Eck, and R. Mertig, Nucl.Phys.Proc.Suppl. **29A**, 204 (1992).

[217] M. Bando, T. Fujiwara, and K. Yamawaki, Prog.Theor.Phys. **79**, 1140 (1988).

[218] R. Casalbuoni, S. De Curtis, D. Dominici, F. Feruglio, and R. Gatto, Int.J.Mod.Phys. **A4**, 1065 (1989).

[219] J. Hirn, A. Martin, and V. Sanz, JHEP **0805**, 084 (2008), 0712.3783.

[220] K. Agashe, C. Csaki, C. Grojean, and M. Reece, JHEP **0712**, 003 (2007), 0704.1821.

[221] G. Cacciapaglia, C. Csaki, C. Grojean, and J. Terning, Phys.Rev. **D71**, 035015 (2005), hep-ph/0409126.

[222] G. Cacciapaglia, C. Csaki, G. Marandella, and J. Terning, Phys.Rev. **D75**, 015003 (2007), hep-ph/0607146.

[223] H. Georgi, Phys.Lett. **B298**, 187 (1993), hep-ph/9207278.

[224] P. Langacker and M.-x. Luo, Phys.Rev. **D45**, 278 (1992).

[225] B. Holdom, Phys.Lett. **B259**, 329 (1991).

[226] G. Altarelli, R. Barbieri, and S. Jadach, Nucl.Phys. **B369**, 3 (1992).

[227] H. Cai, Phys.Rev. **D85**, 115020 (2012), 1204.6622.

[228] M. Baak and R. Kogler, pp. 349–358 (2013), 1306.0571.

[229] J. Alwall, M. Herquet, F. Maltoni, O. Mattelaer, and T. Stelzer, JHEP **1106**, 128 (2011), 1106.0522.

[230] Tech. Rep. CMS-PAS-EXO-12-061, CERN, Geneva (2013).

[231] D. Buttazzo, G. Degrassi, P. P. Giardino, G. F. Giudice, F. Sala, et al., JHEP **1312**, 089 (2013), 1307.3536.

[232] P. Batra, A. Delgado, D. E. Kaplan, and T. M. Tait, JHEP **0402**, 043 (2004), hep-ph/0309149.

[233] A. Maloney, A. Pierce, and J. G. Wacker, JHEP **0606**, 034 (2006), hep-ph/0409127.

[234] S. Dawson, A. Gritsan, H. Logan, J. Qian, C. Tully, et al. (2013), 1310.8361.

[235] H. Baer, T. Barklow, K. Fujii, Y. Gao, A. Hoang, et al. (2013), 1306.6352.

[236] M. Bicer, H. Duran Yildiz, I. Yildiz, G. Coignet, M. Delmastro, et al. (2013), 1308.6176.

[237] A. Djouadi, Phys.Rept. **459**, 1 (2008), hep-ph/0503173.

[238] D. Carmi, A. Falkowski, E. Kuflik, T. Volansky, and J. Zupan, JHEP **1210**, 196 (2012), 1207.1718.

[239] M. Farina, M. Perelstein, and N. Rey-Le Lorier (2013), 1305.6068.

[240] N. Craig, C. Englert, and M. McCullough, Phys.Rev.Lett. **111**, 121803 (2013), 1305.5251.

[241] J. R. Ellis, M. K. Gaillard, and D. V. Nanopoulos, Nucl.Phys. **B106**, 292 (1976).

[242] R. D. Ball et al. (NNPDF), Nucl.Phys. **B877**, 290 (2013), 1308.0598.

[243] A. Avetisyan, J. M. Campbell, T. Cohen, N. Dhingra, J. Hirschauer, et al. (2013), 1308.1636.

[244] C.-Y. Chen, A. Freitas, T. Han, and K. S. Lee, JHEP **1211**, 124 (2012), 1207. 4794.

[245] C. Brust, A. Katz, S. Lawrence, and R. Sundrum, JHEP **1203**, 103 (2012), 1110.6670.

[246] J. Berger, J. Hubisz, and M. Perelstein, JHEP **1207**, 016 (2012), 1205.0013.

[247] G. F. Giudice, M. A. Luty, H. Murayama, and R. Rattazzi, JHEP **9812**, 027 (1998), hep-ph/9810442.

[248] L. Randall and R. Sundrum, Nucl.Phys. **B557**, 79 (1999), hep-th/9810155.

[249] K. Choi, A. Falkowski, H. P. Nilles, and M. Olechowski, Nucl.Phys. **B718**, 113 (2005), hep-th/0503216.

[250] K. Choi, K. S. Jeong, and K.-i. Okumura, JHEP **0509**, 039 (2005), hep-ph/ 0504037.

[251] J. P. Conlon and F. Quevedo, JHEP **0606**, 029 (2006), hep-th/0605141.

[252] J. P. Conlon, S. S. Abdussalam, F. Quevedo, and K. Suruliz, JHEP **0701**, 032 (2007), hep-th/0610129.

[253] B. S. Acharya, K. Bobkov, G. L. Kane, P. Kumar, and J. Shao, Phys.Rev. **D76**, 126010 (2007), hep-th/0701034.

[254] B. S. Acharya, K. Bobkov, G. L. Kane, J. Shao, and P. Kumar, Phys.Rev. **D78**, 065038 (2008), 0801.0478.

[255] J. D. Wells (2003), hep-ph/0306127.

[256] N. Arkani-Hamed and S. Dimopoulos, JHEP **0506**, 073 (2005), hep-th/
0405159.

[257] M. Ibe and T. T. Yanagida, Phys.Lett. **B709**, 374 (2012), 1112.2462.

[258] N. Arkani-Hamed, A. Gupta, D. E. Kaplan, N. Weiner, and T. Zorawski (2012),
1212.6971.

[259] L. J. Hall, Y. Nomura, and S. Shirai, JHEP **1301**, 036 (2013), 1210.2395.

[260] L. J. Hall and Y. Nomura, JHEP **1402**, 129 (2014), 1312.6695.

[261] M. Baumgart, D. Stolarski, and T. Zorawski (2014), 1403.6118.

[262] T. Cohen, M. Lisanti, A. Pierce, and T. R. Slatyer, JCAP **1310**, 061 (2013),
1307.4082.

[263] J. Fan and M. Reece, JHEP **1310**, 124 (2013), 1307.4400.

[264] P. A. R. Ade et al. (Planck) (2015), 1502.02114.

[265] J. Pradler and F. D. Steffen, Phys.Lett. **B648**, 224 (2007), hep-ph/0612291.

[266] V. S. Rychkov and A. Strumia, Phys.Rev. **D75**, 075011 (2007), hep-ph/
0701104.

[267] C. Cheung, G. Elor, and L. Hall, Phys.Rev. **D84**, 115021 (2011), 1103.4394.

[268] L. J. Hall, K. Jedamzik, J. March-Russell, and S. M. West, JHEP **1003**, 080
(2010), 0911.1120.

[269] C. Cheung, G. Elor, L. J. Hall, and P. Kumar, JHEP **1103**, 042 (2011), 1010.
0022.

[270] M. Kawasaki, F. Takahashi, and T. Yanagida, Phys.Lett. **B638**, 8 (2006),
hep-ph/0603265.

[271] M. Kawasaki, F. Takahashi, and T. Yanagida, Phys.Rev. **D74**, 043519 (2006), hep-ph/0605297.

[272] M. Dine, R. Kitano, A. Morisse, and Y. Shirman, Phys.Rev. **D73**, 123518 (2006), hep-ph/0604140.

[273] K. Nakayama, F. Takahashi, and T. T. Yanagida, Phys.Lett. **B718**, 526 (2012), 1209.2583.

[274] M. Kawasaki, K. Kohri, T. Moroi, and A. Yotsuyanagi, Phys.Rev. **D78**, 065011 (2008), 0804.3745.

[275] T. Moroi, M. Nagai, and M. Takimoto, JHEP **1307**, 066 (2013), 1303.0948.

[276] P. Gondolo, J. Edsjo, P. Ullio, L. Bergstrom, M. Schelke, et al., JCAP **0407**, 008 (2004), astro-ph/0406204.

[277] J. Hisano, S. Matsumoto, M. Nagai, O. Saito, and M. Senami, Phys.Lett. **B646**, 34 (2007), hep-ph/0610249.

[278] A. Hryczuk and R. Iengo, JHEP **1201**, 163 (2012), 1111.2916.

[279] A. Hryczuk, Phys.Lett. **B699**, 271 (2011), 1102.4295.

[280] M. Ibe, S. Matsumoto, and R. Sato, Phys.Lett. **B721**, 252 (2013), 1212.5989.

[281] M. Ackermann et al. (Fermi-LAT), Phys.Rev.Lett. **107**, 241302 (2011), 1108.3546.

[282] M. Ackermann et al. (Fermi-LAT), Astrophys.J.Suppl. **203**, 4 (2012), 1206.1896.

[283] M. Ackermann et al. (Fermi-LAT), Phys.Rev. **D88**, 082002 (2013), 1305.5597.

[284] A. Abramowski et al. (H.E.S.S.), Phys.Rev.Lett. **106**, 161301 (2011), 1103.3266.

[285] A. Drlica-Wagner, *Searching for dark matterin dwarf spheroidal satellite galaxies with the fermi-lat*, http://fermi.gsfc.nasa.gov/science/mtgs/symposia/2012/program/fri/ADrlica-Wagner.pdf (2012), [Online; accessed 13-March-2012].

[286] A. Hryczuk, I. Cholis, R. Iengo, M. Tavakoli, and P. Ullio (2014), 1401.6212.

[287] D. Hooper, C. Kelso, and F. S. Queiroz, Astropart.Phys. **46**, 55 (2013), 1209.3015.

[288] A. Abramowski et al. (H.E.S.S.), Phys.Rev.Lett. **110**, 041301 (2013), 1301.1173.

[289] M. Cirelli, A. Strumia, and M. Tamburini, Nucl.Phys. **B787**, 152 (2007), 0706.4071.

[290] T. Moroi and L. Randall, Nucl.Phys. **B570**, 455 (2000), hep-ph/9906527.

[291] R. Easther, R. Galvez, O. Ozsoy, and S. Watson, Phys.Rev. **D89**, 023522 (2014), 1307.2453.

[292] R. Allahverdi, M. Cicoli, B. Dutta, and K. Sinha, Phys.Rev. **D88**, 095015 (2013), 1307.5086.

[293] P. Ade et al. (BICEP2, Planck), Phys. Rev. Lett. **114**, 101301 (2015), 1502.00612.

[294] D. Baumann (2009), 0907.5424.

[295] V. F. Mukhanov, JETP Lett. **41**, 493 (1985).

[296] V. F. Mukhanov, Sov.Phys.JETP **67**, 1297 (1988).

[297] C. Cheung, P. Creminelli, A. L. Fitzpatrick, J. Kaplan, and L. Senatore, JHEP **0803**, 014 (2008), 0709.0293.

181

[298] G. F. Smoot, C. Bennett, A. Kogut, E. Wright, J. Aymon, et al., Astrophys.J. **396**, L1 (1992).

[299] D. Spergel et al. (WMAP), Astrophys.J.Suppl. **170**, 377 (2007), astro-ph/0603449.

[300] D. H. Lyth, Phys.Rev.Lett. **78**, 1861 (1997), hep-ph/9606387.

[301] A. D. Linde, Mod.Phys.Lett. **A1**, 81 (1986).

[302] A. D. Linde, Phys.Lett. **B175**, 395 (1986).

[303] K. Freese, J. A. Frieman, and A. V. Olinto, Phys.Rev.Lett. **65**, 3233 (1990).

[304] K. Harigaya, M. Ibe, K. Schmitz, and T. T. Yanagida (2014), 1403.4536.

[305] K. Harigaya and T. T. Yanagida (2014), 1403.4729.

[306] K. Freese and W. H. Kinney (2014), 1403.5277.

[307] B. A. Bassett, S. Tsujikawa, and D. Wands, Rev.Mod.Phys. **78**, 537 (2006), astro-ph/0507632.

[308] R. Kallosh, L. Kofman, A. D. Linde, and A. Van Proeyen, Phys.Rev. **D61**, 103503 (2000), hep-th/9907124.

[309] G. Giudice, A. Riotto, and I. Tkachev, JHEP **9911**, 036 (1999), hep-ph/9911302.

[310] R. Kallosh, L. Kofman, A. D. Linde, and A. Van Proeyen, Class.Quant.Grav. **17**, 4269 (2000), hep-th/0006179.

[311] A. L. Maroto and A. Mazumdar, Phys.Rev.Lett. **84**, 1655 (2000), hep-ph/9904206.

[312] H. P. Nilles, M. Peloso, and L. Sorbo, JHEP **0104**, 004 (2001), hep-th/0103202.

[313] H. P. Nilles, M. Peloso, and L. Sorbo, Phys.Rev.Lett. **87**, 051302 (2001), hep-ph/0102264.

[314] P. B. Greene, K. Kadota, and H. Murayama, Phys.Rev. **D68**, 043502 (2003), hep-ph/0208276.

[315] J. R. Ellis, C. Kounnas, and D. V. Nanopoulos, Nucl.Phys. **B247**, 373 (1984).

[316] J. Scherk and J. H. Schwarz, Nucl.Phys. **B153**, 61 (1979).

[317] L. J. Hall, Y. Nomura, and S. Shirai (2014), 1403.8138.

[318] N. Craig and D. Green (2014), 1403.7193.

[319] G. Giudice, A. Notari, M. Raidal, A. Riotto, and A. Strumia, Nucl.Phys. **B685**, 89 (2004), hep-ph/0310123.

[320] M. Kamionkowski and J. March-Russell, Phys.Lett. **B282**, 137 (1992), hep-th/9202003.

[321] V. Rubakov and M. Shaposhnikov, Physics Letters B **125**, 139 (1983), ISSN 0370-2693, URL http://www.sciencedirect.com/science/article/pii/0370269383912546.

[322] S. Weinberg, Rev. Mod. Phys. **61**, 1 (1989).

[323] R. Sundrum (2003), hep-th/0312212.

[324] S. S. Gubser, Phys.Rev. **D63**, 084017 (2001), hep-th/9912001.

[325] H. L. Verlinde, Nucl.Phys. **B580**, 264 (2000), hep-th/9906182.

[326] N. Arkani-Hamed, M. Porrati, and L. Randall, JHEP **0108**, 017 (2001), hep-th/0012148.

[327] C. Csaki, M. Graesser, L. Randall, and J. Terning, Phys.Rev. **D62**, 045015 (2000), hep-ph/9911406.

[328] S. Fubini, Nuovo Cim. **A34**, 521 (1976).

[329] R. Contino, A. Pomarol, and R. Rattazzi, *see talks by R. Rattazzi at Planck, 2010 and by A. Pomarol at the XVI IFT XmasWorkshop*, https://indico.cern.ch/event/75810/contribution/163/material/slides/0.pdf, http://www.ift.uam-csic.es/workshops/Xmas10/doc/pomarol.pdf.

[330] Z. Chacko, R. K. Mishra, and D. Stolarski, JHEP **1309**, 121 (2013), 1304.1795.

[331] B. Bellazzini, C. Csaki, J. Hubisz, J. Serra, and J. Terning, Eur.Phys.J. **C74**, 2790 (2014), 1305.3919.

[332] T. Nihei, Phys.Lett. **B465**, 81 (1999), hep-ph/9905487.

[333] N. Kaloper, Phys.Rev. **D60**, 123506 (1999), hep-th/9905210.

[334] P. Creminelli, A. Nicolis, and R. Rattazzi, JHEP **0203**, 051 (2002), hep-th/0107141.

[335] W. D. Goldberger and M. B. Wise, Phys. Rev. Lett. **83**, 4922 (1999), hep-ph/9907447.

[336] L. Randall and G. Servant, JHEP **0705**, 054 (2007), hep-ph/0607158.

[337] S. S. Gubser, Phys. Rev. **D63**, 084017 (2001), hep-th/9912001.

[338] E. Witten, Adv.Theor.Math.Phys. **2**, 505 (1998), hep-th/9803131.

[339] A. H. Guth and E. J. Weinberg, Nucl. Phys. **B212**, 321 (1983).

[340] S. Hawking, I. Moss, and J. Stewart, Phys.Rev. **D26**, 2681 (1982).

[341] G. W. Anderson and L. J. Hall, Phys.Rev. **D45**, 2685 (1992).

[342] S. R. Coleman, Phys.Rev. **D15**, 2929 (1977).

[343] B. Zwiebach, Phys.Lett. **B156**, 315 (1985).

[344] D. G. Boulware and S. Deser, Phys.Rev.Lett. **55**, 2656 (1985).

[345] B. Zumino, Phys.Rept. **137**, 109 (1986).

[346] N. E. Mavromatos and J. Rizos, Phys.Rev. **D62**, 124004 (2000), hep-th/0008074.

[347] S. Nojiri and S. D. Odintsov, Phys.Rept. **505**, 59 (2011), 1011.0544.

[348] T. P. Sotiriou and V. Faraoni, Rev.Mod.Phys. **82**, 451 (2010), 0805.1726.

[349] S. Nojiri and S. D. Odintsov, Phys.Rev. **D68**, 123512 (2003), hep-th/0307288.

[350] S. M. Carroll, V. Duvvuri, M. Trodden, and M. S. Turner, Phys.Rev. **D70**, 043528 (2004), astro-ph/0306438.

[351] A. De Felice and S. Tsujikawa, Living Rev.Rel. **13**, 3 (2010), 1002.4928.

[352] S. Nojiri and S. D. Odintsov, Phys.Rev. **D77**, 026007 (2008), 0710.1738.

[353] V. Faraoni, Phys.Rev. **D76**, 127501 (2007), 0710.1291.

[354] A. Bustelo and D. Barraco, Class.Quant.Grav. **24**, 2333 (2007), gr-qc/0611149.

[355] M. Parry, S. Pichler, and D. Deeg, JCAP **0504**, 014 (2005), hep-ph/0502048.

[356] A. Balcerzak and M. P. Dabrowski, Phys.Rev. **D81**, 123527 (2010), 1004.0150.

[357] M. Faizal, Phys.Rev. **D84**, 106011 (2011), 1111.0213.

[358] B. A. Burrington, A. W. Peet, and I. G. Zadeh, Phys.Rev. **D87**, 106001 (2013), 1211.6699.

[359] G. Gibbons and S. Hawking, Phys.Rev. **D15**, 2752 (1977).

[360] J. York, James W., Phys.Rev.Lett. **28**, 1082 (1972).

[361] E. Dyer and K. Hinterbichler, Phys.Rev. **D79**, 024028 (2009), 0809.4033.

[362] S. S. Gubser, Adv.Theor.Math.Phys. **4**, 679 (2000), hep-th/0002160.

Curriculum Vitae

Personal Data

Date of Birth	1 September 1986
Address	Department of Physics, Syracuse University
	Syracuse, NY 13244, USA
Phone	+1 315 751 2007
email	bjain@syr.edu

Education

2010 –	**PhD in Physics, Syracuse University, Syracuse, NY, USA**
2007 – 2010	MSc in Physics, Indian Institute of Technology , Kanpur, India.
2004 – 2007	BSc in Physics, St Xavier's College, Mumbai, India.

Programming

Mathematica, C++, Python

Awards, etc.

1. Pheno 14 Travel Award, Phenomenology 2014 Symposium,PITT-PACC, University of Pittsburgh, Pittsburgh,PA

2. GSO Travel Grant Graduate Student Organization, Syracuse University, Syracuse, NY - 2014

3. Teaching Mentor, Teaching Assistant Orientation Program, Syracuse University, Syracuse, NY- 2013

4. Henry Levinstein Fellowship Award -awarded in recognition of excellent work in first year graduate courses, Syracuse University, Syracuse, NY -2012

5. Prof. Joseph Selwyn Dias Scholarship- for highest aggregate in Physics in Undergraduate-St Xavier's College, Mumbai, India - 2007

6. Malcolm Pereira Science Scholarship, St Xavier's College, Mumbai, India - 2007

7. Prof. Sam J. Khambatta Scholarship, for highest in III year B.Sc examination, St Xavier's College, Mumbai, India 2007

8. Ranked in top 1%, National Graduate Physics Examinations, Indian Association of Physics, India-2006

9. Honors academic credit - Physics, Ranked in top 1%, St Xavier's College, Mumbai, India- 2004-2007

10. Honors academic credit - Maths, Ranked in top 1%, St Xavier's College, Mumbai, India- 2005

Talks, Posters, Schools and Conferences

1. May 2015, Holographic models with a small cosmological constant at Finite Temperature, Phenomenology 2015 Symposium, University of Pittsburgh, Pittsburgh,PA

2. November 2014, Phenomenology of Spin-1 Top Partner, Theory Seminar, Lund University, Lund, Sweden

3. November 2014, Phenomenology of Spin-1 Top Partner, Theory Seminar, Technische Universitaet Muenchen, Munich, Germany

4. November 2014, Models with small cosmological constant at finite temperature, Theory Seminar, Institut fr Physik (WA THEP) Johannes-Gutenberg-Universitt, Mainz, Germany

5. November 2014, Models with small cosmological constant at finite temperature, Theory Seminar, Institute of High-Energy Physics,Universitat Autonoma de Barcelona, Barcelona, Spain

6. May 2014, Higgs decays in gauge extensions of the standard model, Phenomenology 2014 Symposium, University of Pittsburgh, Pittsburgh,PA

7. Oct 2013, Higgs Decays in Gauge extensions of Standard Model, Laboratory for Elementary-Particle Physics, Cornell University, Ithaca, NY

8. June 2013, Higgs Phenomenology in Gauge extensions of Standard Model, TASI, Student Talk, University of Colorado, Boulder, CO

9. 2014, SLAC Summer Institute, SLAC, Stanford, CA

10. 2014, Phenomenology 2014 Symposium, PITT-PACC, University of Pittsburgh, Pittsburgh,PA

11. 2013, Prospects in Theoretical Physics, Institute for Advanced Study, Princeton,NJ

12. 2013, Theoretical Advanced Study Inspiral in Elementary Particle Physics(TASI), University of Colorado, Boulder,CO

13. 2010, International Linear Collider Workshop, Institute of High Energy Physics, Beijing,China, Indian Institute of Technology, Kanpur, India

14. 2009, Summer school on Particle Physics in LHC Era, International Centre of Theoretical Physics(ICTP), Trieste, Italy

15. 2009, Joint ICTP-INFN-SISSA:Topical Issues in LHC Physics, International Center of Theoretical Physics(ICTP), Trieste, Italy

16. 2008, ERN Summer Student Program, CERN, Geneva, Switzerland

17. 2007, Visiting Student Research Program, Tata Institute of Fundamental Research,Mumbai, India

18. 2007, Summer Student Program, Institute of Mathematical Sciences, Chennai, India